Strategies for rendezvous and formation stabilization of multi-agent systems

by

Stephen L. Smith

A thesis submitted in conformity with the requirements
for the degree of Master of Applied Science
Graduate Department of Electrical and Computer Engineering
University of Toronto

Abstract

Strategies for rendezvous and formation stabilization of multi-agent systems

Stephen L. Smith

Master of Applied Science

Graduate Department of Electrical and Computer Engineering

University of Toronto

2005

In this thesis, four problems in the control of multi-agent systems are studied. First, a hierarchical cyclic pursuit scheme is introduced, and it is shown to yield significant advantages over traditional cyclic pursuit. Second, the control of a heterogeneous group of agents is explored. A global stability analysis is performed for two agents in cyclic pursuit, where each agent has a different kinematic model. Third, the problem of adapting curve shortening theory to the multi-agent setting is addressed. Motivated by this theory, the agents are viewed as the vertices of a polygon, and a linear polygon shortening scheme is proposed which exhibits several analogues to Euclidean curve shortening. Finally, the problem of stabilizing a group of agents to a formation is analyzed. By adapting the linear polygon shortening scheme, a local control strategy is proposed to stabilize the agents to the vertices of an equilateral polygon.

Acknowledgements

I would like to thank Professors Mireille Broucke and Bruce Francis for being exceptional supervisors. I have learned so much from my conversations with them over the past two years, and I will miss that greatly. They have inspired me to continue on in my academic studies – if you told me two years ago that I was going to do 4+ more years of school after my Masters, I wouldn't have believed you. I would also like to thank Professor Manfredi Maggiore for providing wonderful insight into some of the nonlinear problems I encountered throughout my research. His passion for research has not only been inspirational, but also contagious.

Contents

List of Figures

Chapter 1

Introduction

Suppose you have lost a valuable piece of jewelry in the park, and you must find it. You have gathered up some volunteers to help you find the piece of jewelry, and you have roped off the region that contains the object. You instruct the volunteers to set up a perimeter by standing evenly spaced around the boundary of the region, as shown in Figure 1.1(a). How should you tell the volunteers to move so that they will tighten their perimeter around the piece of jewelry? That is, you would like the length of the boundary, and the area inclosed, to decrease. In addition you would like the region enclosed to become convex so that each volunteer has a clear line of sight to every point in the region. A solution, which is developed in this thesis, is for each volunteer to pursue the centroid of its two neighbours. The resulting paths of the volunteers, and the evolving boundary are shown in Figure 1.1(b).

In the above example, the volunteers are agents in a multi-agent system who have been given the task of finding the piece of jewelry. So what exactly is an agent? For our purposes, an agent is a mobile computational system that acquires data through sensors. It can process the data it acquires, and if given a goal, can alter its motion based on the data to attempt to attain the goal. Through its sensors and its computing power the agent can determine the relative positions of objects that it can sense. From

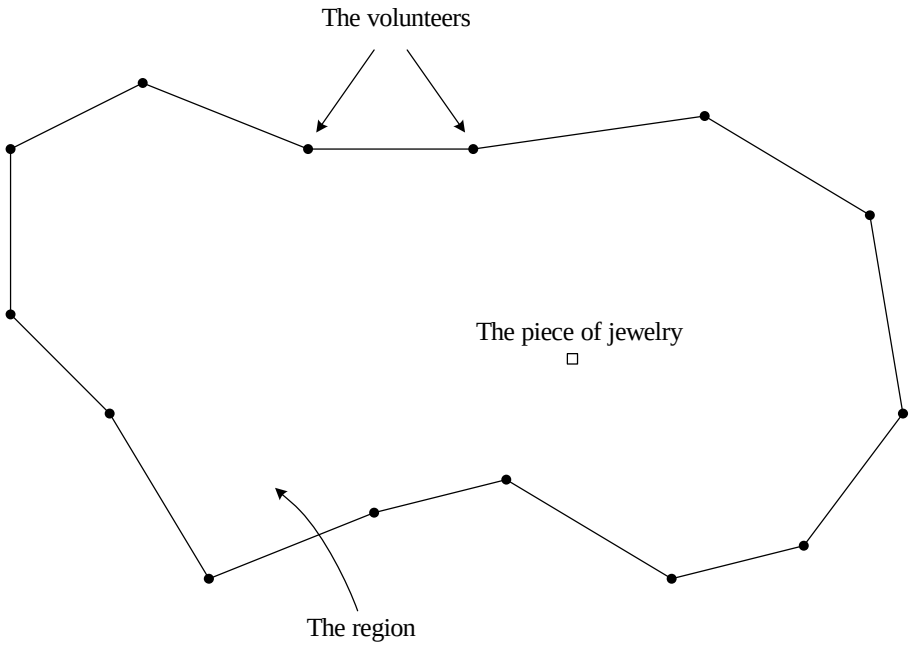

(a) The region which contains the piece of jewelry, and the volunteers positioned around the boundary.

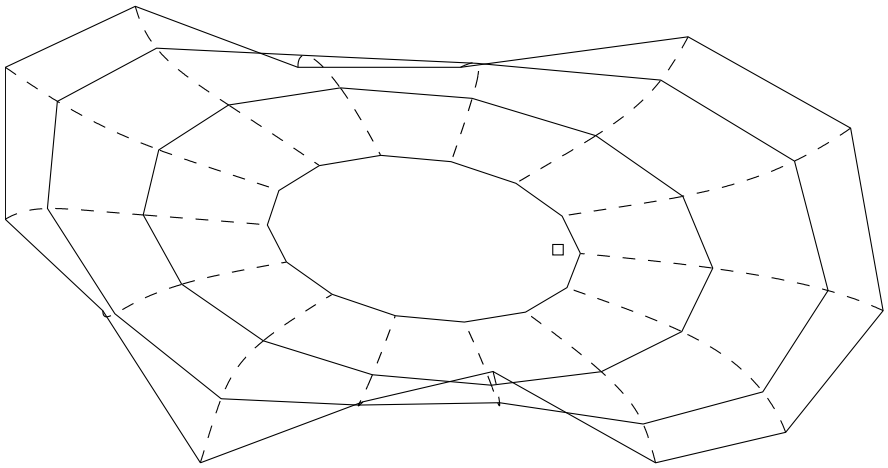

(b) The dashed lines show the path of each volunteer. The solid polygons show the evolution of the region which contains the piece of jewelry as the volunteers tighten their perimeter.

Figure 1.1: Finding the piece of jewelry in the park.

this definition it is clear that the volunteers are agents. A more common example of an agent might be a four-wheeled rover with an onboard computer and an omnidirectional camera. A multi-agent system is then simply a group of agents. Given a desired task for a multi-agent system (such as finding the piece of jewelry), a supervisor must initialize the agents with the information required to complete the task. From this point until task completion the agents are to act without any supervisory intervention. In this sense the agents are autonomous. In addition, the agents attempt to complete the task using only local information. That is, the motion of each agent is based only on quantities that it can compute onboard, such as the relative position of the agents and objects it can sense. In an ideal world the supervisor would not have to provide the agents with any information about their task: They would just do it. Hence, it is desirable to provide the agents with the least amount of information possible before setting them off to complete their task.

Multi-agent systems have an extremely diverse range of possible applications, including search and rescue missions, ocean exploration, land surveying, planetary exploration, and surveillance. It is clear that for many of these applications, the use of robotic agents would be beneficial as it would limit the number of human lives put in danger. What may not initially be as obvious are the advantages of using a multi-agent system over a single agent. However, it is these advantages that provide the truly compelling argument, since a multi-agent system

(i) is inherently robust to failure of single agents,

(ii) can be used to perform distributed sensing tasks,

(iii) can perform a search/explore task more efficiently,

(iv) generally has lower economic cost, and

(v) can achieve a larger range of tasks [28].

Much of the research in the area of multi-agent systems, and in this thesis, has been inspired by these very advantages. Another inspiration is that this research may yield some insight into the social interactions between organisms, such as the way certain organisms travel and collect in swarms. Examples of swarming behavior include schools of fish, flocks of birds, and herds of animals. These groups are all able to achieve an overall group behavior through only local interactions [16]. It is possible that by studying the ways in which global behaviors can be achieved through simple local control strategies in a multi-agent system, we will obtain a better understanding of the way these complex biological systems operate.

1.1 Problem introduction

There have been two approaches to the study of multi-agent systems. The first approach has focused on using artificial intelligence and behavior based techniques to achieve desired group behaviors, for example [17, 29, 42]. These approaches have yielded some very interesting behaviors, but they do not generally admit definite mathematical results [53]. The other approach has been using mathematical analysis to study the behaviors that arise from simple local control strategies. Behaviors which have been studied from this point of view include flocking [51, 52], foraging/searching [27], dispersion/deployment [10], rendezvous [25, 31, 33, 36, 37, 43] (also known as agreement or consensus; in this behavior all agents meet at a common point), and formation stabilization [26, 38, 39, 41, 49, 50] . The local control strategies that are used to achieve these behaviors are generally developed in one of two ways. Either

(i) a local control strategy is known and the interest lies in what global behaviors of the system will emerge; or

(ii) a desired global behavior is known and a local controller is chosen and analyzed in hopes that it will achieve the behavior.

In both cases there are unknowns. In the first, the local control strategy is known, but the global behavior is not, and one hopes that the study will reveal some interesting behavior. In the second case, the global behavior is known, but it is not known whether or not the local control strategy will achieve the desired behavior. In this thesis both approaches are taken. In Chapters 2 and 3 a local control strategy is chosen and the emerging global behavior is studied. In Chapters 4 and 5 a desired global behavior is known and a local controller is chosen to attempt to achieve the global behavior.

The problems addressed in this thesis all have the same structure. We consider n agents lying in the plane. The agents do not know a common direction (i.e., they do not know which way north is) and thus the agents are disoriented. Each agent can sense the position of every other agent, and therefore is equipped with an omnidirectional sensor with a range that is larger than the dimension of its environment. If agent i uses the position of agent j to determine its behavior, we say that agent i has a communication link to agent j. While each agent can see every other agent, we assume that communication comes at a cost, and thus the fewer communication links the better. In addition, each agent is given a unique number from 1 to n. This is the only unique piece of information that each agent possesses, and can be implemented by something as simple as attaching a uniquely colored flag to each agent. The behavior of each agent relative to its neighbours' positions should be identical. That is, one should be able to initialize all the agents with a single local control strategy. The strategy will be defined in terms of some index i. Each agent then simply replaces the index i with its unique number to obtain its strategy. With this problem structure in place, this thesis focuses on solving rendezvous and formation stabilization problems.

1.2 Outline of thesis and contributions

Each chapter of this thesis studies a different problem. At the beginning of each chapter the relevant literature is reviewed and the necessary background material is introduced. All notation is consistent throughout the chapters. The organization is as follows.

In Chapter 2 the rendezvous problem is studied, whereby a group of mobile agents achieves convergence to a common point. A hierarchical cyclic pursuit scheme is introduced, and it is shown that this scheme yields a very significant increase in the rate of convergence to a common point when compared to traditional cyclic pursuit. A second scheme is introduced in which there are more communication links between agents. It is shown that this scheme produces a rate of convergence greater than the traditional scheme but significantly less than the hierarchical scheme.

Contribution of Chapter 2: This chapter marks the introduction of the concept of hierarchy within the sensing structure of a multi-agent system. The strategy developed is the first hierarchical local control strategy in the multi-agent systems literature. Parts of this work originally appeared in [47] by Smith, Broucke, and Francis.

In Chapter 3 the control of a heterogeneous group of agents is explored. Cyclic pursuit is studied for the case of two agents, each with a different kinematic model. It is shown that by varying the gains on the control inputs, different types of formations can be achieved: The agents can spiral into a point, out to infinity, or converge to concentric circles.

Contribution of Chapter 3: This is the first analytical study of a local control strategy for a heterogeneous multi-agent system. A complete global stability analysis is performed for a heterogeneous system consisting of two agents.

In Chapter 4 the problem of adapting curve shortening theory to the multi-agent setting is addressed. Curve shortening theory can be described as follows; If a smooth,

closed, and embedded curve is deformed along its normal vector field at a rate proportional to its curvature, it shrinks to a circular point. This curve evolution is called Euclidean curve shortening and the result is known as the Gage-Hamilton-Grayson Theorem. Motivated by the rendezvous problem in multi-agent systems, the problem of creating a polygon shortening flow is addressed. A simple linear scheme is proposed which exhibits several analogues to Euclidean curve shortening. The polygon shrinks to an elliptical point, convex polygons remain convex, and the perimeter of the polygon is monotonically decreasing.

Contribution of Chapter 4: Inspired by the discrete affine curve shortening scheme in [4], this is the first research to directly relate the theory on curve shortening to multi-agent systems. This theory is used to design a simple local control strategy and to demonstrate some interesting similarities to curve shortening evolution. Parts of this work originally appeared in [46] by Smith, Broucke, and Francis.

In Chapter 5, the problem of stabilizing a group of agents to a formation is analyzed. A novel local control scheme is proposed to stabilize the agents to the vertices of a stationary equilateral polygon. That is, a polygon for which each side has the same length. The centroid of the agents is stationary during the evolution. A full stability analysis is performed for three agents and some interesting results are derived for the general case.

Contribution of Chapter 5: This chapter introduces a local control strategy which stabilizes a group of agents to a novel formation. The agents stabilize to this formation without the use of a common orientation (i.e., a compass).

Finally, in Chapter 6 the thesis is summarized and some areas for future work are outlined.

Chapter 2

Hierarchical cyclic pursuit

In this chapter the *rendezvous problem* is studied whereby a group of mobile agents achieves convergence to a common point. A hierarchical cyclic pursuit scheme is introduced, and it is shown that this scheme yields a very significant increase in the rate of convergence to a common point when compared to traditional cyclic pursuit. A second scheme is introduced in which there are more communication links between vehicles. It is shown that this scheme produces a rate of convergence greater than the traditional scheme but significantly less than the hierarchical scheme.

2.1 Introduction

Much of the current work in multi-agent systems involves the use of simple local control strategies in order to achieve a desired global (or group) behavior. One such behavior is the convergence of a group of agents to a common point. This is a type of *rendezvous problem*, also known as an *agreement* or *consensus problem*. Some recent approaches to solving these types of problems include [25, 31, 33, 36, 37, 46, 43, 51, 52]. As in [4, 31, 46, 51], we assume a fixed topology (i.e., a time-invariant sensor graph). Other references, for example [25, 33, 36, 37, 43, 52], consider dynamic topologies. The approaches in [4, 25, 31] and this paper are based on a strategy called *cyclic pursuit*, which can be

described as follows. A group of n agents, modeled as point masses, are numbered from 1 to n. The position of each of the n agents can be described in the complex plane by the point $z_i = x_i + jy_i$, $i = 1, \ldots, n$, where $j = \sqrt{-1}$. The strategy is for agent i to chase agent $i+1$. The i^{th} agent's velocity points in the direction of agent $i+1$ and the magnitude of the velocity is equal to the distance between agent i and $i+1$. The model for cyclic pursuit is given by

$$\begin{aligned} \dot{z}_i &= z_{i+1} - z_i, \quad i = 1, ..., n-1 \\ \dot{z}_n &= z_1 - z_n. \end{aligned} \tag{2.1}$$

Under this scheme the agents will converge to their stationary centroid.

The scheme above assumes that each agent is equipped with an omnidirectional sensor with an infinite range. Lin et al. [25] consider sensors with a finite range, and directional sensors which can see agents only within some cone of view. Based on these sensor models, control strategies are developed to ensure convergence to a point. Marshall et al. [31] study a similar pursuit strategy but with wheeled vehicles that are subject to a nonholonomic constraint (kinematic unicycles). For models of this type there are two control inputs, namely the forward and angular velocities. The strategy is to pursue the next agent with linear velocity proportional to the distance to the next agent, and angular velocity proportional to the difference between the desired and actual heading. By appropriate choice of gains on the velocities, the vehicles can either spiral in to a point, converge to a circle of some radius, or diverge. These are two examples of the application of local control strategies to achieve a global group behavior. There are many other results, and a more complete review of these can be found in [25] and [31].

Williams et al. [54] study the problem of achieving an overall formation with n groups of homogeneous vehicle formations. In each group there is one leader, which is the only vehicle that can communicate to the other groups. By using a simple linear control law, and by modeling the vehicles as point masses, hierarchical formations, such as groups achieving a common heading, are attained.

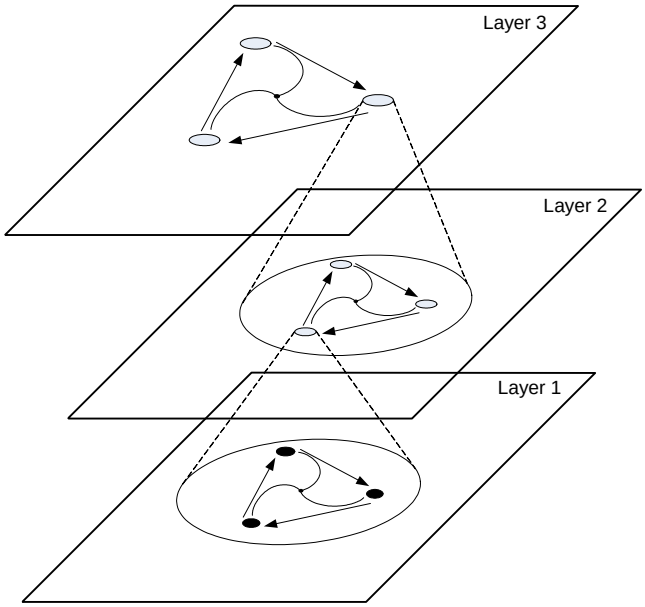

Figure 2.1: Three layers of hierarchy in cyclic pursuit.

In this chapter, the concept of hierarchy is applied to cyclic pursuit. The simplest hierarchical cyclic pursuit scheme, which we call a two layer hierarchical scheme, can be described as follows. A collection of N_2 agents is divided into n_2 groups, each containing n_1 agents ($n_1 \times n_2 = N_2$). The local control strategy is chosen such that the agents within each group are in cyclic pursuit. In addition, the centroid of each group is pursuing the centroid of the next in order (i.e., the centroids are also in cyclic pursuit). This idea can be extended to more layers of hierarchy as shown in Figure 2.1. In Sections 2.4 and 2.5 this discussion will be formalized, and it will be shown that this scheme yields a very significant increase in the rate of convergence of a group of vehicles to their centroid when compared to traditional cyclic pursuit (2.1). The hierarchical scheme requires more communication links between agents than the traditional scheme. Because of this, in Section 2.6 the rate of convergence of the hierarchical scheme is compared to an alternate scheme with an equal number of communication links. It is shown that the hierarchical scheme still yields a significantly greater rate of convergence than this alternate scheme.

2.2 Background in circulant matrices

In order to proceed we require a few mathematical tools. This section gives a summary of the theory of circulant matrices and is based on [12] by Davis.

Consider an n-tuple $(c_1, c_2, \ldots, c_n)$ of real numbers. This n-tuple along with its $n-1$ cyclic permutations can be used to form the rows of

$$C = \begin{bmatrix} c_1 & c_2 & c_3 & \cdots & c_n \\ c_n & c_1 & c_2 & \cdots & c_{n-1} \\ c_{n-1} & c_n & c_1 & \cdots & c_{n-2} \\ \vdots & \vdots & \vdots & \vdots & \vdots \\ c_2 & c_3 & c_4 & \ldots & c_1 \end{bmatrix}. \tag{2.2}$$

This is the general form of a circulant matrix, which can be written more compactly as

$$C =: \operatorname{circ}(c_1, c_2, \ldots, c_n).$$

There is a well-developed theory which gives a structured approach for diagonalizing matrices of this form. Consider the $n \times n$ circulant matrix

$$P = \begin{bmatrix} 0 & 1 & 0 & \cdots & 0 \\ 0 & 0 & 1 & \cdots & 0 \\ \vdots & \vdots & \vdots & \vdots & \vdots \\ 1 & 0 & 0 & \cdots & 0 \end{bmatrix} = \operatorname{circ}(0, 1, 0, \ldots, 0). \tag{2.3}$$

We refer to P as the *permutation matrix*. This matrix has the special property that

$$P^2 = \operatorname{circ}(0, 0, 1, 0, \ldots, 0), \quad P^3 = \operatorname{circ}(0, 0, 0, 1, 0, \ldots, 0),$$

and so on. Because of this, the matrix C can be written as

$$C = c_n P^{n-1} + c_{n-1} P^{n-2} + \cdots + c_2 P + c_1 I.$$

By defining the polynomial

$$q_C(s) = c_n s^{n-1} + c_{n-1} s^{n-2} + \cdots + c_2 s + c_1 s^0,$$

we have that $C = q_C(P)$. In order to determine the eigenvalues of this polynomial we will now introduce a special case of the Spectral Mapping Theorem.

Definition 2.1. The set of all eigenvalues of a matrix A is called the *spectrum* of A and will be written $\text{eigs}(A)$.

Theorem 2.2 (Spectral Mapping Theorem)**.** *For every $n \times n$ matrix A and every polynomial $p(s)$, the spectrum of $p(A)$ is $p(eigs(A))$.*

Based on this theorem, the eigenvalues of C are,

$$\text{eigs}(C) = \{q_C(\lambda) : \lambda \in \text{eigs}(P)\}.$$

Matrix P is in companion form and its characteristic polynomial is $s^n - 1$. The eigenvalues of P are the n^{th} roots of unity:

$$\text{eigs}(P) = \{1, \mathrm{e}^{2\pi j/n}, \mathrm{e}^{4\pi j/n}, \ldots, \mathrm{e}^{2(n-1)\pi j/n}\}.$$

So, if we define $\omega := \mathrm{e}^{2\pi j/n}$ then

$$\text{eigs}(P) = \{1, \omega, \omega^2, \ldots, \omega^{n-1}\}. \tag{2.4}$$

Therefore,

$$\text{eigs}(C) = \left\{q_C(1), q_C(\omega), q_C(\omega^2), \ldots, q_C(\omega^{n-1})\right\}. \tag{2.5}$$

Now we will look at diagonalizing the matrix C. It can easily be seen that normalized eigenvectors of P corresponding to the eigenvalues in (2.4) are given by

$$\frac{1}{\sqrt{n}}\begin{bmatrix}1\\1\\1\\\vdots\\1\end{bmatrix}, \frac{1}{\sqrt{n}}\begin{bmatrix}1\\\omega\\\omega^2\\\vdots\\\omega^{n-1}\end{bmatrix}, \frac{1}{\sqrt{n}}\begin{bmatrix}1\\\omega^2\\\omega^4\\\vdots\\\omega^{2(n-1)}\end{bmatrix}, \cdots, \frac{1}{\sqrt{n}}\begin{bmatrix}1\\\omega^{n-1}\\\omega^{2(n-1)}\\\vdots\\\omega^{(n-1)(n-1)}\end{bmatrix}.$$

Therefore, by defining the matrices consisting of the eigenvalues and eigenvectors as

$$\Omega = \begin{bmatrix} 1 & 0 & \cdots & 0 \\ 0 & \omega & \cdots & 0 \\ \vdots & & \ddots & \vdots \\ 0 & \cdots & 0 & \omega^{n-1} \end{bmatrix} \quad \text{and} \quad F = \frac{1}{\sqrt{n}} \begin{bmatrix} 1 & 1 & \cdots & 1 \\ 1 & \omega & \cdots & \omega^{n-1} \\ \vdots & \vdots & \vdots & \vdots \\ 1 & \omega^{n-1} & \cdots & \omega^{(n-1)(n-1)} \end{bmatrix},$$

we get

$$PF = F\Omega \quad \text{or} \quad P = F\Omega F^*,$$

where * represents the complex conjugate transpose. By pre-multiplying $PF = F\Omega$ by P we see that $P^2F = F\Omega^2$ from which it follows that $P^3F = F\Omega^3$, $P^4F = F\Omega^4$, and so on. Since

$$C = c_n P^{n-1} + c_{n-1}P^{n-2} + \cdots + c_2 P + c_1 I,$$

we have that $CF = Fq_C(\Omega)$ or $C = F\Lambda F^*$, where Λ is the diagonal matrix taking the form

$$\Lambda := q_C(\Omega) = \begin{bmatrix} q_C(1) & 0 & \cdots & 0 \\ 0 & q_C(\omega) & \cdots & 0 \\ \vdots & & \ddots & \vdots \\ 0 & \cdots & 0 & q_C(\omega^{n-1}) \end{bmatrix}.$$

In this manner all circulant matrices can be diagonalized to reveal their eigenvalues.

2.2.1 Block circulant matrices

To extend this concept to block circulant matrices we introduce an operation between two matrices called the Kronecker product. The Kronecker product, $\otimes$, between an $n \times m$ matrix A, and a matrix B, is defined as

$$A \otimes B = \begin{bmatrix} a_{11}B & \cdots & a_{1m}B \\ \vdots & & \vdots \\ a_{n1}B & \cdots & a_{nm}B \end{bmatrix}.$$

In other words, the Kronecker product replaces the ij^{th} element of A by the block $a_{ij}B$. The eigenvalues of $A \otimes B$ are given by all possible products of the eigenvalues of A and B.

Now consider the matrix (2.2) but with each real number entry replaced by an $m \times m$ matrix D_i:

$$D = \begin{bmatrix} D_1 & D_2 & D_3 & \cdots & D_n \\ D_n & D_1 & D_2 & \cdots & D_{n-1} \\ D_{n-1} & D_n & D_1 & \cdots & D_{n-2} \\ \vdots & \vdots & \vdots & \vdots & \vdots \\ D_2 & D_3 & D_4 & \dots & D_1 \end{bmatrix} = \text{circ}(D_1, D_2, \dots, D_n).$$

The matrix D is of dimension $nm \times nm$ and has a block circulant form. This matrix can be written in terms of the $n \times n$ circulant matrix P as

$$D = P^{n-1} \otimes D_n + P^{n-2} \otimes D_{n-1} + \cdots + P \otimes D_2 + I \otimes D_1.$$

The matrix D can be block diagonalized using F from above, as follows:

$$\Lambda := (F \otimes I_m)^* D (F \otimes I_m).$$

Here I_m is the $m \times m$ identity matrix. It can be shown that the block diagonal matrix Λ has the following entries along its diagonal:

$$\begin{aligned} &D_1 + D_2 + D_3 + \cdots + D_n \\ &D_1 + \omega D_2 + \omega^2 D_3 + \cdots + \omega^{n-1} D_n \\ &\qquad \vdots \\ &D_1 + \omega^{n-1} D_2 + \omega^{2(n-1)} D_3 + \cdots + \omega^{(n-1)(n-1)} D_n. \end{aligned} \tag{2.6}$$

Therefore, if $D_1, \dots, D_n$ are circulant matrices, the expressions in (2.6) can be combined with the expression for the eigenvalues of a circulant matrix in (2.5) to obtain the eigenvalues of a block circulant matrix.

2.3 Traditional cyclic pursuit

Consider n agents, modeled as point masses, numbered from 1 to n, and performing cyclic pursuit as described by (2.1). This system can be written in vector form as

$$\dot{z} = A_1 z, \tag{2.7}$$

where $A_1 = \text{circ}(-1, 1, 0, \ldots, 0)$. The matrix A_1 can also be written as $A_1 = P - I$, where P is given in (2.3). The eigenvalues of P are the n^{th} roots of unity; thus, the eigenvalues of A_1 are the n^{th} roots of unity shifted left by one. The following theorem describes two main properties of cyclic pursuit.

Theorem 2.3 (Bruckstein et al. [4])**.** *Consider the cyclic pursuit scheme in* (2.7)*. For every initial condition, the centroid of the agents $z_1(t), \ldots, z_n(t)$ is stationary and every $z_i(t)$ converges to this centroid.*

Proof. We include a proof of this theorem as it helps to demonstrate the properties of cyclic pursuit. The eigenvector for the zero eigenvalue of A_1 satisfies

$$A_1 v = 0 \text{ or } Pv = v,$$

so all of v's components are equal. For simplicity take them all to be 1. Denote the corresponding one-dimensional eigenspace as $\mathcal{E}_0$. Let $\mathcal{E}_1$ denote the sum of all the other eigenspaces. Let λ be a nonzero eigenvalue, and $w \in \mathcal{E}_1$ be a corresponding eigenvector. So we have

$$A_1 w = \lambda w$$

$$Pw = w + \lambda w.$$

Pre-multiplying by v^T and using the fact that $v^T P = v^T$ we get,

$$v^T w = v^T w + \lambda v^T w.$$

Therefore $v^T w = 0$ and thus $\mathcal{E}_0$ and $\mathcal{E}_1$ are orthogonal eigenspaces.

We will now use this result to show that the agents converge to their stationary centroid. Consider $\dot{z} = A_1 z$. The initial condition can be written in terms of the orthogonal eigenspaces as

$$z(0) = \tilde{z}v + w(0),$$

where $\tilde{z}$ is a constant and so $\tilde{z}v \in \mathcal{E}_0$ and $w(0) \in \mathcal{E}_1$. Pre-multiplying this expression by v^T and using the fact that $v^T w(0) = 0$ and $v^T v = n$, we get that

$$v^T z(0) = \tilde{z} v^T v + v^T w(0) = \tilde{z} n.$$

Hence, $\tilde{z} = (z_1(0) + \cdots + z_n(0))/n$ is the centroid of the agents' initial positions. The trajectories of the system can be written as

$$z(t) = \tilde{z}v + w(t)$$

since the eigenvalue associated with v is the zero eigenvalue. Pre-multiplying by v^T again we see that

$$v^T z(t) = \tilde{z} n,$$

which implies that the centroid of the agents, $z_1(t), \ldots, z_n(t)$, is stationary. Finally, $w(t) \to 0$ since $w(t) \in \mathcal{E}_1$ and all the eigenvalues of $\mathcal{E}_1$ are in the open left half-plane. Therefore, we have $z(t) \to \tilde{z}v$ so every agent converges to the centroid $\tilde{z}$. □

Note that the rate of convergence of the agents to the centroid $\tilde{z}$ will be determined by the nonzero eigenvalue with the smallest absolute real part.

Now consider the situation where each agent follows a displacement of the next agent:

$$\dot{z}_i = (z_{i+1} + d_i) - z_i, \quad i = 1, ..., n-1$$
$$\dot{z}_n = (z_1 + d_n) - z_n.$$

In vector form, this can be written as

$$\dot{z} = A_1 z + d.$$

Pre-multiplying by v^T we obtain

$$v^T \dot{z} = v^T A_1 z + v^T d$$
$$v^T \dot{z} = v^T d.$$

Since v is a vector of 1's we get that

$$\sum_{i=1}^{n} \dot{z}_i = \sum_{i=1}^{n} d_i. \tag{2.8}$$

If we denote the centroid of the agents as $\tilde{z}$, (2.8) becomes

$$\dot{\tilde{z}} = \frac{1}{n} \sum_{i=1}^{n} d_i. \tag{2.9}$$

This implies that we can control the centroid of a group of agents using the d_i's. By properly selecting the d_i's we can create hierarchy within cyclic pursuit.

2.4 Two layer hierarchy

We will start by looking at the two layer hierarchical scheme, as described in Section 2.1, where N_2 agents are divided into n_2 groups of n_1 agents ($n_1 \times n_2 = N_2$). Each agent will be described by the subscripts $z_{p,q}$ where $p = 1, \ldots, n_2$ is the group index, and $q = 1, \ldots, n_1$ is the agent index. Therefore, the two layer hierarchy system can be

written as,

$$\text{group } 1 \left\{ \begin{array}{l} \dot{z}_{1,1} = z_{1,2} - z_{1,1} + d_{1,1} \\ \dot{z}_{1,2} = z_{1,3} - z_{1,2} + d_{1,2} \\ \quad \vdots \\ \dot{z}_{1,n_1} = z_{1,1} - z_{1,n_1} + d_{1,n_1} \end{array} \right\}$$
$$\vdots \tag{2.10}$$
$$\text{group } n \left\{ \begin{array}{l} \dot{z}_{n_2,1} = z_{n_2,2} - z_{n_2,1} + d_{n_2,1} \\ \dot{z}_{n_2,2} = z_{n_2,3} - z_{n_2,2} + d_{n_2,2} \\ \quad \vdots \\ \dot{z}_{n_2,n_1} = z_{n_2,1} - z_{n_2,n_1} + d_{n_2,n_1}. \end{array} \right\}$$

where the $d_{p,q}$'s are the displacements. We require the centroids of the groups to be in cyclic pursuit. Therefore, the desired equations of motion for the centroids of each group are

$$\begin{aligned} \dot{\tilde{z}}_p &= \tilde{z}_{p+1} - \tilde{z}_p, \quad p = 1, \ldots, n_2 - 1 \\ \dot{\tilde{z}}_{n_2} &= \tilde{z}_1 - \tilde{z}_{n_2}, \end{aligned} \tag{2.11}$$

where the centroid of the p^{th} group is defined as

$$\tilde{z}_p := \frac{1}{n_1} \sum_{q=1}^{n_1} z_{p,q}.$$

The question is how to choose the displacements, $d_{p,q}$'s, to achieve this motion in the centroids. From (2.9), the dynamics of group p's centroid is

$$\dot{\tilde{z}}_p = \frac{1}{n_1} \sum_{q=1}^{n_1} d_{p,q}.$$

Combining this with (2.11) we get that

$$\sum_{q=1}^{n_1} d_{p,q} = n_1(\tilde{z}_{p+1} - \tilde{z}_p). \tag{2.12}$$

Looking at (2.12) and summing over all of the $d_{p,q}$'s we can see that

$$\sum_{p=1}^{n_2} \sum_{q=1}^{n_1} d_{p,q} = n_1 \sum_{p=1}^{n_2} \dot{\tilde{z}}_p = 0,$$

and therefore the centroid of the N_2 agents is stationary.

Several different $d_{p,q}$'s can be chosen that will satisfy (2.12). One such choice is

$$d_{p,q} = z_{p+1,q} - z_{p,q}. \tag{2.13}$$

This means that the q^{th} agent in the p^{th} group chases the q^{th} agent in the $(p+1)^{th}$ group. By substituting the expression for the $d_{p,q}$'s into (2.10) it can be seen that each agent has a communication link to two other agents ($z_{p+1,q}$ and $z_{p,q+1}$). Therefore, with this scheme, there is a total of $2N_2$ communication links. This system can be further examined by looking at the vector form

$$\dot{z} = Bz + Dz,$$

where B is the block diagonal matrix describing the cyclic pursuit within the groups, and is given by

$$B = \text{diag}(A_1, \ldots, A_1), \ (n_2 \text{ blocks}),$$

and $A_1 = (P - I)_{n_1 \times n_1}$ as in (2.7). The eigenvalues of B are n_2 sets of the n_1^{th} roots of unity, shifted left by 1. The matrix D represents the $d_{p,q}$'s and has the form

$$\begin{aligned} D &= \text{circ}(-1, 1, 0, \ldots, 0)_{n_2 \times n_2} \otimes I_{n_1} \\ &= (P - I)_{n_2 \times n_2} \otimes I_{n_1}. \end{aligned} \tag{2.14}$$

The matrix $I_{n_1} =: S$ in (2.14) represents the sensor connections of each agent in one group to the agents in the next group. A '1' in the fg^{th} position of the S matrix, $f, g = 1, \ldots, n_1$, indicates that the f^{th} agent in each group senses the g^{th} agent in the next group (modulo n_2). Therefore, $S = I$ indicates that the f^{th} agent of each group sees the f^{th} agent in the next group.

If we compute $A_2 := B + D$, it has the block circulant structure (with each block being of size $n_1 \times n_1$)

$$A_2 = \text{circ}(A_1 - I, I, 0, \ldots, 0)_{N_2 \times N_2}. \tag{2.15}$$

This matrix can be block diagonalized to obtain the following matrices along the diagonal:

$$(A_1 - I) + \omega^{r-1} I, \quad r = 1, \ldots, n_2,$$

where $\omega = \mathrm{e}^{2\pi j/n_2}$. The eigenvalues of A_2 are the union of the eigenvalues of these matrices. That is, we have n_2 sets of n_1 eigenvalues, the r^{th} set being comprised of the eigenvalues of A_1 shifted by $\omega^{r-1} - 1$. This can be written more compactly as

$$\mathrm{eigs}(A_2) = \bigcup_{r=1}^{n_2} \mathrm{eigs}\left(A_1 + (\mathrm{e}^{2\pi j(r-1)/n_2} - 1)I\right). \tag{2.16}$$

Example 2.4 (Nine agents with two layers of hierarchy)**.** Consider 9 agents which are split into 3 groups, each containing 3 agents. In the notation introduced above, this can be written as $n_1 = n_2 = 3$, giving a total of $n_1 n_2 = N_2 = 9$ agents. The matrix A_1 is

$$A_1 = \begin{bmatrix} -1 & 1 & 0 \\ 0 & -1 & 1 \\ 1 & 0 & -1 \end{bmatrix} = \mathrm{circ}(-1, 1, 0).$$

From (2.15) we have

$$A_2 = \mathrm{circ}(A_1 - I, I, 0, \ldots, 0) = \mathrm{circ}(-2, 1, 0, 1, 0, 0, 0, 0, 0)$$

The trajectories generated by the nine agents are shown in Figure 2.2 for initial conditions equally spaced around a circle.

2.4.1 Rate of convergence to the centroid

By examining (2.16) it can be seen that A_2 has one eigenvalue at zero and all others lie in the open left half-plane. The matrices on the right hand side of (2.16) are circulant, thus when A_2 is block diagonalized, each block is circulant. But since the blocks are circulant, they can be further diagonalized, thereby fully diagonalizing A_2. Therefore, the zero eigenvalue of A_2 dictates that the agents converge to their centroid rather than to the origin. The rate of convergence of the agents to their centroid is determined by

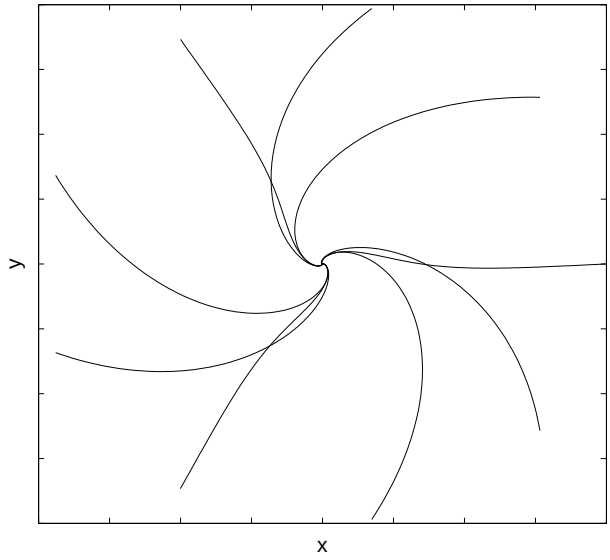

Figure 2.2: Trajectories of nine agents in a two layer hierarchy scheme with $n_1 = n_2 = 3$.

the nonzero eigenvalue of A_2 with the smallest absolute real part. In order to simplify the subsequent discussion the following definition is introduced.

Definition 2.5. The *γ-value* of a set of eigenvalues, which lie in the left half-plane, is the nonzero eigenvalue with the smallest absolute real part.

The eigenvalues of A_1 are the n_1^{th} roots of unity shifted left by one and can be written as

$$\lambda_p = \mathrm{e}^{2\pi j(p-1)/n_1}, \quad p = 1, \ldots, n_1.$$

If we define $\sigma_2(r) := \mathrm{e}^{2\pi j(r-1)/n_2} - 1$, the real part takes values in the range

$$-2 \leq \Re(\sigma_2(r)) \leq 0, \quad \forall r = 1, \ldots, n_2, \tag{2.17}$$

and (2.16) can be written as

$$\mathrm{eigs}(A_2) = \bigcup_{r=1}^{n_2} \mathrm{eigs}\left(A_1 + \sigma_2(r) I\right).$$

Now, looking for the γ-value of A_2, we know from (2.17) that $\sigma_2(r)I$ shifts the r^{th} set of eigenvalues of A_1 to the left by some amount between 0 and 2. In order to find the γ-value

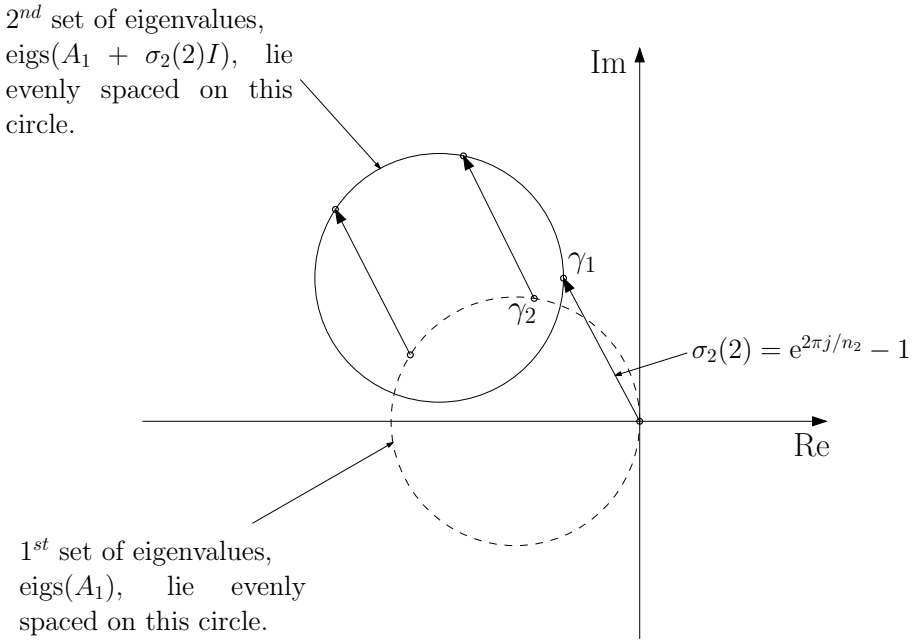

Figure 2.3: Finding the γ-value of A_2. The shift of $\sigma_2(2)$ as well as γ_1 and γ_2 are shown.

of A_2 we need to find the set of eigenvalues which is shifted by the smallest amount to the left, and then we need to find the γ-value of that set.

The set of eigenvalues of A_1 that is not shifted at all is the first ($r = 1$) set which has the shift $\sigma_2(1) = 0$. The eigenvalues of this set are simply the eigenvalues of A_1. The rightmost eigenvalue of A_1 lies at zero ($\lambda_1 = 0$), and thus the next eigenvalue to the left of 0 provides the γ-value, which is $\lambda_2 = e^{2\pi j/n_1} - 1 =: \gamma_1$ (or equivalently λ_{n_1}). The eigenvalues of A_1 are shown in Figure 2.4.

The set of eigenvalues that is shifted to the left by the next smallest amount is given by $\sigma_2(2)$ (or equivalently $\sigma_2(n_2 - 1)$). The rightmost eigenvalue of this set is given by

$$\lambda_1 + \sigma_2(2) = 0 + e^{2\pi j/n_2} - 1,$$

as shown in Figure 2.3. This eigenvalue is nonzero and is therefore the γ-value of the set:

$$\gamma_2 := e^{2\pi j/n_2} - 1.$$

Both γ_1 and γ_2 are shown in Figure 2.5 and the process of finding the γ-value is shown

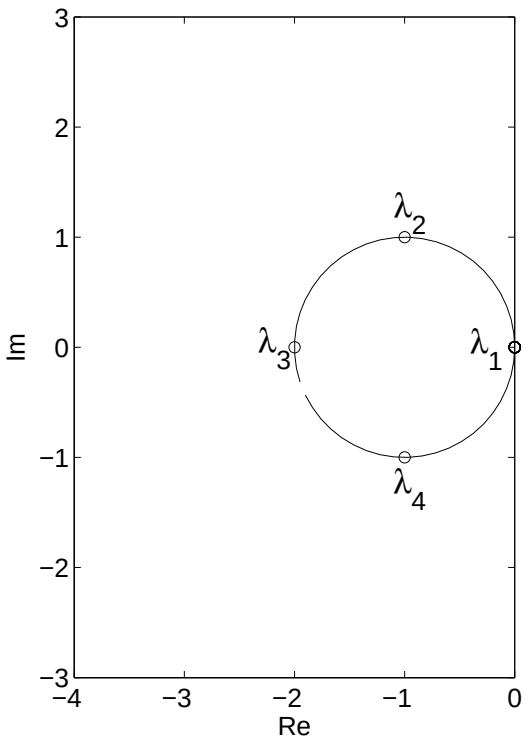

Figure 2.4: The eigenvalues of A_1 for $n_1 = 4$, showing $\lambda_1, \ldots, \lambda_4$.

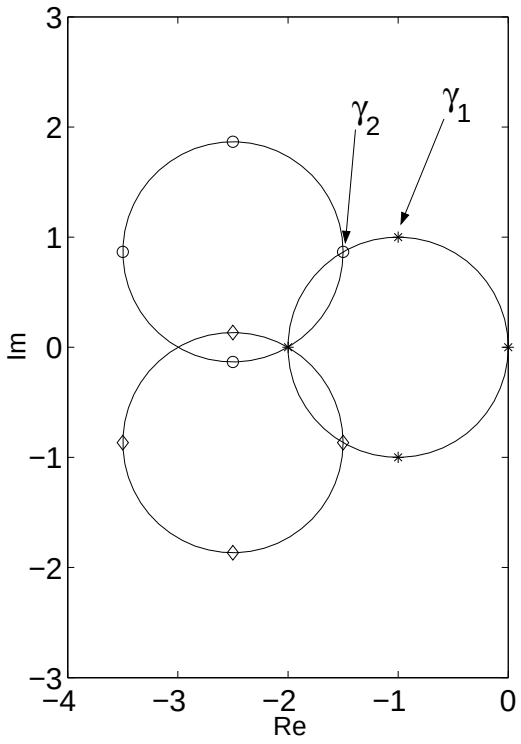

Figure 2.5: Eigenvalue structure for $n_1 = 4$, and $n_2 = 3$ showing γ_1 and γ_2

in Figure 2.3.

The question arises as to which eigenvalue has a smaller absolute real part: γ_1, or γ_2? We have

$$\gamma_1 = \mathrm{e}^{2\pi j/n_1} - 1$$
$$\Re(\gamma_1) = \cos(2\pi/n_1) - 1$$

and,

$$\gamma_2 = \mathrm{e}^{2\pi j/n_2} - 1$$
$$\Re(\gamma_2) = \cos(2\pi/n_2) - 1.$$

Therefore, the γ-value is given by γ_1 if $n_1 \geq n_2$, and by γ_2 if $n_1 \leq n_2$. The real part of

the γ-value of A_2 can be written as

$$\chi := \cos(2\pi/w) - 1, \tag{2.18}$$

where

$$w = \max\{n_1, n_2\}. \tag{2.19}$$

In comparing the real part of the γ-value for the two cyclic pursuit schemes, hierarchical and traditional, we get that the increase in the rate of convergence to the centroid when using hierarchical cyclic pursuit is

$$\frac{\text{hierarchical}}{\text{traditional}} = \frac{\cos(2\pi/w) - 1}{\cos(2\pi/N_2) - 1}.$$

Expanding the cos terms to the first order and using the fact that $N_2 = n_1 \times n_2$, and $w = \max\{n_1, n_2\}$, we arrive at the following theorem.

Theorem 2.6 (Two layers of hierarchy)**.** *Suppose we have two layers of hierarchy in cyclic pursuit, where N_2 agents are divided into n_2 groups, with each group containing n_1 agents. Then the increase in the rate of convergence of the two layer hierarchy scheme, when compared to traditional cyclic pursuit, is approximated by*

$$R := \frac{\textit{hierarchical}}{\textit{traditional}} \approx \min\{n_1, n_2\}^2 =: R_2. \tag{2.20}$$

As the total number of agents becomes large ($N_2 \to \infty$), $R/R_2 \to 1$.

Thus in the special case where $n_1 = n_2 = \sqrt{N_2}$, the N_2 agents will converge to their centroid approximately N_2 times faster using the hierarchy scheme than using traditional cyclic pursuit.

2.5 The generalized scheme

In the most general setting, we have L layers of hierarchy (in the previous section we had two layers). We call the layer consisting of n_1 agents the first layer. The second layer

then consists of n_2 subgroups of n_1 agents, the third layer, n_3 groups of n_2 subgroups of n_1 agents, and so on. In total we have N_L agents, where

$$\prod_{m=1}^{L} n_m = N_L.$$

The system can be written in the form

$$\dot{z} = A_L z, \tag{2.21}$$

where z is a column vector of length N_L, and A_L is an N_L by N_L matrix. For $L = 1$, we have $N_L = N_1 = n_1$ and the A_1 matrix is $A_1 = (P - I)_{n_1 \times n_1}$. Each time we add a new layer we would like the behavior in the layer below to remain the same. For example, with one layer, we have traditional cyclic pursuit. When we add another layer and have several groups, we would still like the agents within each individual group to be in cyclic pursuit. We then add sensor connections between each of the groups to achieve cyclic pursuit at the new level (between the centroids of the groups). In looking at the A_2 matrix in (2.15) this becomes evident. The A_1 matrices along the diagonal represent the cyclic pursuit within each group. The I's along the off-diagonal and $-I$'s along the diagonal represent the sensor connections between groups to create the new layer of hierarchy; each agent in a group takes the position of an agent in the next group, minus its own position (as described in (2.13)), to create the new layer.

Lemma 2.7. *An L-layer hierarchy scheme can be put into the form of* (2.21). *The matrix A_L is given by the recursive expression*

$$\begin{aligned} A_1 &= \text{circ}(-1, 1, 0, \ldots, 0) \\ A_m &= \text{circ}(A_{m-1} - I, I, 0, \ldots, 0), \quad m = 2, \ldots, L \end{aligned} \tag{2.22}$$

where A_m is composed of n_m blocks of dimension $N_{m-1} \times N_{m-1}$.

Notice that in order to add a layer of hierarchy, each agent must have an additional communication link to another agent. This is described by the off-diagonal identity

matrices in (2.22). Therefore, if the total number of agents in an L-layer hierarchy scheme is N_L, the total number of communication links in the system is LN_L.

The matrix A_m is block circulant and the eigenvalues are given by

$$\text{eigs}(A_m) = \bigcup_{r=1}^{n_m} \text{eigs}\left(A_{m-1} + (\mathrm{e}^{2\pi j(r-1)/n_m} - 1)I\right).$$

So, the eigenvalues of A_m are n_m sets of the eigenvalues of A_{m-1}, with the r^{th} set of eigenvalues shifted by $\sigma_m(r) := \mathrm{e}^{2\pi j(r-1)/n_m} - 1$. In examining the expression for $\sigma_m(r)$, it can be seen that all n_m sets of eigenvalues are shifted to the left by some amount between 0 and 2 since,

$$-2 \leq \Re(\sigma_m(r)) \leq 0 \quad \forall r = 1, \ldots, n_m.$$

In order to find the rate of convergence to the centroid we need to determine all the possible γ-values of eigs(A_m). These γ-values will come from the sets of eigenvalues with the smallest leftward shift. The first set of eigenvalues of A_m are simply the eigenvalues of A_{m-1} shifted by $\sigma_m(1) = 0$. Therefore, the possible γ-values of this set are the γ-values of eigs(A_{m-1}).

The set of eigenvalues with the next smallest leftward shift is given by $A_{m-1}+\sigma_m(2)I$, (or equivalently $A_{m-1}+\sigma_m(n_m)I$), as is shown in Figure 2.3 for the case of $m = 2$. In this set, the zero eigenvalue of A_{m-1} (which is the rightmost eigenvalue of A_{m-1}) is shifted to $\sigma_m(2)$. Thus, this is the γ-value of this set and is given by

$$\gamma_m := \mathrm{e}^{2\pi j/n_m} - 1.$$

The γ-value of eigs(A_m) must be either the γ-value of eigs(A_{m-1}) or γ_m. Therefore, this is a recursive scheme. For each additional layer, another eigenvalue is added to the set of possible γ-values (this additional eigenvalue is γ_m which corresponds to the set shifted by $\sigma_m(2)$). This is shown in Figure 2.6.

As an example, for eigs(A_1) the γ-value is given by

$$\gamma_1 := e^{2\pi j/n_1} - 1.$$

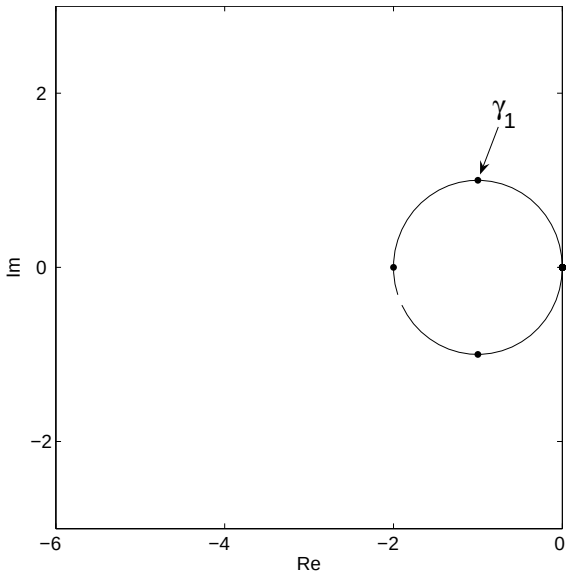

(a) The eigenvalues of A_1.

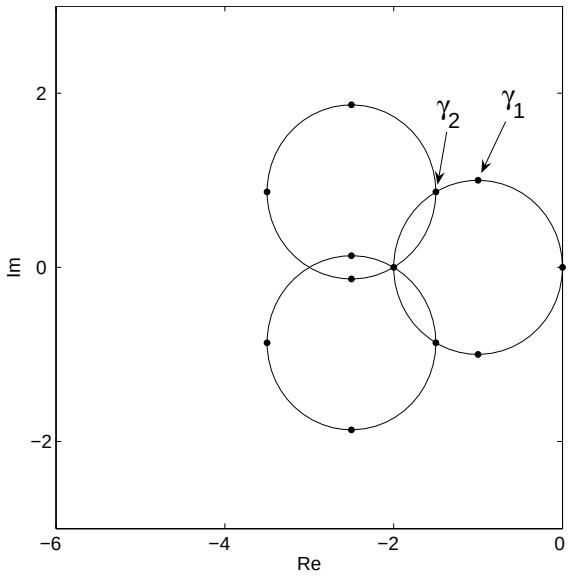

(b) The eigenvalues of A_2.

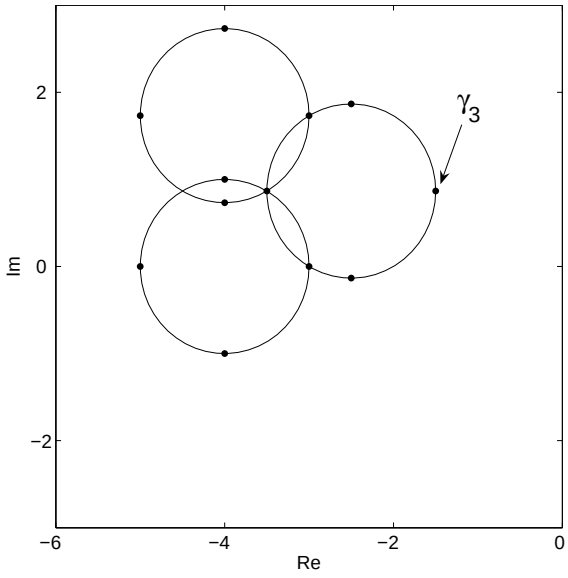

(c) The eigenvalues of A_2 shifted by $\sigma_3(2) = e^{2\pi j/3} - 1$.

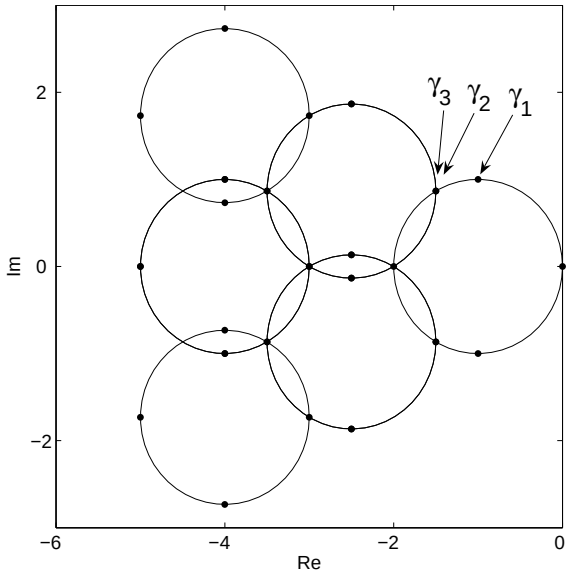

(d) The eigenvalues of A_3.

Figure 2.6: Determining the possible γ-values for eigs(A_3). For this distribution of agents, $n_3 = 3$ groups of $n_2 = 3$ subgroups of $n_1 = 4$ agents (total of 36 agents) the γ-value is γ_1.

The γ-value of eigs(A_2) is either the γ-value of eigs(A_1), which is γ_1, or

$$\gamma_2 := e^{2\pi j/n_2} - 1.$$

The γ-value of eigs(A_3) is either one of the possible γ-values of eigs(A_2), namely γ_1 or γ_2, or

$$\gamma_3 := e^{2\pi j/n_3} - 1.$$

For eigs(A_m), the γ-value is given by

$$\gamma := \mathrm{e}^{2\pi j/w} - 1 \qquad w = \max_m\{n_m\}, \quad m = 1, \ldots, L.$$

The increase in rate of convergence over the traditional cyclic pursuit is given by

$$R = \frac{\text{hierarchical}}{\text{traditional}} = \frac{\Re\left(\mathrm{e}^{2\pi j/w} - 1\right)}{\Re\left(\mathrm{e}^{2\pi j/N_L} - 1\right)} = \frac{\cos(2\pi/w) - 1}{\cos(2\pi/N_L) - 1}.$$

Expanding the cos terms to the first order we obtain the following result.

Theorem 2.8 (L layers of hierarchy)**.** *Consider a group of N_L agents, divided into L layers of hierarchy. The increase in the rate of convergence of the L-layer hierarchy scheme when compared to traditional cyclic pursuit is approximated by*

$$R \approx \left(\frac{N_L}{\max_m\{n_m\}}\right)^2 =: R_L. \tag{2.23}$$

As the number of agents becomes very large ($N_L \to \infty$), $R/R_L \to 1$.

In order to determine the distribution of agents in a hierarchy which results in the highest rate of convergence we introduce the following definition.

Definition 2.9. A distribution of n_m's satisfying $\prod_{m=1}^{L} n_m = N_L$ which yields the highest rate of convergence is an *optimal distribution.*

Theorem 2.10. *In the case where $\sqrt[L]{N_L}$ is an integer, the uniform distribution of n_m's*

$$n_1 = n_2 = \cdots = n_L = \sqrt[L]{N_L}, \tag{2.24}$$

which yields an increase in the rate of convergence of

$$R_L = N_L^{2(L-1)/L}, \tag{2.25}$$

is an optimal distribution. Moreover, it is the only optimal distribution.

Proof. First we show that distribution (2.24) is optimal. Since the numerator of (2.23) is a constant, the highest rate of convergence is obtained when the denominator is minimized. Therefore, an optimal distribution is one which minimizes the maximum n_m. Suppose there exists a distribution which yields a rate of convergence greater than (2.25). This implies there exists a distribution $\{n_m\}$, $m = 1, \ldots, L$, such that

$$\max_m\{n_m\} =: M < \sqrt[L]{N_L} \quad \text{and} \quad \prod_{m=1}^{L} n_m = N_L.$$

Thus, $M \geq n_m$ for all m. But then $M^L \geq \prod_{m=1}^{L} n_m = N_L$ which is a contradiction, since we assumed $M < \sqrt[L]{N_L}$. Therefore $\max_m\{n_m\} \geq \sqrt[L]{N_L}$ and

$$R_L \leq N_L^{2(L-1)/L}$$

for all distributions, and thus (2.24) is an optimal distribution.

Now suppose a distribution which is not identical to (2.24) is also optimal. This implies there exists a distribution, $\{n_m\}$, $m = 1, \ldots, L$, where $n_{m_1} > n_{m_2}$ for some $m_1, m_2 \in \{1, \ldots, L\}$, such that

$$\max_m\{n_m\} = M = \sqrt[L]{N_L} \quad \text{and} \quad \prod_{m=1}^{L} n_m = N_L.$$

Thus, $M \geq n_m$ for all m, with $M > n_{m_2}$. But then $M^L > \prod_{m=1}^{L} n_m = N_L$, which is a contradiction since we assumed $M \leq \sqrt[L]{N_L}$. Therefore, for any distribution not identical to (2.24), $\max_m\{n_m\} > \sqrt[L]{N_L}$, and

$$R_L < N_L^{2(L-1)/L},$$

which is not optimal. Therefore, (2.24) is the optimal distribution. □

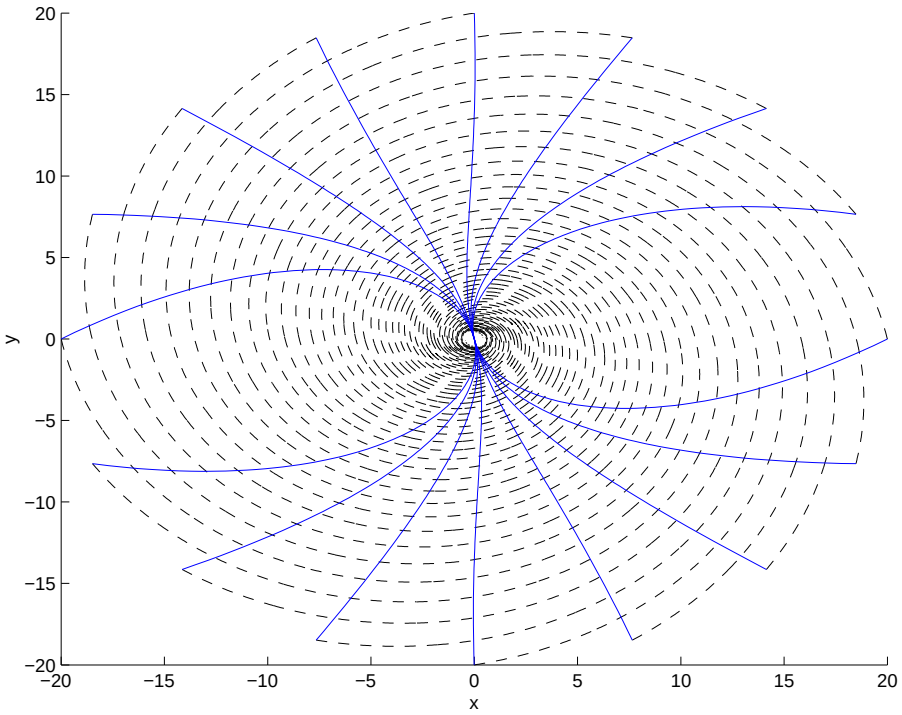

Figure 2.7: Trajectories for 16 agents in traditional cyclic pursuit (dashed line) and 16 agents with 4 layers of hierarchy (solid line).

When $\sqrt[L]{N_L}$ is not an integer there may be multiple optimal distributions. For example, if $N_L = 12$ and $L = 2$, there are two optimal distributions, $\{n_1, n_2\} = \{3, 4\}$ and $\{n_1, n_2\} = \{4, 3\}$, since they both yield the highest rate of convergence.

In Figure 2.7 trajectories are shown for 16 agents in traditional cyclic pursuit and 16 agents with $L = 4$ ($n_1 = n_2 = n_3 = n_4 = 2$).

2.6 A new comparison

We have obtained a significant increase in the rate of convergence of a group of agents to the centroid when comparing hierarchical cyclic pursuit to the traditional cyclic pursuit scheme. However, the hierarchical scheme has more communication; each agent sees more than one other agent, whereas in the traditional scheme each agent only sees one other

agent. Because of this, a rate of convergence comparison will now be performed between the hierarchy scheme and a scheme in which each agent chases the centroid of a group of agents.

In an L-layer hierarchy scheme, each agent has a communication link to L other agents. If there is a total of N_L agents, then the entire system consists of LN_L communication links. Now, consider another scheme involving a group of N_L agents. The strategy in this scheme is that agent i chases the centroid of agents $i+1$ to $i+L$ modulo N_L. This can be written as

$$\dot{z}_i = \frac{1}{L}\sum_{m=1}^{L} z_{i+m \pmod{N_L}} - z_i \quad i = 1, \ldots, N_L. \tag{2.26}$$

This scheme has the same number of total communication links as an L layer hierarchy scheme (i.e., there is a total of LN_L communication links). The system (2.26) can be written in the vector form as

$$\dot{z} = Az,$$

where A is the circulant matrix given by

$$A = \frac{1}{L}\text{circ}(-L, \underbrace{1, \ldots, 1}_{L \text{ ones}}, 0, \ldots, 0).$$

Matrix A can be written in terms of the matrix P and the polynomial

$$q_C(s) = \frac{1}{L}s^L + \frac{1}{L}s^{L-1} + \cdots + \frac{1}{L}s - s^0,$$

as $A = q_C(P)$. The eigenvalues of A are given by

$$\text{eigs}(A) = \{q_C(1), q_C(\omega), q_C(\omega^2), \ldots, q_C(\omega^{N_L-1})\},$$

where $\omega = \mathrm{e}^{2\pi j/N_L}$.

Lemma 2.11. *The matrix A has one eigenvalue at zero, $q_C(1)$, and all others lie in the open left half-plane. If N_L is sufficiently large when compared to L, the γ-value of* $\text{eigs}(A)$ *is given by $\gamma := q_C(\omega)$.*

The reason for the condition that N_L be sufficiently large in comparison to L can be better understood by looking at Figure 2.8. In Figures 2.8(a) and 2.8(b) the rightmost nonzero eigenvalue is clearly given by γ, which is the first eigenvalue arrived upon when following the curve counterclockwise from the zero eigenvalue. However, when looking at Figure 2.8(c) all four nonzero eigenvalues have same real part, and in Figure 2.8(d), γ is no longer the rightmost nonzero eigenvalue. Therefore, only when N_L is sufficiently large in comparison to L, will γ be the γ-value. However, when performing the comparison between this scheme and the hierarchical scheme it is the limiting case when $N_L \to \infty$ that is of interest and in this case it is clear that the γ-value of eigs(A) is given by γ.

Now to compare the rate of convergence of this scheme with the hierarchical scheme we have

$$q_C(\omega) = \frac{1}{L}\left(\omega + \omega^2 + \ldots + \omega^L\right) - 1 = \frac{1}{L}\sum_{m=1}^{L} e^{2\pi j m/N_L} - 1$$

The real part of γ can be written as

$$\Re(\gamma) = \frac{1}{L}\sum_{m=1}^{L}\left(\cos(2m\pi/N_L)\right) - 1,$$

If we call this new scheme "L-link", then comparing the rate of convergence of the L-link scheme with the L-layer hierarchy scheme we obtain

$$R_{new} := \frac{\text{hierarchical}}{L-\text{link}} = \frac{\cos(2\pi/w) - 1}{\frac{1}{L}(\cos(2\pi/N_L) + \cos(4\pi/N_L) + \ldots + \cos(2L\pi/N_L)) - 1},$$

where $w = \max\{n_1, n_2, \ldots, n_L\}$. Using this result and taking the first order expansion of the cos terms we arrive at the following theorem.

Theorem 2.12 (Equal communication comparison)**.** *In comparing the L-layer hierarchy scheme, which has a total of LN_L communication links, to the L-link scheme which has an equal amount of communication, the increase in the rate of convergence is approximated by*

$$R_{new} \approx \left(\frac{L}{\sum_{m=1}^{L} m^2}\right)\frac{N_L^2}{w^2}, \tag{2.27}$$

where $w = \max\{n_1, n_2, \ldots, n_L\}$. As $N_L \to \infty$ this approximation approaches an equality.

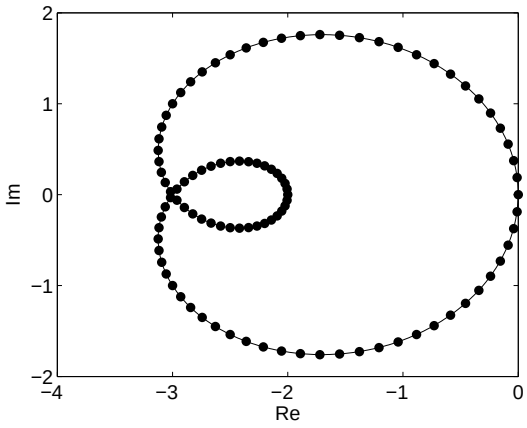

(a) Eigenvalues of A with $N_L = 100$ and $L = 2$.

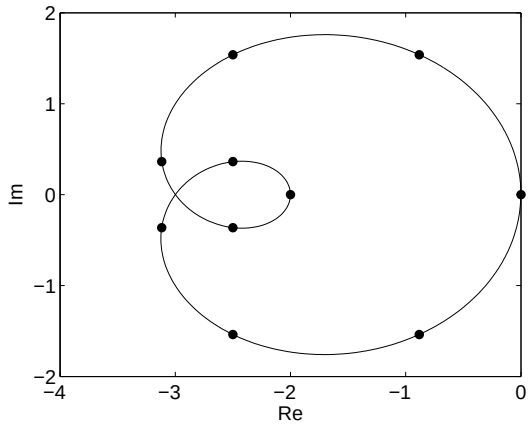

(b) Eigenvalues of A with $N_L = 10$ and $L = 2$.

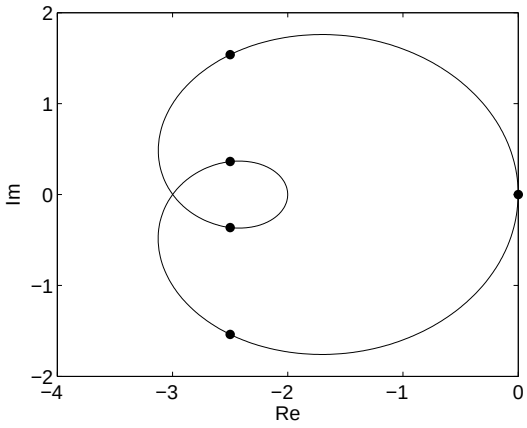

(c) Eigenvalues of A with $N_L = 5$ and $L = 2$.

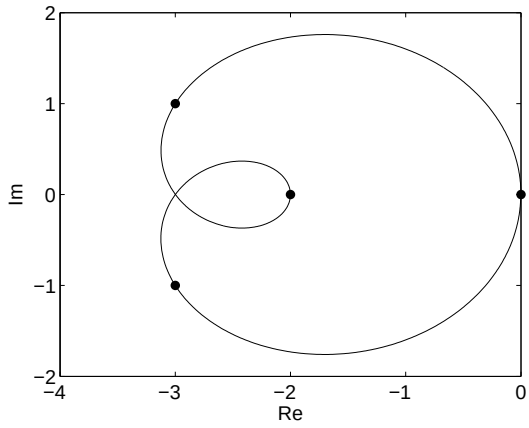

(d) Eigenvalues of A with $N_L = 4$ and $L = 2$. The eigenvalue $q_C(\omega)$ is no longer the γ-value, it is now given by $q_C(\omega^2)$.

Figure 2.8: N_L must be sufficiently large when compared to L.

Table 2.1: Comparing the rate of convergence of an $L = 3$ hierarchy scheme to the traditional and three-link schemes.

Number of agents	hierarchy/trad.	hierarchy/three-link
$3^3 = 27$	56	12
$4^3 = 64$	208	45
$10^3 = 1000$	9675	2075

Table 2.1 shows some comparisons between the different schemes for $L = 3$. The hierarchical scheme has a much greater rate of convergence than the L-link scheme. The trajectories of 16 agents in 4-link pursuit and in hierarchical pursuit with $L = 4$ ($n_1 = n_2 = n_3 = n_4 = 2$) are shown in Figure 2.9.

Some visually appealing images can be created by using the hierarchical cyclic pursuit scheme. In Figure 2.10 the trajectories of 256 agents in a four layer hierarchy scheme are shown. The initial conditions are created by placing the agents equally spaced around a circle, and then displacing each agent in both angle and radius by some random amount.

Remark 2.13. In this chapter we have created a hierarchical structure for cyclic pursuit. Cyclic pursuit can be written as $\dot{z} = A_1 z$ where A_1 is the circulant matrix $\text{circ}(-1, 1, 0, \ldots, 0)$. This method, however, can be applied to any system whose dynamics are governed by a circulant pursuit matrix. That is, a circulant matrix with one eigenvalue at zero and all others in the open left half-plane. For example, we could create a hierarchical version of the L-link scheme and perform a rate of convergence analysis as was done in this chapter. As another example, a hierarchical version of the system $\dot{z} = B_1 z$ where $B_1 = \text{circ}(-1, 1/2, 0, \ldots, 0, 1/2)$ can be created. This system is studied in Chapter 4. It turns out that for this system

$$\text{eigs}(B_1) = \Re\{\text{eigs}(A_1)\}.$$

For an L-layer hierarchical scheme, $\dot{z} = B_L z$, the matrix B_L is given by the recursive

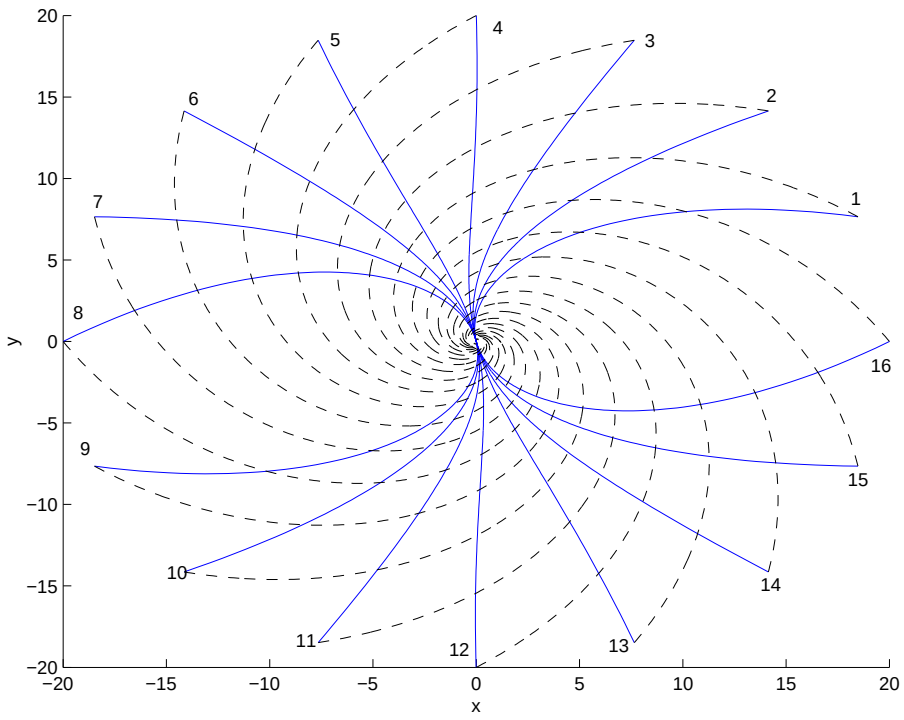

Figure 2.9: Trajectories for 16 agents in 4-link cyclic pursuit (dashed line) and 16 agents with 4 layers of hierarchy (solid line).

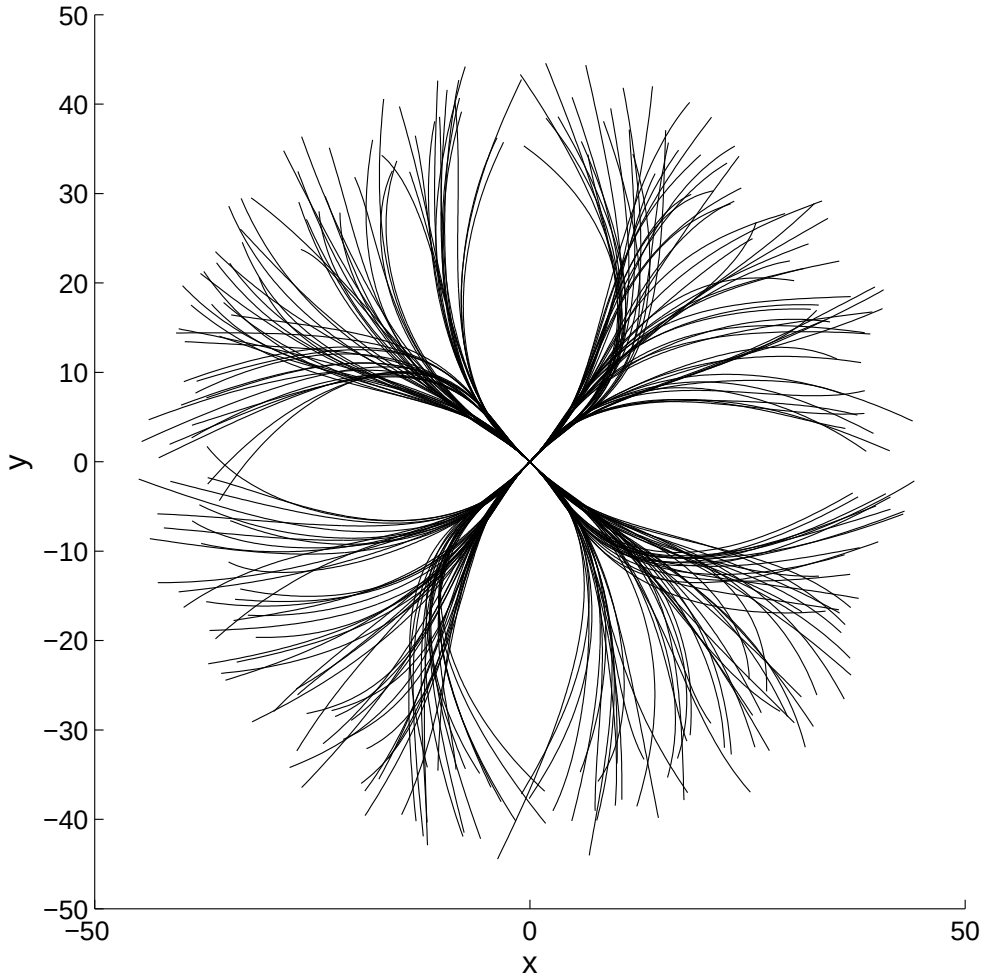

Figure 2.10: Trajectories for 256 agents in a 4 layer hierarchical cyclic pursuit with $n_1 = n_2 = n_3 = n_4 = 4$. The initial positions of the agents created by spacing them equally around a circle and then displacing each agent randomly.

expression

$$B_1 = \text{circ}(-1, 1/2, 0, \ldots, 0, 1/2)$$
$$B_m = \text{circ}(B_{m-1} - I, 1/2I, 0, \ldots, 0, 1/2I), \quad m = 2, \ldots, L.$$

The increase in the rate of convergence of the L-layer scheme over the traditional $\dot{z} = B_1 z$ scheme is given by the exact same expression as in Theorem 2.10,

$$R \approx \left(\frac{N_L}{\max_m \{n_m\}} \right)^2.$$

◀

2.7 Summary

In this chapter a hierarchical cyclic pursuit scheme has been introduced. It has been shown that this scheme yields a higher rate of convergence of a group of vehicles to their centroid than either the traditional cyclic pursuit or the equal communication scheme.

Chapter 3

Heterogeneous multi-agent systems

In this chapter the control of a heterogeneous group of agents is explored. Cyclic pursuit is studied for the case of two agents, each with a different kinematic model. One agent is modeled as a point mass, and the other is modeled as a kinematic unicycle. It is shown that by varying the gains on the control inputs, different types of formations can be achieved: The agents can spiral in to a point, out to infinity, or converge to concentric circles.

3.1 Introduction

A heterogeneous group of agents is simply a group in which there are differences between the agents. The differences may lie in their kinematic models, or in their sensing/computing capabilities. There has been a considerable amount of applied research in the area of heterogeneous multi-robot systems, for example [17, 29, 42]. In this research, controllers are heuristically designed to achieve a desired group behavior, and then implemented on a heterogeneous group of robots. Much of the work is focused on groups with different sensing/computing capabilities. As an example, in [42], a group of robots is studied in which there are sensor-rich robots that are given the role of leaders, and sensor-limited robots who require assistance. Using a map of their environment the sensor rich

robots are able to aid the sensor-limited robots in dispersing themselves throughout the environment. Research is also being done on groups of agents with different kinematic models. One example is the research being performed at the Center for Collaborative Control of Unmanned Vehicles (C3UV), at UC Berkeley [21]. The center has developed a test-bed consisting of unmanned air vehicles (UAVs) and unmanned ground vehicles (UGVs). The agents are outfitted with GPS receivers which are used to receive waypoints to dictate their path. The goal is for the agents to work in a self-directed and collaborative manner to perform tasks that would not be possible with homogeneous groups. In terms of mathematical analysis of heterogeneous multi-agent systems, the research is very limited. Nearly all of the literature is focused on homogeneous groups of agents. However, one interesting study is by Tabuada et al. [50], where the feasibility of formations of heterogeneous systems is considered. In this research, formation stabilization is studied. Nonconstructive conditions are determined on each agent, given its kinematic model, that guarantee there exists a feasible trajectory driving the agent to a desired formation.

In this chapter we consider two agents with different kinematic models. We prescribe a simple local control strategy to each agent, and then study the emerging global behavior. We model one agent as a point mass (i.e., it can instantaneously move in any direction), and the other as a kinematic unicycle (i.e., its motion is subject to a single nonholonomic constraint). The local control strategy used is cyclic pursuit. For each type of agent, a homogeneous cyclic pursuit study has previously been performed. From Chapter 2 we know that if a group of point masses is in cyclic pursuit they will converge to their stationary centroid. Also, as described in Chapter 2, if a group of unicycles is in cyclic pursuit, depending on the linear and angular velocity gains, the unicycles can either spiral in to a point, converge to a circle of some radius, or diverge [31]. For our heterogeneous system it is discovered that the behavior is similar to cyclic pursuit for unicycles. Depending on the gains on the velocities, the agents can either spiral in to a

point, converge to concentric circles, or diverge.

The organization of this chapter is as follows. In Section 3.2 the problem is formalized and a model of the two agent system is derived in local coordinates. In Section 3.3 the cyclic pursuit control strategy is introduced and the equilibrium formations of the system are determined. Finally, in Section 3.4 the stability of the equilibria are analyzed and plots of the behaviors are shown.

3.2 Relative coordinates

We begin with two agents lying in the plane. We represent their positions as points in the complex plane. The first agent's position is given by $z_1 := x_1 + jy_1$. The dynamics of this agent is given by a simple integrator

$$\dot{z}_1 = u,$$

where u is the velocity input. Due to this agent's ability to instantaneously move in any direction, we will call it a *beetle*. The second agent's position is given by $z_2 := x_2 + jy_2$. This agent has a more complicated dynamical model which is given by

$$\dot{z}_2 = v\mathrm{e}^{j\theta}$$

$$\dot{\theta} = \omega,$$

where v and ω are the linear and angular velocity inputs respectively. This is known as the unicycle model since instantaneously the agent can move only in the direction $\mathrm{e}^{j\theta}$.

The unicycle and beetle are shown in the complex plane in Figure 3.1. We define the unit vector pointing in the direction of the unicycle's heading as

$$r := \mathrm{e}^{j\theta}.$$

We would like to express the beetle-unicycle system in local coordinates. To do this we define the distance between the two agents to be

$$\rho := |z_1 - z_2|.$$

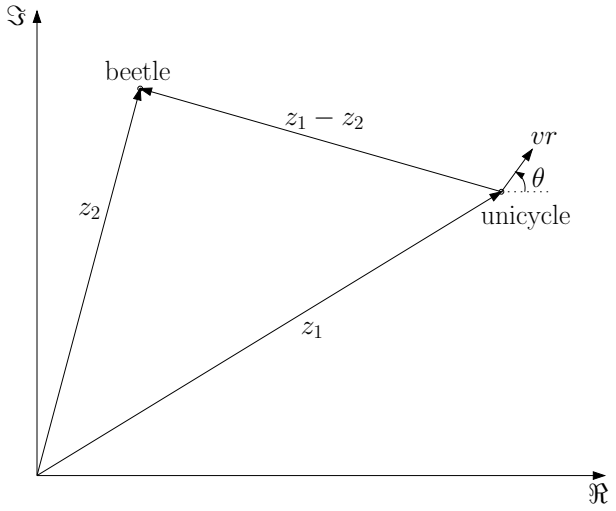

Figure 3.1: A unicycle and a beetle in the complex plane.

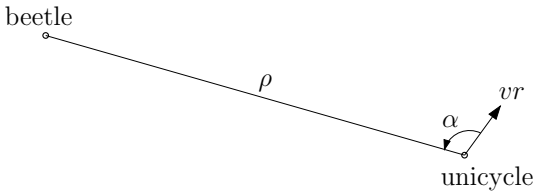

Figure 3.2: Relative coordinates for the unicycle and beetle.

Also, we define α to be the angle from the current heading of the unicycle to the heading that would take it to the beetle. This is shown in Figure 3.2. If we rotate r by α and scale it by ρ we get $z_1 - z_2$:

$$z_1 - z_2 = \rho r \mathrm{e}^{j\alpha}.$$

Differentiating this expression we get

$$\dot{z}_1 - \dot{z}_2 = \dot{\rho} r \mathrm{e}^{j\alpha} + \rho \dot{r} \mathrm{e}^{j\alpha} + \rho r j \dot{\alpha} \mathrm{e}^{j\alpha}.$$

Using the fact that

$$\dot{r} = j\dot{\theta}\mathrm{e}^{j\theta} = j\omega r,$$

and substituting the expressions for $\dot{z}_1$ and $\dot{z}_2$ we have

$$u - vr = \dot{\rho} r \mathrm{e}^{j\alpha} + j\rho r \omega \mathrm{e}^{j\alpha} + \rho r j \dot{\alpha} \mathrm{e}^{j\alpha}.$$

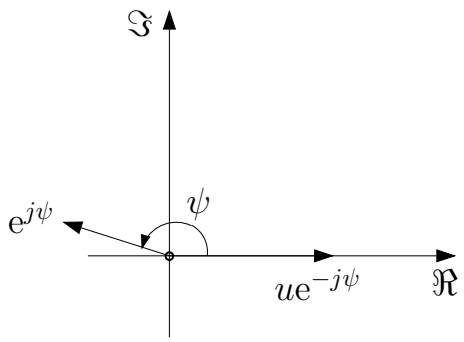

Figure 3.3: If $ue^{-j\psi}$ lies on the positive real axis then $u = ce^{j\psi}$ for some $c > 0$.

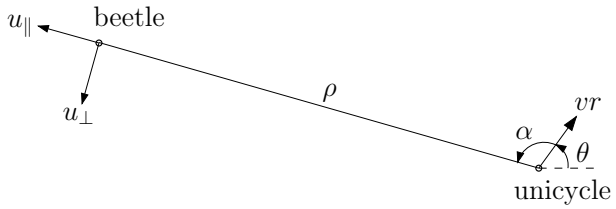

Figure 3.4: The components of u parallel and perpendicular to $z_1 - z_2$.

Bringing vr to the right side and dividing through by $re^{j\alpha}$ we obtain

$$ue^{-j(\alpha+\theta)} = \dot{\rho} + j\rho\omega + j\rho\dot{\alpha} + ve^{-j\alpha}. \tag{3.1}$$

Defining $\psi := \alpha + \theta$ we can write the left-hand side of (3.1) as $ue^{-j\psi}$. To understand this quantity, consider the case where $ue^{-j\psi} = c \in \mathbb{R}$. This is shown in Figure 3.3. It follows that $u = ce^{j\psi}$. Therefore, $ue^{-j\psi}$ takes on a real value if and only if u is aligned with $e^{j\psi}$. But since $z_1 - z_2 = \rho e^{j\psi}$, we have that $ue^{-j\psi}$ is real if and only if u is aligned with $z_1 - z_2$. Likewise, $ue^{-j\psi}$ is imaginary if and only if u is perpendicular to $z_1 - z_2$. Therefore, we have

$$ue^{-j\psi} = u_\parallel + ju_\perp,$$

where $u_\parallel$ is the component of u aligned with $z_1 - z_2$, and $u_\perp$ is the component of u perpendicular to $z_1 - z_2$ as shown in Figure 3.4. Because of this we can rewrite (3.1) as

$$u_\parallel + ju_\perp = \dot{\rho} + j\rho\omega + j\rho\dot{\alpha} + ve^{-j\alpha}. \tag{3.2}$$

Taking the real and imaginary parts and rearranging we get

$$\begin{aligned} \dot{\rho} &= u_{\parallel} - v\cos\alpha \\ \dot{\alpha} &= \frac{1}{\rho}(v\sin\alpha + u_{\perp}) - \omega, \end{aligned} \tag{3.3}$$

respectively. The domain of validity of (3.3) is $\rho \in \mathbb{R} \setminus \{0\}$, $\alpha \in \mathbb{R}$.

3.3 Equilibrium formations

We will now apply the strategy of cyclic pursuit to the beetle and unicycle. For a group of beetles in cyclic pursuit, the control law is

$$u_i = k_{v_1}(z_{i+1} - z_i),$$

where the constant $k_{v_1} > 0$ is the gain on the velocity. Therefore, for our system we have $\dot{z}_1 = k_{v_1}(z_2 - z_1)$ which can be written in relative coordinates as

$$u_{\parallel} = -k_{v_1}\rho \quad \text{and} \quad u_{\perp} = 0.$$

From [31], a group of unicycles in cyclic pursuit use the following strategy. Each unicycle pursues the next with linear velocity proportional to the distance to the next unicycle, and angular velocity proportional to the difference between the desired and actual heading. In our notation this is written as

$$v_i = k_{v_2}|z_{i+1} - z_i| \quad \text{and} \quad \omega_i = k_{\alpha}\alpha_i.$$

where $k_{v_2}, k_{\alpha} > 0$ are constants. Hence, in relative coordinates, this can be written as

$$v = k_{v_2}\rho \quad \text{and} \quad \omega = k_{\alpha}\alpha.$$

In studies of homogeneous cyclic pursuit, it is always assumed that the linear velocity gains, k_{v_1} and k_{v_2}, are the same for each agent. In this study, we will allow the possibility

of different gains in order to remain as general as possible (i.e., k_{v_1} is not necessarily equal to k_{v_2}) . Substituting these control laws into (3.3) we get

$$\begin{aligned} \dot{\rho} &= -k_{v_1}\rho - k_{v_2}\rho\cos\alpha \\ \dot{\alpha} &= k_{v_2}\sin\alpha - k_\alpha\alpha. \end{aligned} \tag{3.4}$$

Notice that the singularity at $\rho = 0$ is no longer present in the α dynamics of (3.4) and thus we can extend the domain of validity of the system to $(\rho, \alpha) \in \mathbb{R}^2$. Since ρ is a distance, it has physical significance only when $\rho \geq 0$. Also, since α is an angle, it takes unique values only on $(-\pi, \pi]$ (i.e., π and $-\pi$ correspond to the same physical situation).

To determine the equilibria of this system, we set $\dot{\rho} = 0$ and $\dot{\alpha} = 0$ and get

$$\rho(k_{v_1} + k_{v_2}\cos\alpha) = 0, \tag{3.5}$$

$$k_{v_2}\sin\alpha - k_\alpha\alpha = 0. \tag{3.6}$$

The solutions ρ and α, to (3.5) and (3.6) depend on the values of the gains k_{v_1}, k_{v_2}, and k_α. The equation (3.5) is satisfied if $\rho = 0$ or

$$\cos\alpha = -\frac{k_{v_1}}{k_{v_2}}. \tag{3.7}$$

Notice that since $-k_{v_1}/k_{v_2} < 0$ a solution to (3.7) must lie in $(-\pi, -\pi/2)$ or $(\pi/2, \pi]$. The equation (3.6) can be rewritten as

$$\sin\alpha = \frac{k_\alpha}{k_{v_2}}\alpha. \tag{3.8}$$

We will split the study of the equilibrium formations into three cases, which are defined by gain ranges.

Case 1 ($k_\alpha \geq k_{v_2}$): Since $k_\alpha/k_{v_2} \geq 1$, the only solution to (3.8) is $\alpha = 0$. We can also see that $\alpha = 0$ does not satisfy (3.7). Therefore the only solution to (3.5) is $\rho = 0$. Because of this, the only equilibrium is

$$(\rho, \alpha) = (0, 0). \tag{3.9}$$

Case 2 ($k_\alpha < k_{v_2}$ and $k_{v_1} \geq k_{v_2}$): Since $k_\alpha/k_{v_2} < 1$, there are now two non-zero solutions to (3.8), which we call $\pm\alpha^*$, where $\alpha^* \in (0, \pi)$. However, since $k_{v_1}/k_{v_2} \leq -1$, $\alpha = 0, \pm\alpha^*$ are not solutions to (3.7). Thus, the only solution to (3.5) is $\rho = 0$. Therefore, the equilibria are (3.9) and

$$(\rho, \alpha) = (0, \pm\alpha^*) \quad \text{where } \alpha^* \in (0, \pi) \text{ satisfies} \quad \sin\alpha^* = \frac{k_\alpha}{k_{v_2}}\alpha^*.$$

Case 3 ($k_\alpha < k_{v_2}$ and $k_{v_1} < k_{v_2}$): The point in (3.9) is still an equilibrium in this case. Since k_{v_1}/k_{v_2} takes values in the range $(0, 1)$, equation (3.7) is now satisfied for some $\alpha = \pm\alpha^*$, where $\alpha^* \in (\pi/2, \pi)$. The gain k_α can be chosen such that $\pm\alpha^*$ are also solutions to (3.8). Hence, there is an equilibrium point of (3.4), given by $(\rho^*, \pm\alpha^*)$, where $\rho^* \in \mathbb{R}$, and α^* and the gains $k_{v_1}, k_{v_2}, k_\alpha$ satisfy

$$\sin\alpha^* = \frac{k_\alpha}{k_{v_2}}\alpha^* \quad \text{and} \quad \cos\alpha^* = -\frac{k_{v_1}}{k_{v_2}}.$$

These two conditions can be combined using the fact that $e^{j\alpha} = \sin\alpha + j\cos\alpha$ to obtain

$$e^{j\alpha^*} = \frac{1}{k_{v_2}}(-k_{v_1} + jk_\alpha\alpha^*), \quad \alpha^* \in (\pi/2, \pi). \tag{3.10}$$

Figure 3.5 shows a situation where (3.10) is satisfied. If (3.10) is not satisfied then there does not exist an α^* which satisfies both (3.7) and (3.8), and thus the non-zero equilibria are

$$(\rho, \alpha) = (0, \pm\alpha^*) \quad \text{where } \alpha^* \in (0, \pi) \text{ satisfies} \quad \sin\alpha^* = \frac{k_\alpha}{k_{v_2}}\alpha^*.$$

Thus the equilibrium formations in Case 3 are:

(i) $(\rho, \alpha) = (0, 0)$, and

(ii) if (3.10) is satisfied, $(\rho, \alpha) = (\rho^*, \pm\alpha^*)$, where $\rho^* \in \mathbb{R}$, or

(iii) if (3.10) is not satisfied, $(\rho, \alpha) = (0, \pm\alpha^*)$ where $\alpha^* \in (0, \pi)$ satisfies $\sin\alpha^* = \frac{k_\alpha}{k_{v_2}}\alpha^*$.

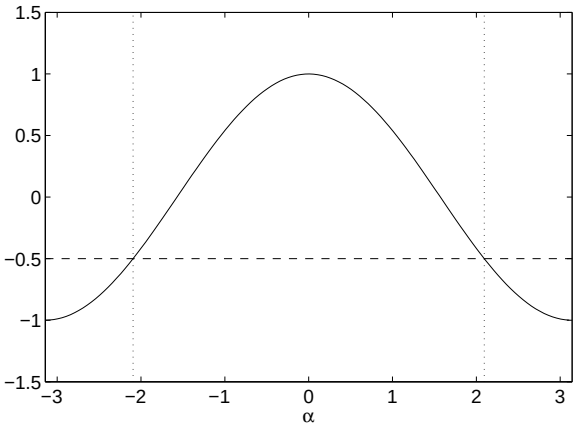

(a) A plot of $\cos\alpha$ (solid line) and $-k_{v_1}/k_{v_2}$ (dashed line). The intersection points are $\alpha = \pm 2\pi/3$.

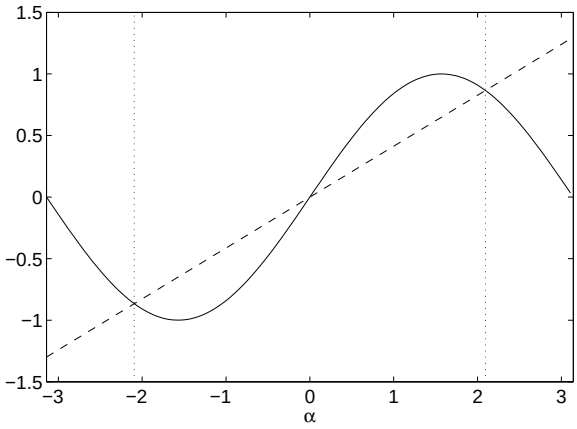

(b) A plot of $\sin\alpha$ (solid line) and $\alpha k_\alpha/k_{v_2}$ (dashed line). The nonzero intersection points are $\alpha = \pm 2\pi/3$.

Figure 3.5: The situation in Case 3 where (3.7) and (3.8) are satisfied by the same α^*. Here $\alpha^* = 2\pi/3$, and the gains are $(k_{v_1}, k_{v_2}, k_\alpha) = (1, 2, \frac{3\sqrt{3}}{2\pi})$.

Based on this analysis there are essentially three types of equilibrium points:

(i) $\rho = 0$, $\alpha = 0$.

(ii) $\rho = 0$, $\alpha \neq 0$.

(iii) $\rho \neq 0$, $\alpha \neq 0$.

3.4 Stability of the equilibria

Introducing the notation

$$\xi = \begin{bmatrix} \rho \\ \alpha \end{bmatrix},$$

we can linearize the system $\dot{\xi} = f(\xi)$, defined in (3.4), about an equilibrium point ξ^* as follows:

$$\dot{\xi} = \left.\frac{\partial f}{\partial \xi}\right|_{\xi^*} \xi.$$

We can write this system in the form $\dot{\xi} = A\xi$, where

$$A := \left.\frac{\partial f}{\partial \xi}\right|_{\xi^*} = \left[\begin{array}{cc} -k_{v_1} - k_{v_2}\cos\alpha & k_{v_2}\rho\sin\alpha \\ 0 & k_{v_2}\cos\alpha - k_\alpha \end{array}\right]_{\xi^*}. \tag{3.11}$$

As can be seen from (3.4) and (3.11), the function f and the Jacobian $\partial f/\partial\xi$ are continuous on $\mathbb{R}^2$, and therefore $f : \mathbb{R}^2 \to \mathbb{R}^2$ is a locally Lipschitz map.

In what follows we will consider the linearization about the equilibrium points to determine local stability for each case. We will then use nonlinear analysis to obtain global stability results. However, first we will quickly look at the three cases from a purely intuitive point of view.

In Case 1, $k_\alpha \geq k_{v_2}$. That is, the turning gain for the unicycle is at least as large as the linear velocity gain. This is in essence saying that the unicycle can turn quickly when compared to its forward velocity. Hence, a large heading error can be corrected with a relatively small linear motion. Therefore, one might conjecture that the unicycle will quickly turn around to face the beetle and the two will move towards each other, asymptotically converging to a common point.

In Case 2 we have $k_\alpha < k_{v_2}$ and $k_{v_1} \geq k_{v_2}$. In this case the beetle is at least as fast as the unicycle. Also, the unicycle cannot turn very fast relative to its linear velocity. Therefore, one might guess that the beetle will catch the unicycle, but the unicycle may not be able to completely turn around to face the beetle before capture.

In Case 3 we have $k_\alpha < k_{v_2}$ and $k_{v_1} < k_{v_2}$. Here the unicycle is faster than the beetle but the unicycle cannot turn very quickly when compared to its linear velocity. The beetle is too slow too catch the unicycle, but the unicycle might regulate its heading error too slowly to catch the beetle. Because of this, it is difficult to intuitively determine whether or not the unicycle and beetle will meet at a point.

With the intuitive picture of the three cases in mind, we will now perform a stability analysis.

3.4.1 Case 1 ($k_\alpha \geq k_{v_2}$)

In Case 1 the only equilibrium is $(\rho, \alpha) = (0, 0)$, from which we get that

$$A = \begin{bmatrix} -(k_{v_1} + k_{v_2}) & 0 \\ 0 & k_{v_2} - k_\alpha \end{bmatrix}. \tag{3.12}$$

When $k_\alpha > k_{v_2}$, this matrix has two real negative eigenvalues and thus locally the equilibrium $(\rho, \alpha) = (0, 0)$ is a stable node. If $k_\alpha = k_{v_2}$, the A matrix drops rank and thus the linearization tells us nothing. Since $(0, 0)$ is the only equilibrium for this range of gains, we can study its stability properties on the domain $\mathbb{R}^2$.

Theorem 3.1. *Provided that $k_\alpha > k_{v_2}$, the origin of* (3.4) *is globally exponentially stable. If $k_\alpha = k_{v_2}$, the origin is globally asymptotically stable.*

Proof. First we will show that the $\dot{\alpha}$ subsystem of (3.4) is globally exponentially stable (GES) when $k_\alpha > k_{v_2}$. From Theorem 4.10 of Khalil [24], if we find a continuously differentiable Lyapunov function $V : \mathbb{R} \to \mathbb{R}$ such that

$$k_1|\alpha|^a \leq V(\alpha) \leq k_2|\alpha|^a \tag{3.13}$$

$$\dot{V}(\alpha) \leq -k_3|\alpha|^a \tag{3.14}$$

for all $\alpha \in \mathbb{R}$, where k_1, k_2, k_3, and a are positive constants, then, $\alpha = 0$ is GES.

Consider the choice

$$V(\alpha) = \frac{1}{2}\alpha^2.$$

Clearly by choosing $k_1 = k_2 = 1/2$ and $a = 2$, condition (3.13) is satisfied. Now evaluating the Lie derivative using (3.4) we get

$$\dot{V} = \alpha\dot{\alpha} = -k_\alpha\alpha^2 + k_{v_2}\alpha\sin\alpha$$

but since $\alpha^2 \geq \alpha\sin\alpha$ for all $\alpha \in \mathbb{R}$ we have

$$\dot{V} \leq -(k_\alpha - k_{v_2})\alpha^2.$$

If $k_\alpha - k_{v_2} > 0$, then by choosing $k_3 = k_\alpha - k_{v_2}$ condition (3.14) is satisfied. Therefore, $\alpha = 0$ is GES if $k_\alpha > k_{v_2}$.

Next we will show that the $\dot{\alpha}$ subsystem of (3.4) is globally asymptotically stable (GAS) when $k_\alpha = k_{v_2}$. In this case the expression for $\dot{V}$ becomes

$$\dot{V} = -k_\alpha(\alpha^2 + \alpha \sin \alpha).$$

But $\alpha^2 > \alpha \sin \alpha$ for all $\alpha \in \mathbb{R} \setminus \{0\}$. Hence $\dot{V} < 0$ on $\mathbb{R} \setminus \{0\}$ with $\dot{V} = 0$ if and only if $\alpha = 0$. Hence, if $k_\alpha = k_{v_2}$, $\alpha = 0$ is GAS.

Finally we will show that for all $k_\alpha \geq k_{v_2}$, the equilibrium $\rho = 0$ is GES for the ρ dynamics, provided $\alpha(t) \to 0$ as $t \to \infty$. Consider rewriting the ρ dynamics from (3.4) (adding and subtracting $k_{v_2}\rho$ on the right hand side) as

$$\dot{\rho} = -(k_{v_1} + k_{v_2})\rho + k_{v2}(1 - \cos \alpha)\rho.$$

These dynamics can then be rewritten as the linear system

$$\dot{\rho} = [A + B(t)]\rho,$$

where $B(t)$ is the continuous function

$$B(t) = k_{v2}(1 - \cos \alpha(t))$$

and $A = -(k_{v_1} + k_{v_2})$ is negative. Now, since $\alpha(t) \to 0$ as $t \to \infty$ we can conclude that

$$B(t) \to 0 \quad \text{as} \quad t \to \infty. \tag{3.15}$$

Since A is negative, the origin of

$$\dot{\rho} = A\rho \tag{3.16}$$

is GES. Finally, the perturbation term $B(t)\rho$ satisfies the inequality

$$|B(t)\rho| \leq |B(t)||\rho|. \tag{3.17}$$

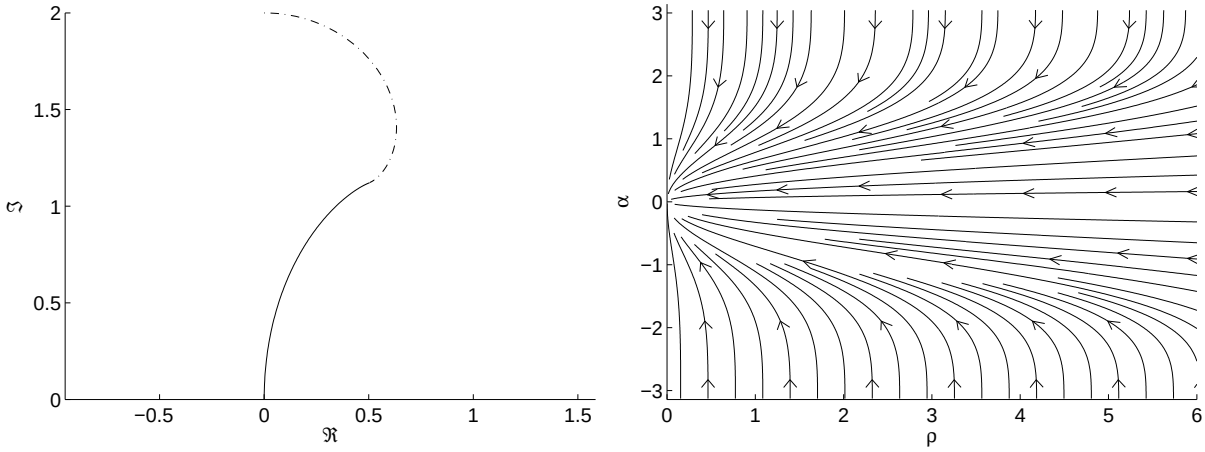

(a) A unicycle (dashed line) and a beetle (solid line) approaching the $(\rho, \alpha) = (0, 0)$ equilibrium.

(b) The corresponding phase portrait.

Figure 3.6: Case 1. In this plot $(k_{v_1}, k_{v_2}, k_\alpha) = (1, 1, 2)$.

Therefore, since the nominal system is GES and perturbation is bounded and vanishing, by Corollary 9.1 and Lemma 9.5 of Khalil [24], the origin of the ρ dynamics is GES. Since the ρ dynamics is GES provided that $\alpha(t) \to 0$ as $t \to \infty$, and the α dynamics is GES provided $k_\alpha > k_{v_2}$, system (3.4) is GES provided $k_\alpha > k_{v_2}$. If $k_\alpha = k_{v_2}$, the α dynamics is GAS and the ρ dynamics is GES, which implies system (3.4) is GAS. □

Figure 3.6 shows the trajectories of a unicycle and beetle as they approach the $(\rho, \alpha) = (0, 0)$ equilibrium of Case 1.

3.4.2 Case 2 ($k_\alpha < k_{v_2}$ and $k_{v_1} \geq k_{v_2}$)

In Case 2 the equilibria are $(\rho, \alpha) = (0, 0)$ and

$$(\rho, \alpha) = (0, \pm\alpha^*) \quad \text{where } \alpha^* \in (0, \pi) \text{ satisfies} \quad \sin\alpha^* = \frac{k_\alpha}{k_{v_2}}\alpha^*.$$

Linearizing the system (3.4) about the $(0, 0)$ equilibrium we obtain (3.12). The first diagonal term is negative, but since $k_\alpha < k_{v_2}$, the second diagonal term is positive. Therefore, the equilibrium point $(0, 0)$ is a saddle. The other equilibrium points for Case

2 are $(0, \alpha^*)$ and $(0, -\alpha^*)$. Linearizing about the $(0, \alpha^*)$ equilibrium we obtain

$$A = \begin{bmatrix} -k_{v_1} - k_{v_2} \cos\alpha^* & 0 \\ 0 & k_{v_2} \cos\alpha^* - k_\alpha \end{bmatrix}. \tag{3.18}$$

Since $k_{v_1} \geq k_{v_2}$, and $\alpha^* \in (0, \pi)$, the first diagonal term is negative. The second diagonal term is $T_2 := k_{v_2} \cos\alpha^* - k_\alpha$. To see that this term is negative for all $\alpha^* \in (0, \pi)$ consider the following. Using the fact that $\sin\alpha^* = \alpha^* k_\alpha / k_{v_2}$, we can rewrite this term as

$$T_2 := k_{v_2} \left(\cos\alpha^* - \frac{\sin\alpha^*}{\alpha^*} \right) = k_{v_2} \alpha^* (\alpha^* \cos\alpha^* - \sin\alpha^*) = k_{v_2} \alpha^* g(\alpha^*),$$

where $g(\alpha) := \alpha\cos\alpha - \sin\alpha$. Since $\alpha^* \in (0, \pi)$, $k_{v_2}\alpha^* > 0$. Also, differentiating $g(\alpha)$ we obtain

$$\frac{dg}{d\alpha} = -\alpha \sin\alpha < 0, \quad \text{for all } \alpha \in (0, \pi).$$

since $g(0) = 0$, we have that $g(\alpha^*) < 0$ for all $\alpha^* \in (0, \pi)$. Therefore $T_2 < 0$ for all $\alpha^* \in (0, \pi)$, and hence the equilibrium $(\rho, \alpha) = (0, \alpha^*)$ is locally stable. Using the same argument it can be shown that the equilibrium $(0, -\alpha^*)$ is locally stable.

If we were to study this case on the domain $\mathbb{R}^2$, then $(0, \alpha^*)$, $(0, \alpha^* + 2\pi)$, $(0, \alpha^* + 4\pi)$, etc., would all be equilibrium points. However, all of these equilibria correspond to the same physical situation. Therefore, we restrict our attention to the domain $(\rho, \alpha) \in \mathcal{D} := \mathbb{R} \times (-\pi, \pi)$. This is an open and connected set and thus we can use it as a domain for Lyapunov analysis. (Notice that the situation where the unicycle is pointing directly away from the beetle, and thus $\alpha = \pm\pi$, is not included in this domain. This is simply a technicality, and could be easily remedied by, for example, defining this situation as $\alpha = +\pi$ and redefining our domain as $\mathbb{R} \times (-\pi, \pi + \epsilon)$, $\epsilon > 0$.)

We will now study the stability properties of (3.4) on the domain $\mathcal{D} = \mathbb{R} \times (-\pi, \pi)$.

Theorem 3.2. *For gains satisfying $k_\alpha < k_{v_2}$ and $k_{v_1} \geq k_{v_2}$, there are three equilibrium points of (3.4) on $\mathcal{D}$: $(0, 0)$, $(0, \alpha^*)$, and $(0, -\alpha^*)$, where $\alpha^* \in (0, \pi)$ satisfies*

$$\sin\alpha^* = \frac{k_\alpha}{k_{v_2}} \alpha^*.$$

The stability properties of these equilibria are

(i) $(0,0)$ *is a saddle. The only trajectory going to this equilibrium is* $(\rho(0),0)$.

(ii) For every $\epsilon \in (0,\alpha^*)$*, the equilibrium* $(\rho,\alpha)=(0,\alpha^*)$ *is exponentially stable on the domain* $\mathbb{R}\times(\epsilon,\pi)$*. On the domain* $\mathbb{R}\times(0,\pi)$*, the equilibrium* $(0,\alpha^*)$ *is asymptotically stable.*

(iii) For every $\epsilon \in (-\alpha^*,0)$*, the equilibrium* $(\rho,\alpha)=(0,-\alpha^*)$ *is exponentially stable on the domain* $\mathbb{R}\times(-\pi,\epsilon)$*. On the domain* $\mathbb{R}\times(-\pi,0)$*, the equilibrium* $(0,-\alpha^*)$ *is asymptotically stable.*

Proof. In order to study these equilibria, we will study the α dynamics, which is given by

$$\dot{\alpha} = k_{v_2}\sin\alpha - k_\alpha\alpha.$$

Both $\sin\alpha$ and $-\alpha$ are anti-symmetric about $\alpha=0$, and therefore, so is $\dot{\alpha}$. Because of this, by studying the equilibrium α^* on the interval $\alpha\in(0,\pi)$, we will also determine the behavior of $-\alpha^*$ on the interval $\alpha\in(-\pi,0)$. Therefore, we will simply study the equilibrium α^*. We begin by showing asymptotic stability of the equilibrium α^* on the interval $(0,\pi)$.

From the definition of α^* we have $k_{v_2}=k_\alpha\alpha^*/\sin\alpha^*$, which can be substituted into the α dynamics in (3.4) to obtain

$$\dot{\alpha} = k_\alpha\left(\alpha^*\frac{\sin\alpha}{\sin\alpha^*}-\alpha\right).$$

Consider the shifted Lyapunov function

$$V=\frac{1}{2}(\alpha-\alpha^*)^2.$$

Computing the Lie derivative we get

$$\begin{aligned}\dot{V} &= k_\alpha(\alpha-\alpha^*)\left(\alpha * \frac{\sin\alpha}{\sin\alpha^*}-\alpha\right)\\ &= k_\alpha\alpha(\alpha^*-\alpha)\left(1-\frac{\alpha^*\sin\alpha}{\alpha\sin\alpha^*}\right) = k_\alpha\alpha(\alpha^*-\alpha)\left(1-\frac{\operatorname{sinc}(\alpha)}{\operatorname{sinc}(\alpha^*)}\right),\end{aligned}$$

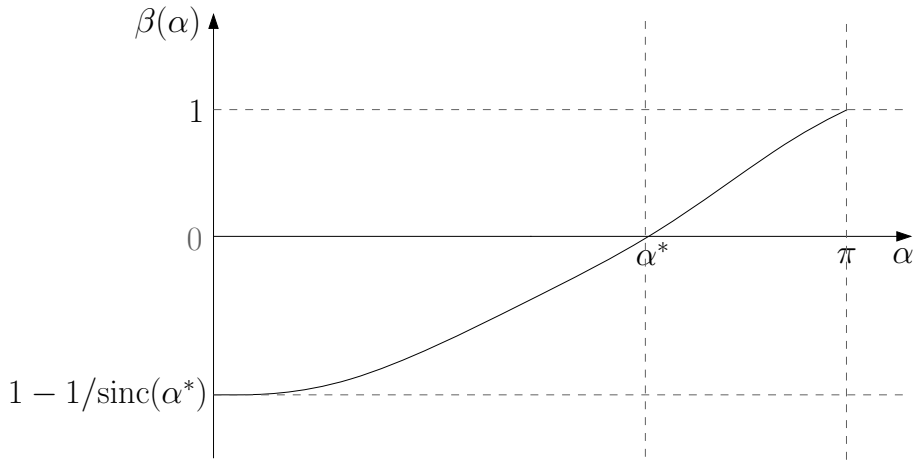

Figure 3.7: The strictly increasing function $\beta(\alpha)$ on the interval $\alpha \in (0, \pi]$.

where $\text{sinc}(a) := \sin(a)/a$, which is well-defined on the interval $a \in (0, \pi)$. The function $\text{sinc}(\alpha)$ is a positive, strictly decreasing, and continuous function on this interval, where $\lim_{\alpha \to 0} \text{sinc}(\alpha) = 1$, and $\text{sinc}(\pi) = 0$. Defining

$$\beta(\alpha) := \left(1 - \frac{\text{sinc}(\alpha)}{\text{sinc}(\alpha^*)}\right),$$

we can see that on $\alpha \in (0, \pi)$, $\beta(\alpha)$ is strictly increasing and continuous, with $\lim_{\alpha \to 0} \beta(\alpha) = 1 - 1/\text{sinc}(\alpha^*) < 0$, $\beta(\alpha^*) = 0$, and $\beta(\pi) = 1$. The function $\beta(\alpha)$ is shown in Figure 3.7. Using this function we can write $\dot{V}$ as

$$\dot{V} = k_\alpha \alpha(\alpha^* - \alpha)\beta(\alpha).$$

When $\alpha = \alpha^*$, $\dot{V} = 0$. Also, when $\alpha \in (0, \alpha^*)$, we have $(\alpha^* - \alpha) > 0$, and $\beta(\alpha) < 0$, giving $\dot{V} < 0$. Similarly, when $\alpha \in (\alpha^*, \pi)$, we have $(\alpha^* - \alpha) < 0$ and $\beta(\alpha) > 0$, giving $\dot{V} < 0$. Therefore, the equilibrium α^* is asymptotically stable for all $\alpha \in (0, \pi)$.

Now we will show exponential stability of the equilibrium α^* for all $\alpha \in (\epsilon, \pi)$, where $\epsilon \in (0, \alpha^*)$. Notice that on this interval, if $(\alpha - \alpha^*) < 0$ then $\beta(\alpha) < 0$, and if $(\alpha - \alpha^*) > 0$ then $\beta(\alpha) > 0$. Therefore, we have

$$\dot{V} = -k_\alpha \alpha(\alpha - \alpha^*)\beta(\alpha) = -k_\alpha |\alpha||\alpha - \alpha^*||\beta(\alpha)|.$$

For any $\alpha \in (\epsilon, \pi)$, $|\alpha| > \epsilon$. Also, since $\beta(\alpha)$ has a positive derivative at every point in (ϵ, π), $|\beta(\alpha)| \geq c_1|\alpha - \alpha^*|$, for some $c_1 > 0$. Using these relations, we can write $\dot{V}$ as

$$\begin{aligned}\dot{V} = -k_\alpha \epsilon |\alpha - \alpha^*|(c_1|\alpha - \alpha^*|) &= -c_2|\alpha - \alpha^*|^2 \\ &= -2c_2 V,\end{aligned}$$

where $c_2 = k_\alpha c_1 \epsilon > 0$. Therefore, for every $\epsilon \in (0, \alpha^*)$, α^* is exponentially stable for all $\alpha \in (\epsilon, \pi)$.

Finally, we will show that when $\alpha(t) \to \pm\alpha^*$ as $t \to \infty$, the equilibrium $\rho = 0$ is GES for the ρ dynamics. Consider rewriting the ρ dynamics in (3.4) (adding and subtracting $k_{v_2}\rho\cos\alpha^*$ on the right hand side) as

$$\dot{\rho} = -(k_{v_1} + k_{v_2}\cos\alpha^*)\rho + k_{v2}(\cos\alpha^* - \cos\alpha)\rho.$$

These dynamics can then be rewritten as the linear system

$$\dot{\rho} = [A + B(t)]\rho,$$

where $B(t)$ is the continuous function

$$B(t) = k_{v2}(\cos\alpha^* - \cos\alpha(t))$$

and $A = -(k_{v_1} + k_{v_2}\cos\alpha^*)$ is negative (since $k_{v_1} \geq k_{v_2}$ and $\alpha^* \in (0, \pi)$). Since $\alpha(t) \to \pm\alpha^*$ as $t \to \infty$, we can conclude that $B(t) \to 0$ as $t \to \infty$. Also, the perturbation term $B(t)\rho$ satisfies the inequality $|B(t)\rho| \leq |B(t)||\rho|$. Therefore, again applying Corollary 9.1 and Lemma 9.5 of Khalil [24], the origin of the ρ dynamics is GES.

We have now shown (ii) and (iii) of Theorem 3.2. All that remains is to show (i). From the above analysis we have shown that for every $\alpha \in (-\pi, \pi) \setminus \{0\}$, $\alpha(t) \to \pm\alpha^*$, as $t \to \infty$. Hence the equilibrium $(0, 0)$ is unstable. The only portion of the domain that we have not explored is $(\rho, \alpha) \in \mathbb{R} \times \{0\}$. If $\alpha = 0$ then from (3.4), $\dot{\alpha} = 0$. Also from (3.4), this implies that $\dot{\rho} = -(k_{v_1} + k_{v_2})\rho$, and thus $\rho(t) \to 0$ as $t \to \infty$. Therefore $(\rho(t), \alpha(t)) \to (0, 0)$ as $t \to \infty$ if and only if $(\rho(0), \alpha(0)) \in \mathbb{R} \times \{0\}$. Hence, $(0, 0)$ is a saddle. □

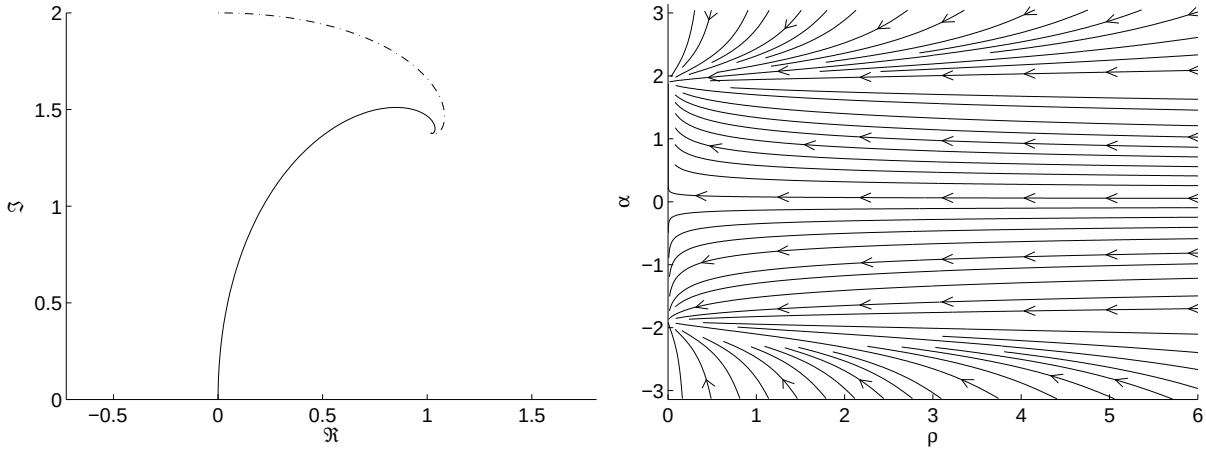

(a) A unicycle (dashed line) and a beetle (solid line) approaching the $(\rho, \alpha) = (0, \alpha^*)$ equilibrium.

(b) The corresponding phase portrait.

Figure 3.8: Case 2. In this plot $(k_{v_1}, k_{v_2}, k_\alpha) = (3, 2, 1)$.

Remark 3.3. For our system, ρ is a distance, and thus has physical significance only when it is non-negative. Since there is an equilibrium point at $\rho = 0$, if $\rho(0)$ is non-negative, then $\rho(t)$ is non-negative for all time (as would be expected).

Figure 3.8 shows the trajectories of a unicycle and beetle as they approach the $(\rho, \alpha) = (0, \alpha^*)$ equilibrium of Case 2.

3.4.3 Case 3 ($k_\alpha < k_{v_2}$ and $k_{v_1} < k_{v_2}$)

In Case 3 there are three types of equilibria; $(\rho, \alpha) = (0, 0)$; if (3.10) is satisfied, then $(\rho, \alpha) = (\rho^*, \pm\alpha^*)$, where $\rho^* \in \mathbb{R}$; and if (3.10) is not satisfied, $(\rho, \alpha) = (0, \pm\alpha^*)$ where $\alpha^* \in (0, \pi)$ satisfies $\sin\alpha^* = \frac{k_\alpha}{k_{v_2}}\alpha^*$. The equilibrium $(0, 0)$ is again a saddle. Looking at the equilibria $(0, \pm\alpha^*)$, the linearization yields (3.18). However, we now have that $k_{v_1} < k_{v_2}$ and so the first diagonal term is negative only if

$$\cos\alpha^* > -\frac{k_{v_1}}{k_{v_2}}. \tag{3.19}$$

Using the argument from Case 2, the second diagonal term is negative for all $\alpha^* \in (0, \pi)$. Therefore, the equilibria $(0, \pm\alpha^*)$ are locally stable if (3.19) is satisfied. We will now

explore the stability properties of these equilibria on the domain $\mathcal{D} = \mathbb{R} \times (-\pi, \pi)$.

Theorem 3.4. *Consider gains satisfying $k_\alpha < k_{v_2}$ and $k_{v_1} < k_{v_2}$, but for which (3.10) is not satisfied. Then the equilibria of (3.4) on $\mathcal{D}$ are: $(0,0)$, $(0,\alpha^*)$, and $(0,-\alpha^*)$, where $\alpha^* \in (0,\pi)$ depends on the gains. The equilibrium (0,0) is a saddle. The equilibria $(\rho,\alpha) = (0,\pm\alpha^*)$ have the following stability properties provided*

$$\cos\alpha^* > -\frac{k_{v_1}}{k_{v_2}} \tag{3.20}$$

is satisfied:

(i) For every $\epsilon \in (0,\alpha^*)$, the equilibrium $(\rho,\alpha) = (0,\alpha^*)$ is exponentially stable on the domain $\mathbb{R}\times(\epsilon,\pi)$. On the domain $\mathbb{R}\times(0,\pi)$, the equilibrium $(0,\alpha^*)$ is asymptotically stable.

(ii) For every $\epsilon \in (-\alpha^*,0)$, the equilibrium $(\rho,\alpha) = (0,-\alpha^*)$ is exponentially stable on the domain $\mathbb{R} \times (-\pi,\epsilon)$. On the domain $\mathbb{R} \times (-\pi,0)$, the equilibrium $(0,-\alpha^*)$ is asymptotically stable.

If (3.20) is not satisfied, $(0,\pm\alpha^*)$ are unstable.

Proof. The proof of this is identical to that for Theorem 3.2. □

Figure 3.9 shows the trajectories of the system as they approach the equilibrium $(0,-\alpha^*)$, of Case 3. Figure 3.10 shows the unstable spiral that results in Case 3 when (3.19) is not satisfied.

The other possibility for Case 3 is that (3.10) is satisfied. In this case the equilibria are $(0,0)$ and $(\rho^*,\pm\alpha^*)$, with $\alpha^* \in (0,\pi)$, where α^* and the gains satisfy

$$\sin\alpha^* = \frac{k_\alpha}{k_{v_2}}\alpha^* \quad \text{and} \quad \cos\alpha^* = -\frac{k_{v_1}}{k_{v_2}}.$$

The equilibrium $(0,0)$ is still a saddle. By linearizing (3.4) about (ρ^*,α^*) or $(\rho^* - \alpha^*)$, and substituting in the expression for $\cos\alpha^*$, the A matrix drops rank and thus the

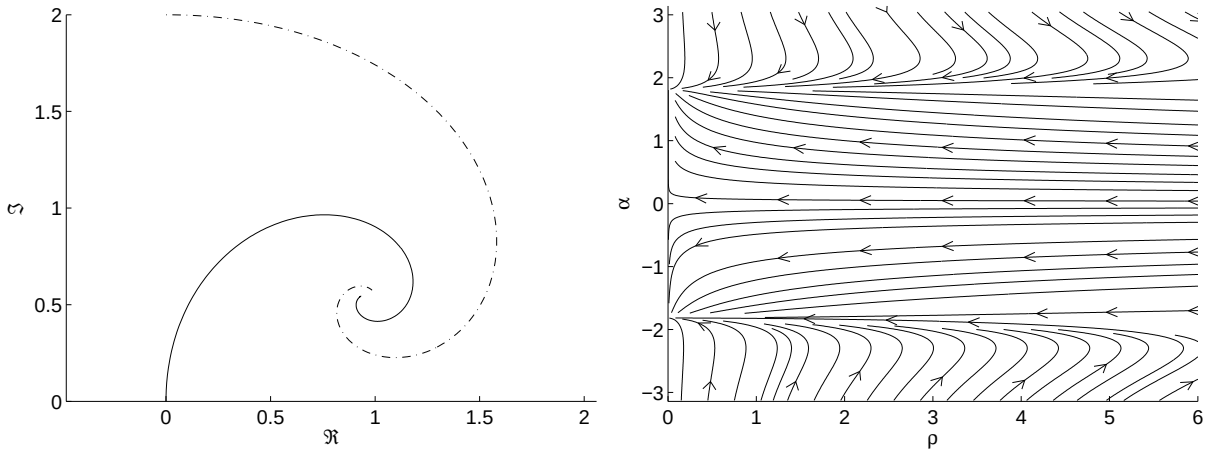

(a) A unicycle (dashed line) and a beetle (solid line) approaching the $(\rho, \alpha) = (0, \alpha^*)$ equilibrium.

(b) The corresponding phase portrait.

Figure 3.9: Case 3. In this plot $(k_{v_1}, k_{v_2}, k_\alpha) = (1, 1.5, 0.8)$.

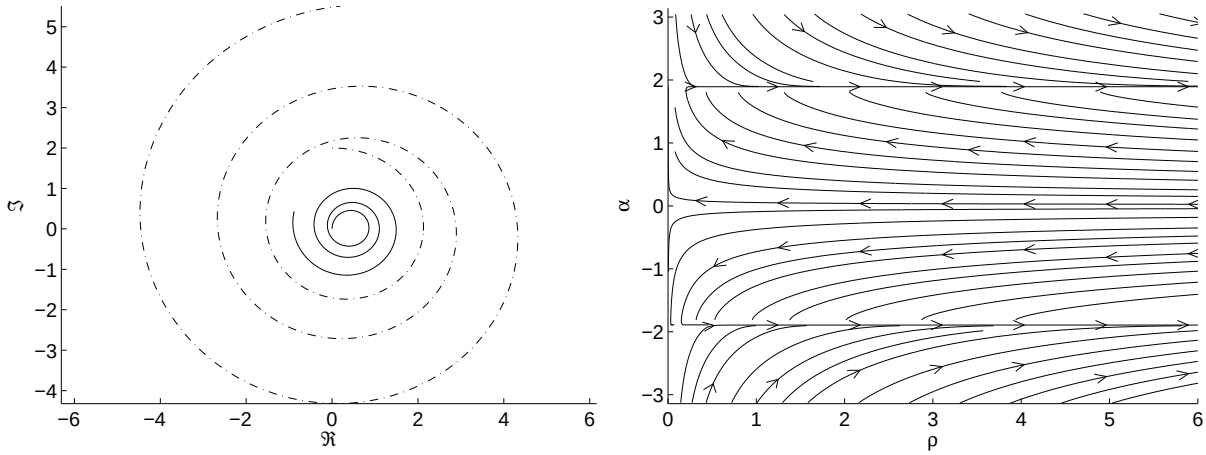

(a) A unicycle (dashed line) and a beetle (solid line) spiraling out to infinity.

(b) The corresponding phase portrait.

Figure 3.10: Case 3. In this plot $(k_{v_1}, k_{v_2}, k_\alpha) = (0.5, 2, 1)$ and thus $\cos\alpha^* < -k_{v_1}/k_{v_2}$.

linearization tells us nothing about the stability of the equilibrium. However, by studying the α dynamics we arrive upon the following result.

Theorem 3.5. *Suppose k_{v_1}, k_{v_2}, k_α, α^* satisfy $k_\alpha < k_{v_2}$, $k_{v_1} < k_{v_2}$, and*

$$e^{j\alpha^*} = \frac{1}{k_{v_2}}(-k_{v_1} + jk_\alpha\alpha^*), \quad \alpha^* \in (\pi/2, \pi).$$

The resulting equilibria $(\rho^*, \pm\alpha^*)$, $\rho^* \in \mathbb{R}$, of (3.4) have the following stability properties:

(i) For every $\epsilon \in (0, \alpha^*)$, the equilibrium $(\rho, \alpha) = (\rho^*, \alpha^*)$ is exponentially stable on the domain $\mathbb{R} \times (\epsilon, \pi)$.

(ii) For every $\epsilon \in (-\alpha^*, 0)$, the equilibrium $(\rho, \alpha) = (\rho^*, -\alpha^*)$ is exponentially stable on the domain $\mathbb{R} \times (-\pi, \epsilon)$.

In addition, if $\rho(0) \in \mathbb{R}^+$ then $\rho(t) \to c \in \mathbb{R}^+$ as $t \to \infty$.

Proof. We begin by looking at the α dynamics which are given by $\dot{\alpha} = k_{v_2} \sin\alpha - k_\alpha\alpha$. We know from Theorem 3.4 that if $\alpha(0) \in (0, \pi)$ then $\alpha(t) \to \alpha^*$ as $t \to \infty$, and if $\alpha(0) \in (-\pi, 0)$ then $\alpha(t) \to -\alpha^*$ as $t \to \infty$. Since the α dynamics is anti-symmetric, we can again determine the behavior of both α^* and $-\alpha^*$ by studying the equilibrium α^*. When α converges to α^*, $\dot{\rho} \to 0$ since

$$\dot{\rho}(\alpha^*) = -\rho(k_{v_1} + k_{v_2}\cos\alpha^*) = 0.$$

It remains to be shown that this implies that ρ tends to a constant (i.e., ρ does not tend to infinity). We begin by fixing ϵ as some value in the set $(0, \alpha^*)$. Using the definition of α^*, we have $k_{v_1} = -k_{v_2}\cos\alpha^*$, and the ρ dynamics in (3.4) can be written as

$$\dot{\rho} = k_{v_2}\rho\left(\cos\alpha^* - \cos(\alpha(t))\right).$$

Solving for $\rho(t)$ we obtain

$$\rho(t) = C\exp\left(k_{v_2}\int_0^t (\cos\alpha^* - \cos(\alpha(\tau)))d\tau\right), \quad C \in \mathbb{R}.$$

Therefore, as $t \to \infty$, $\rho(t) \to c \in \mathbb{R}$, if

$$\int_0^\infty |\cos\alpha^* - \cos(\alpha(\tau))|\, d\tau < \infty. \tag{3.21}$$

That is, $\rho(t)$ tends to a constant if $\cos\alpha^* - \cos(\alpha(\tau))$ is L_1-integrable. From Theorem 3.4, we know that for every $\epsilon \in (0, \alpha^*)$, and for every $\alpha(0) \in (\epsilon, \pi)$, $\alpha(t)$ converges to α^* exponentially. That is, there exist positive constants k_1 and λ such that

$$|\alpha^* - \alpha(t)| \leq k_1 |\alpha^* - \alpha(0)| \mathrm{e}^{-\lambda t}, \quad \forall\, \alpha(0) \in (\epsilon, \pi).$$

Therefore $\alpha^* - \alpha(t)$ is L_1-integrable which implies that

$$\int_0^\infty |\alpha^* - \alpha(\tau)| d\tau < \infty.$$

But, this implies that $\cos(\alpha^*) - \cos(\alpha(t))$ must also be L_1-integrable, since there exists a positive constant k_2 such that $|\cos\alpha^* - \cos\alpha| \leq k_2 |\alpha^* - \alpha|$, $\forall \alpha \in (\epsilon, \pi)$ (In fact, since $\alpha^* \in (0, \pi)$, we can choose $k_2 = 1$). This is shown in Figure 3.11. Therefore, (3.21) is satisfied, and so $\rho(t)$ converges to a constant. In addition, since (3.21) is satisfied, if $\rho(0) \in \mathbb{R}^+$ then $\rho(t) \to c \in \mathbb{R}^+$ as $t \to \infty$. □

In Theorem 3.5 we have shown that if (3.10) is satisfied, $\rho(0)$ is positive, and $\alpha(0)$ is non-zero, then the agents converge to concentric circles. Figure 3.12 shows the trajectories of the beetle-unicycle system as they approach the equilibrium (ρ^*, α^*) of Case 3.

3.5 Summary

In this chapter we have analyzed a beetle and unicycle in cyclic pursuit. A global stability analysis has been performed based on the selection of the linear velocity gain of the beetle and the linear and angular velocity gains of the unicycle. By varying these gains several interesting phenomenon can be achieved. The agents can spiral in to a point, out to infinity, or converge to concentric circles.

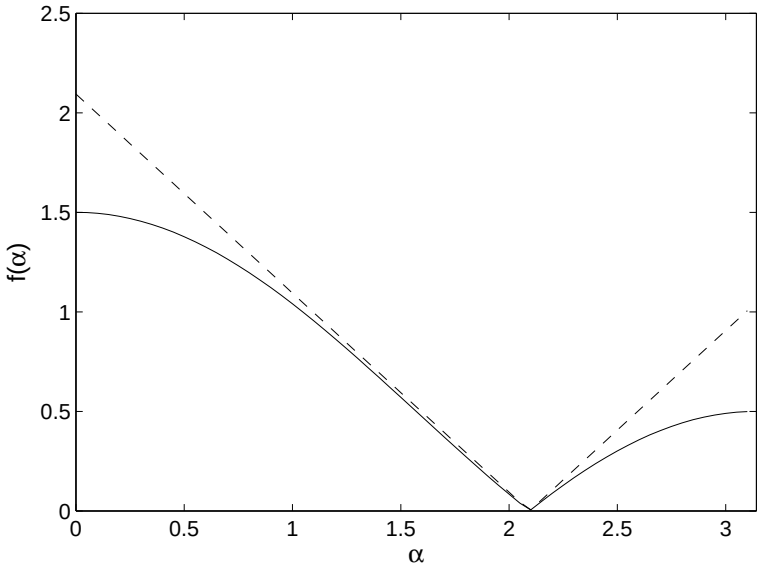

Figure 3.11: The dashed line shows the function $f(\alpha) = |\alpha^* - \alpha|$, and the solid line, $f(\alpha) = |\cos\alpha^* - \cos\alpha|$. It is clear that $|\cos\alpha^* - \cos\alpha| \leq |\alpha^* - \alpha|$, $\forall\alpha \in [0, \pi]$. In this plot $\alpha^* = 2\pi/3$.

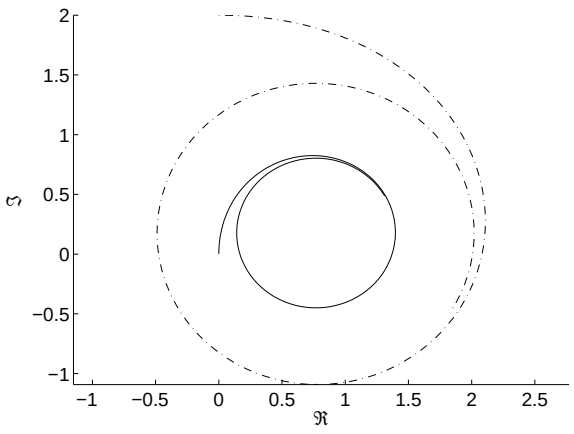

(a) A unicycle (dashed line) and a beetle (solid line) in the $(\rho, \alpha) = (\rho^*, \alpha^*)$ equilibrium.

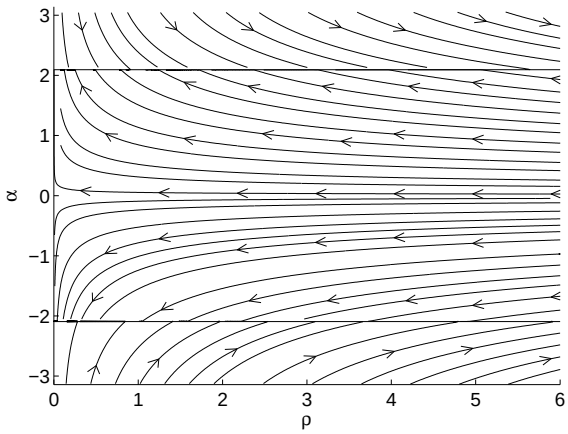

(b) The corresponding phase portrait. Notice that all trajectories go the horizontal lines at $+2\pi/3$ and $-2\pi/3$.

Figure 3.12: Case 3. In this plot $(k_{v_1}, k_{v_2}, k_\alpha) = (1, 2, \frac{3\sqrt{3}}{2\pi})$, and the final angle is $\alpha^* = 2\pi/3$.

Chapter 4

Curve shortening applied to multi-agent systems

If a smooth, closed, and embedded curve is deformed along its normal vector field at a rate proportional to its curvature it shrinks to a circular point. This curve evolution is called Euclidean curve shortening and the result is known as the Gage-Hamilton-Grayson Theorem. Motivated by the rendezvous problem in multi-agent systems, we address the problem of creating a polygon shortening flow. A simple linear scheme is proposed which exhibits several analogues to Euclidean curve shortening. The polygon shrinks to an elliptical point; convex polygons remain convex, and; the perimeter of the polygon is monotonically decreasing.

4.1 Introduction

The rendezvous problem addressed in this chapter can be stated as follows; given a group of n agents whose positions are represented in the complex plane by $z_i = x_i + jy_i$, $i = 1, \ldots, n$, $j = \sqrt{-1}$, and whose dynamics are given by $\dot{z}_i = u_i$, find a local control strategy that will ensure convergence of all z_i's to a point. Some approaches to this problem, as well as a new solution based on hierarchy, were presented in Chapter 2. In

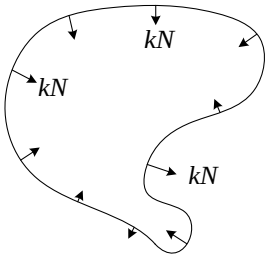

Figure 4.1: The Euclidean curve shortening flow.

this chapter we propose a strategy which solves this problem with a fixed communication topology. The strategy is motivated by the theory of curve shortening. Because of this, the formation of the group of agents as they converge to a common point has properties which are analogous to the curve shortening theory.

Consider a family of smooth, closed curves $\mathbf{x}(p,t)$ lying in the plane. Here, p parameterizes the points along each individual curve, and t parameterizes the family of curves (i.e., the initial curve $\mathbf{x}(p,0)$ evolves as a function of time to $\mathbf{x}(p,t)$). The *Euclidean curve shortening* flow is given by

$$\frac{\partial \mathbf{x}}{\partial t}(p,t) = k(p,t)\mathbf{N}(p,t), \tag{4.1}$$

where $k(p,t)$ is the Euclidean curvature, and $\mathbf{N}(p,t)$ is the inner Euclidean normal. Hence, if a curve evolves according to (4.1), it is deformed along its normal vector field at a rate proportional to its curvature. Intuitively, the curvature at a point on a curve is the inverse of the radius of the largest tangent circle to the curve (on the concave side) at the point. The Euclidean curve shortening flow is depicted in Figure 4.1. We also define $L(t)$ to be the length of the curve at time t, and $A(t)$ the area enclosed by the curve. The isoperimetric inequality [40] states that

$$\frac{L(t)^2}{A(t)} \geq 4\pi.$$

Equality is achieved if and only if the curve is a circle. Therefore, the ratio L^2/A gives a measure of "how circular" the curve is. In 1983, Gage [13] showed that when a convex

curve evolves according to (4.1), $A(t) \to 0$, and the ratio L^2/A is decreasing. In 1984, Gage [14] showed that under (4.1), if the curvature does not blow up prematurely (i.e., a cusp does not form) then for a convex curve $L^2/A \to 4\pi$ and the curve shrinks to a circular point. The term "circular point" means that the curve is collapsing to a point, and if we zoom in on the curve as it is collapsing, the curve is becoming circular. In 1986 Gage and Hamilton [15] showed that for convex curves evolving according to (4.1) the curvature does not blow up prematurely, and in 1987, Grayson [18] showed that any embedded (non-self-intersecting) curve shrinks to a circular point. The Euclidean curve shortening flow also has the property that it shrinks the length of the curve $L(t)$ as fast as possible using only local information [19]. The notion of shrinking "as fast as possible" will be clarified later.

The Euclidean curve shortening flow is defined in terms of the Euclidean curvature and the Euclidean normal. These quantities are invariant under Euclidean transformations (i.e., rotations, translations, and reflections). In application, curve shortening can be used to smooth an image. However, the image may have undergone a geometric viewing transformation in the capturing process. Because of this, there has been interest in flows which are invariant under various groups of viewing transformations. We say that a flow is invariant under a transformation if the flow and transformation commute. One such transformation is called an *affine transformation*. Sapiro and Tannenbaum [45] create a new curve shortening flow which is defined in terms of quantities that are invariant under affine transformations. This flow is called the *affine curve shortening flow*. In [45] it is shown that if a smooth convex curve evolves according to the affine curve shortening flow, the curve shrinks to an elliptical point. In [1] this result is extended to smooth embedded curves (not necessarily convex). For a complete account of many of the results of curve shortening see [9].

The elegant results obtained in the curve shortening literature have motivated research in creating discrete analogues of the flows; that is, to create a shortening flow for polygons

which exhibits similar attributes to the Euclidean (or affine) curve shortening flow. This research has been driven by both theoretical interest [4, 22, 34], and by applications such as crystal growth [44]. In [4], the evolution of planar polygons is studied in discrete time. An affine polygon shortening scheme is proposed and it is shown that it shrinks polygons to elliptical points. This means that the vertices are collapsing to a point, and if we zoom in on the polygon as it is collapsing, the vertices are converging to an ellipse. In addition, two Euclidean polygon shortening schemes are proposed. In [22] a polygon shortening scheme based on the Menger-Melnikov curvature [32] is studied. It is shown that under this scheme most quadrilaterals shrink to circular points. In [34] a discrete curve shortening equation is developed which tends to (4.1) as the number of points tends to infinity. The main results in this paper are that the area inclosed by the polygon vanishes in finite time, and the perimeter monotonically decreases.

There are two contributions of this chapter. The first is to introduce the problem of polygon shortening as it relates to multi-agent systems and the rendezvous problem. The second is to study a polygon consisting of vertices $z_1, \ldots, z_n$ as it evolves according to

$$\dot{z}_i = \frac{1}{2}(z_{i+1} - z_i) + \frac{1}{2}(z_{i-1} - z_i). \tag{4.2}$$

Intuitively, when a polygon evolves according to (4.2), each vertex chases the centroid of its two neighboring vertices. This scheme is studied in discrete time in [4], where it is referred to as an affine polygon shortening scheme. In this chapter we show the following properties of this scheme: 1) Polygons shrink to elliptical points, 2) Convex polygons remain convex, 3) If vertices are arranged in a star formation about their centroid, they will remain in a star formation for all time (i.e, the vertices (agents) will not collide) 4) The perimeter of the polygon is a monotonically decreasing function of time.

This chapter is organized as follows. In Section 4.2 we give a more detailed development of Euclidean and affine curve shortening including a review of pertinent topics in geometry and differential geometry. In Section 4.3 we give two polygon shortening

schemes, shortening by Menger-Melnikov curvature, and linear scheme (4.2). In Sections 4.4 and 4.5 we show that under (4.2) star formations are invariant and that convex polygons remain convex. Finally, in Section 4.6 we derive the optimal direction for perimeter shortening and show that under (4.2) the perimeter of the polygon is monotonically decreasing.

4.2 Background

In this section we will give some background on Euclidean and affine geometry and derive the Euclidean and affine curve shortening flows. The sections on Euclidean and affine geometry follow the development of [3], and the proofs of the theorems can be found within. The section on Euclidean curve shortening follows [20]. A more thorough treatment of affine differential geometry and affine curve shortening can be found in [5, 35, 45].

4.2.1 Euclidean geometry

A *Euclidean transformation* of $\mathbb{R}^2$ is a function $L : \mathbb{R}^2 \to \mathbb{R}^2$ of the form

$$L(\mathbf{x}) = U\mathbf{x} + a,$$

where U is an orthogonal 2×2 matrix and $a \in \mathbb{R}^2$. Recall that a matrix U is orthogonal if $U^{-1} = U^T$ (where ^{T} denotes transpose), which is equivalent to saying that the columns of U are orthonormal. The set of all Euclidean transformations of $\mathbb{R}^2$ is denoted $E(2)$ and is the set of all rotations, translations, and reflections of a figure in $\mathbb{R}^2$. Roughly speaking, *Euclidean geometry* is the study of properties of figures which remain unchanged by Euclidean transformations. These properties are called *Euclidean properties*, and include distance, angle, curvature, and collinearity of points. From this we will now introduce the concept of congruence.

Definition 4.1. A figure F_1 is *Euclidean-congruent* to a figure F_2 if there is a Euclidean transformation which maps F_1 onto F_2.

A few examples of sets of figures which are Euclidean-congruent to each other are: The set of all line segments of a fixed length, and the set of all squares of a fixed area. It can easily be verified that Euclidean-congruence is an equivalence relation, and thus the previous sets are equivalence classes.

4.2.2 Euclidean curve shortening

Consider a family of smooth closed curves $\mathbf{x}(p,t) : [0,1] \times [0,\tau] \to \mathbb{R}^2$, where $p \in [0,1]$ parameterizes the curve, and $t \in [0,\tau]$ the family. For now we fix t and study a single curve $\mathbf{x}(p)$. The tangent vector to the curve is given by $d\mathbf{x}/dp =: \dot{\mathbf{x}}$ and thus we define the unit tangent as $\mathbf{T}(p) := \dot{\mathbf{x}}/\|\dot{\mathbf{x}}\|$. Introducing coordinates in $\mathbb{R}^2$ we can write $\mathbf{x}(p) = (x_1(p), x_2(p))$. The unit tangent is $(\dot{x}_1, \dot{x}_2)/\|\dot{\mathbf{x}}\|$ and the unit normal is then given by $\mathbf{N}(p) := (-\dot{x}_2, \dot{x}_1)/\|\dot{\mathbf{x}}\|$. When $\mathbf{T}$ runs in the counterclockwise direction around the curve, $\mathbf{N}$ is the inner unit normal.

It is convenient and customary to use arc-length to describe distance around the curve instead of p. The Euclidean arc-length s is defined via $ds := \|\dot{\mathbf{x}}\|dp$. We can re-parameterize the curve by s as $\mathbf{x}(s) = (x_1(s), x_2(s))$. The unit tangent and normal vectors can be written in terms of s as

$$\mathbf{T}(s) = (x_1', x_2'), \quad \text{and} \quad \mathbf{N}(s) = (-x_2', x_1'),$$

where $'$ denotes differentiation with respect to s. Using column vector notation we define

$$A(s) := \begin{bmatrix} \mathbf{T}^T \\ \mathbf{N}^T \end{bmatrix} = \begin{bmatrix} x_1' & x_2' \\ -x_2' & x_1' \end{bmatrix}.$$

The matrix $A(s)$ is a rotation matrix which rotates the standard basis to the coordinate frame $\mathbf{T}, \mathbf{N}$ attached to the curve. Differentiating $A(s)$ we get

$$A' = A'A^{-1}A =: C(s)A. \tag{4.3}$$

Now, since A is a rotation matrix it is orthogonal and so $A^TA = AA^T = I$. Using this, we can show that $C(s)$ is skew-symmetric as follows. Differentiating the expression $I = AA^T$ we obtain

$$0 = (AA^T)' = A'A^T + A(A^T)' = A'A^{-1} + (A^{-1})^T(A')^T = A'A^{-1} + (A'A^{-1})^T,$$

which implies that $C(s) = -C(s)^T$. Computing $C(s)$ and using the fact that it is a skew symmetric matrix we get

$$C(s) = \begin{bmatrix} 0 & k(s) \\ -k(s) & 0 \end{bmatrix}, \tag{4.4}$$

where the curvature $k(s)$ is given by

$$k(s) := x_1'x_2'' - x_1''x_2' = \det(\mathbf{x}', \mathbf{x}''),$$

and $\det(\cdot,\cdot)$ denotes the determinant of the 2×2 matrix created by the two 2×1 vectors. Since $ds = \|\dot{\mathbf{x}}\|dp$ we can also write k in terms of the parameter p as $k(p) = (\dot{\mathbf{x}}, \ddot{\mathbf{x}})/\|\dot{\mathbf{x}}\|^3$. From (4.3) and (4.4) we obtain the Frenet equation:

$$\frac{d\mathbf{T}}{ds} = k\mathbf{N}$$
$$\frac{d\mathbf{N}}{ds} = -k\mathbf{T}.$$

The curvature of the curve $\mathbf{x}(s)$ is given by $k(s)$ and the radius of curvature is defined to be $1/|k(s)|$.

In the Euclidean curve shortening flow the curve $\mathbf{x}(p,t)$ is deformed along its unit normal vector $\mathbf{N}(p,t)$ at a rate proportional to its curvature $k(p,t)$. This can be written as

$$\frac{\partial \mathbf{x}}{\partial t}(p,t) = k(p,t)\mathbf{N}(p,t).$$

Using the Frenet equation we have $k\mathbf{N} = d\mathbf{T}/ds = d^2\mathbf{x}/ds^2$. Therefore the Euclidean curve shortening flow can be written as

$$\frac{\partial \mathbf{x}}{\partial t}(p,t) = \frac{\partial^2 \mathbf{x}}{\partial s^2}(p,t). \tag{4.5}$$

The equation (4.5) is called the *heat equation* or *diffusion equation.* (Note: in this equation, on the right hand side, p is a function of s.)

To clarify the concepts introduced on the Euclidean curve shortening flow, we will carry out a calculation of the curve shortening flow for a very simple example. It should be noted that since the governing equation is a partial differential equation, completing an example for a generalized curve is a very difficult task.

Example 4.2 (Euclidean curve shortening)**.** Consider a circle which is fixed at the origin and whose parametric equation is given by

$$\mathbf{x}(p,t) = a(t)\left(\cos(2\pi p), \sin(2\pi p)\right), \quad p \in [0,1], \tag{4.6}$$

where $a(0) > 0$ is the radius of the circle at $t = 0$. We will compute the curve shortening flow for this circle using two methods; first using the parameter $p \in [0,1]$, and then using the arc-length s, where $ds = \|\dot{\mathbf{x}}\|dp$. We begin by using the parameter p and the expression for the curve shortening flow in (4.1). We have

$$\frac{\partial \mathbf{x}}{\partial p} = 2\pi a(t)(-\sin(2\pi p), \cos(2\pi p)),$$

and thus

$$\|\dot{\mathbf{x}}\| = \left\|\frac{\partial \mathbf{x}}{\partial p}\right\| = 2\pi a(t). \tag{4.7}$$

The tangent vector is given by

$$\mathbf{T}(p) = \frac{1}{\|\dot{\mathbf{x}}\|}\frac{\partial \mathbf{x}}{\partial p} = (-\sin(2\pi p), \cos(2\pi p)),$$

and thus the inner normal is given by

$$\mathbf{N}(p) = (-\cos(2\pi p), -\sin(2\pi p)).$$

The curvature $k(p,t)$ is given by

$$\begin{aligned} k(p,t) &= \det(\dot{\mathbf{x}}, \ddot{\mathbf{x}})/\|\dot{\mathbf{x}}\|^3 \\ &= \frac{1}{(2\pi a)^3} \begin{vmatrix} -2\pi a \sin(2\pi p) & -(2\pi)^2 a \cos(2\pi p) \\ 2\pi a \cos(2\pi p) & -(2\pi)^2 a \sin(2\pi p) \end{vmatrix} \\ &= \frac{1}{a}(\sin^2(2\pi p) + \cos^2(2\pi p)) = \frac{1}{a(t)}. \end{aligned}$$

Therefore, from (4.1) we have

$$\begin{aligned} \frac{\partial \mathbf{x}}{\partial t}(p,t) &= k(t)\mathbf{N}(p) \\ \frac{da(t)}{dt}\left(\cos(2\pi p), \sin(2\pi p)\right) &= \frac{1}{a(t)}(-\cos(2\pi p), -\sin(2\pi p)) \end{aligned}$$

And therefore the flow is given by

$$\frac{da(t)}{dt} = -\frac{1}{a(t)}.$$

Solving this we obtain

$$a(t) = (a(0)^2 - 2t)^{1/2}, \tag{4.8}$$

and so the circle will collapse to a point in finite time.

Equation (4.8) can also be calculated by using (4.5) and the Euclidean arc-length s. To begin, we would like to calculate $s(p)$. Using the relation $ds = \|\dot{\mathbf{x}}\|dp$, the expression in (4.7), and letting $s(0) = 0$, we have

$$s(p) = 2\pi a(t)p.$$

Combining the expression for $s(p)$ and (4.6) we can write the curve as

$$\mathbf{x}(s,t) = a\left(\cos(s/a), \sin(s/a)\right), \quad s \in [0, 2\pi a].$$

The tangent vector is given by

$$\mathbf{T}(s,t) = \frac{\partial \mathbf{x}(s,t)}{\partial s} = \left(-\sin(s/a), \cos(s/a)\right).$$

Differentiating $\mathbf{T}(s,t)$ we obtain

$$\frac{\partial^2 \mathbf{x}(s,t)}{\partial s^2} = \frac{1}{a(t)} \left(-\cos(s/a), -\sin(s/a)\right).$$

Finally we can write this in terms of p as

$$\frac{\partial^2 \mathbf{x}(p,t)}{\partial s^2} = \frac{1}{a(t)} \left(-\cos(2\pi p), -\sin(2\pi p)\right).$$

Combining this with the curve shortening flow in (4.5) we again obtain (4.8). ◀

4.2.3 Shrinking the length optimally

In [19] it is stated that the length, $L(t)$, of a curve which is evolving according to the Euclidean curve shortening flow is shrinking as fast as possible using only local information. To see why and in what sense this is true, consider the following. We can write the perimeter at a fixed time t as

$$L(t) = \int_0^{L(t)} ds = \int_0^1 \left\| \frac{\partial \mathbf{x}}{\partial p} \right\| dp, \tag{4.9}$$

since the arc-length element is $ds = \|\dot{\mathbf{x}}\| dp$. In order to take the time derivative of this expression, first consider taking the time derivative of $\|\partial \mathbf{x}/\partial p\|^2$:

$$\frac{\partial}{\partial t} \left\| \frac{\partial \mathbf{x}}{\partial p} \right\|^2 = \frac{\partial}{\partial t} \left\langle \frac{\partial \mathbf{x}}{\partial p}, \frac{\partial \mathbf{x}}{\partial p} \right\rangle = 2 \left\langle \frac{\partial \mathbf{x}}{\partial p}, \frac{\partial}{\partial p} \frac{\partial \mathbf{x}}{\partial t} \right\rangle,$$

where $\langle \cdot\, , \cdot \rangle$ is the inner product (for $u, v \in \mathbb{R}^n$, $\langle u, v \rangle = u^T v$). We also have that

$$\frac{\partial}{\partial t} \left\| \frac{\partial \mathbf{x}}{\partial p} \right\|^2 = 2 \left\| \frac{\partial \mathbf{x}}{\partial p} \right\| \frac{\partial}{\partial t} \left(\left\| \frac{\partial \mathbf{x}}{\partial p} \right\| \right).$$

Therefore, combining these expressions and using the notation $\|\partial \mathbf{x}/\partial p\| = \|\dot{\mathbf{x}}\|$, we have

$$\frac{\partial}{\partial t} \left(\left\| \frac{\partial \mathbf{x}}{\partial p} \right\| \right) = \frac{1}{\|\dot{\mathbf{x}}\|} \left\langle \frac{\partial \mathbf{x}}{\partial p}, \frac{\partial}{\partial p} \frac{\partial \mathbf{x}}{\partial t} \right\rangle,$$

and thus using (4.9)

$$\frac{dL}{dt} = \int_0^1 \frac{1}{\|\dot{\mathbf{x}}\|} \left\langle \frac{\partial \mathbf{x}}{\partial p}, \frac{\partial}{\partial p} \frac{\partial \mathbf{x}}{\partial t} \right\rangle dp.$$

Now,

$$\frac{1}{\|\dot{\mathbf{x}}\|}\frac{\partial \mathbf{x}}{\partial p} = \frac{1}{\|\dot{\mathbf{x}}\|}\frac{\partial s}{\partial p}\frac{\partial \mathbf{x}}{\partial s} = \frac{\partial \mathbf{x}}{\partial s},$$

since $ds = \|\dot{\mathbf{x}}\|dp$. This gives us

$$\frac{dL}{dt} = \int_0^1 \left\langle \frac{\partial \mathbf{x}}{\partial s}, \frac{\partial}{\partial p}\frac{\partial \mathbf{x}}{\partial t} \right\rangle dp.$$

Integrating by parts we obtain

$$\frac{dL}{dt} = \left\langle \frac{\partial \mathbf{x}}{\partial s}, \frac{\partial \mathbf{x}}{\partial t} \right\rangle \Big|_0^1 - \int_0^1 \frac{\partial}{\partial p}\left(\frac{\partial \mathbf{x}}{\partial s}\right)^T \frac{\partial \mathbf{x}}{\partial t} dp.$$

The first term on the right hand side is zero, since the curve is smooth and $\mathbf{x}(0,t) = \mathbf{x}(1,t)$. Then, since

$$\frac{\partial}{\partial p} = \frac{\partial s}{\partial p}\frac{\partial}{\partial s},$$

we get

$$\frac{dL}{dt} = -\int_0^L \left(\frac{\partial^2 \mathbf{x}}{\partial s^2}\right)^T \frac{\partial \mathbf{x}}{\partial t} ds.$$

Finally, since $\partial \mathbf{x}/\partial s = \mathbf{T}$ and $\partial \mathbf{T}/\partial s = k\mathbf{N}$, we have

$$\frac{dL}{dt} = -\int_0^L \left\langle k\mathbf{N}, \frac{\partial \mathbf{x}}{\partial t} \right\rangle ds \tag{4.10}$$

Therefore, the direction of $\partial \mathbf{x}/\partial t$ in which $L(t)$ is decreasing most rapidly is $\partial \mathbf{x}/\partial t = k\mathbf{N}$, which is Euclidean curve shortening (see (4.1)). Note that this flow is optimal in the sense that the velocity of the curve at each point always points in the direction which maximizes the rate of decrease of $L(t)$. However, the magnitude of the velocity of the curve at each point is not in general the speed which maximizes the rate of decrease of $L(t)$.

4.2.4 Affine geometry

The following sections provide an introduction to affine geometry, affine differential geometry, and affine curve shortening. While the results of these sections are not directly applied in this chapter, there are two reasons for their inclusion. The first is that the work in [4], which was a motivation for the work in this chapter, is based on affine curve

shortening. The second is that limiting shape for both the linear scheme proposed in this chapter, and the affine curve shortening flow, is an elliptical point.

A *general affine transformation* of $\mathbb{R}^2$ is a function $L : \mathbb{R}^2 \to \mathbb{R}^2$ of the form

$$L(x) = A\mathbf{x} + b, \tag{4.11}$$

where A is a real invertible 2×2 matrix and $b \in \mathbb{R}^2$. Notice that every Euclidean transformation of $\mathbb{R}^2$ is an affine transformation of $\mathbb{R}^2$ since every orthogonal matrix is invertible. Affine transformations

(i) map straight lines to straight lines;

(ii) map parallel straight lines to parallel straight lines;

(iii) preserve ratios of lengths along a given straight line.

Another interesting property of affine transformations is stated in the following theorem.

Theorem 4.3. *Let p, q, r and p', q', r' be two sets of three non-collinear points in $\mathbb{R}^2$. Then*

(i) there is an affine transformation L which maps p, q, r to p', q', r', respectively;

(ii) the affine transformation L is unique.

An immediate corollary of this theorem is that all triangles are affine-congruent (in analogy with Definition 4.1). That is, given a triangle, the set of all possible triangles can be created by affine transformations of the original triangle.

Yet another interesting feature of affine transformations is their effect on non-degenerate conic sections. *Conic* is the name given to a shape that is obtained by taking a plane slice of the double cone. *Non-degenerate conic sections* are parabolas, hyperbolas, and ellipses (note that a circle is just a special case of an ellipse). Some properties of conics are:

(i) Every ellipse is affine-congruent to the unit circle with equation $x^2 + y^2 = 1$.

(ii) Every hyperbola is affine-congruent to the rectangular hyperbola with equation $xy = 1$.

(iii) Every parabola is affine-congruent to the parabola with equation $y^2 = x$.

(iv) Affine transformations map ellipses to ellipses, parabolas to parabolas, and hyperbolas to hyperbolas.

From this description we can see that Euclidean properties are not preserved (or invariant) under a general affine transformation. For example, the distance between two points after an affine transformation can become larger or smaller, or the angles between the sides of a triangle can change (since all triangles are affine-congruent). Also note that the Euclidean curvature is not invariant since an ellipse, whose curvature at a point (x, y) on the ellipse is a function of x and y, is affine-congruent to a circle, which has constant curvature.

The final result that we require from affine geometry is stated in the following theorem:

Theorem 4.4. *Let L be an affine transformation, and let $\mathbf{T}$ be a tangent to a conic C. Then $L(\mathbf{T})$ is a tangent to the conic $L(C)$.*

It turns out that this result holds for any smooth curve. The importance of this result can be seen when considering the Frenet frame attached to a smooth curve $\mathbf{x}$. This frame consists of the tangent vector $\mathbf{T}$, and a perpendicular normal vector $\mathbf{N}$. Consider transforming $\mathbf{x}$ via an affine transformation L, to $L(\mathbf{x})$. From the previous result, $L(\mathbf{T})$ will be a tangent to $L(\mathbf{x})$. However, $L(\mathbf{N})$ will not, in general, be perpendicular to $L(\mathbf{T})$ because an affine transformation does not, in general, preserve the angle between vectors.

The Euclidean curve shortening flow is invariant under Euclidean transformations. The curve may be rotated or translated, but the evolution of the curve will remain the same. However, if the curve undergoes a general affine transformation, the curvature of

$$\begin{array}{ccc} \mathbf{x}(p,0) & \xrightarrow{flow} & \mathbf{x}(p,t) \\ \downarrow L & & \downarrow L \\ L(\mathbf{x}(p,0)) & \xrightarrow{flow} & L(\mathbf{x}(p,t)) \end{array}$$

Figure 4.2: A flow which is invariant under a transformation L.

the curve will change, the normal vector will no longer be normal to the curve, and thus the evolution will be drastically changed. The goal of affine curve shortening is to find a flow which is invariant under affine transformations. See Figure 4.2. We will look at this in more depth in the next section.

4.2.5 Affine differential geometry

For affine curve evolution we will restrict ourselves to *equiaffine geometry*, also called the group of *special affine motions*, in which the matrix A of (4.11) satisfies $\det(A) = 1$ (that is, $A \in SL_2(\mathbb{R})$). What this restriction means is that under any equiaffine transformation, the unit square will be transformed into a parallelogram with area 1. Therefore, equiaffine transformations are area preserving. With this in mind, consider a smooth closed curve $\mathbf{x}(p,t) : [0,1] \times [0,\tau] \to \mathbb{R}^2$, where $p \in [0,1]$ parameterizes the curve. We would like to attach two vectors to the curve, which create a coordinate system, such that there exists a relationship between the vectors that is invariant under equiaffine transformations. The Euclidean tangent and normal vectors will not suffice since the relation $\mathbf{T} \cdot \mathbf{N} = 0$ is not preserved under a general equiaffine transformation. Since we know that tangent vectors remain tangent, we can choose one vector, $a_1(p)$, to be $\dot{\mathbf{x}} = d\mathbf{x}/dp$. We then look for a second vector $a_2(p)$ which along with $a_1(p)$ spans the unit area: $\det(a_1(p), a_2(p)) = 1$. Since equiaffine transformations are area preserving, these vectors are related by an invariant property. The only problem is that we don't have an expression for computing $a_2(p)$. To solve this problem, we introduce a new parameter ν for the curve, such that

$$\det(\mathbf{x}', \mathbf{x}'') = 1, \tag{4.12}$$

where $'$ now denotes the derivative with respect to ν. We then define the *affine tangent* to the newly parameterized curve as $\mathbf{T_a} := \mathbf{x}'$ and the *affine normal* as $\mathbf{N_a} := \mathbf{x}''$. These vectors span the unit area and thus are related by an invariant property (hence, $\det(\mathbf{T_a}, \mathbf{N_a}) = 1$ although in general $\mathbf{T_a} \cdot \mathbf{N_a} \neq 0$). The parameter ν is called the *affine arc-length*. We can write it in terms of the old parameter p as

$$\begin{aligned} &\det(\mathbf{x}', \mathbf{x}'') = \det\left(\frac{\partial \mathbf{x}}{\partial p}\frac{\partial p}{\partial \nu}, \frac{\partial^2 \mathbf{x}}{\partial p^2}\left(\frac{\partial p}{\partial \nu}\right)^2\right) = 1 \\ &\Rightarrow \left(\frac{d\nu}{dp}\right)^3 = \det\left(\frac{\partial \mathbf{x}}{\partial p}, \frac{\partial^2 \mathbf{x}}{\partial p^2}\right) \\ &\Rightarrow \nu(p) = \int_0^p \det(\dot{\mathbf{x}}, \ddot{\mathbf{x}})^{1/3} dp. \end{aligned} \tag{4.13}$$

In order for this re-parametrization $p \mapsto \nu$ to exist, we require that $\det(\dot{\mathbf{x}}, \ddot{\mathbf{x}}) \neq 0$ for every p. This is essentially requiring that the curve have no points of inflection.

Differentiating the expression in (4.12) we get

$$\det(\mathbf{x}', \mathbf{x}''') = 0,$$

and hence the two vectors $\mathbf{x}'$ and $\mathbf{x}'''$ are linearly dependent. This implies that

$$\mathbf{x}''' + \mu \mathbf{x}' = 0, \tag{4.14}$$

for some scalar quantity $\mu(\nu)$. Multiplying both sides of (4.12) by μ we get

$$\mu = \det(\mu \mathbf{x}', \mathbf{x}'') = -\det(\mathbf{x}'', \mu \mathbf{x}'),$$

and from (4.14) we obtain

$$\mu = \det(\mathbf{x}'', \mathbf{x}''').$$

The scalar μ is invariant under equiaffine transformations and is called the *affine curvature*. To clarify, consider a curve $\mathbf{x}(\nu)$ in the plane with affine arc-length parameter ν and curvature $\mu(\nu)$, which is transformed under an equiaffine transformation, L, to $L(\mathbf{x}(\nu))$. The new curve $L(\mathbf{x}(\nu))$ still has ν as its affine arc-length parameter and the affine curvature of $\mathbf{x}(\nu)$ is equal to the affine curvature of $L(\mathbf{x}(\nu))$ at each value of ν. In

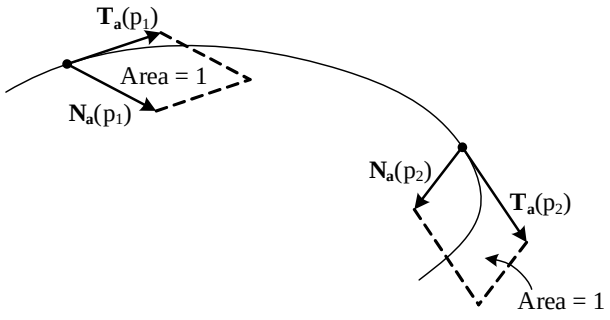

Figure 4.3: The affine normal and tangent at two points $\mathbf{x}(p_1)$ and $\mathbf{x}(p_2)$ on a curve $\mathbf{x}(p)$.

this sense the affine quantities ν and μ are analogous to the Euclidean quantities s and k.

The important quantities introduced in this section are: (1) the affine arc-length, which is chosen such that $\det(\mathbf{x}', \mathbf{x}'') = 1$; (2) the affine tangent $\mathbf{T_a} := \mathbf{x}'$, which is collinear with the Euclidean tangent at each point on a curve, but is not in general a unit vector; and (3) the affine normal $\mathbf{N_a} := \mathbf{x}''$, which is not in general perpendicular to $\mathbf{T_a}$ but is chosen such that the area of the parallelogram created by $\mathbf{x}'$ and $\mathbf{x}''$ is 1. The affine tangent and normal are shown in Figure 4.3.

4.2.6 Affine curve shortening

In affine curve shortening we deform the curve $\mathbf{x}(p, t)$ along the affine normal $\mathbf{N_a} = \mathbf{x}''$ at a rate proportional to the length of the affine normal. This can be written as

$$\frac{\partial \mathbf{x}}{\partial t}(p, t) = \frac{\partial^2 \mathbf{x}}{\partial \nu^2}(p, t) = \mathbf{N_a}(p, t). \tag{4.15}$$

If an embedded curve evolves according to (4.15), the curve shrinks to an elliptical point. In order to get a better feeling of what this curve evolution is doing, we would like to express the affine normal vector, $\mathbf{x}''$, in terms of Euclidean quantities. Consider the case where the parameter p, the original parameter of the curve, is the Euclidean arc-length.

Then we have

$$\frac{\partial \mathbf{x}}{\partial p} = \dot{\mathbf{x}} = \mathbf{T} \quad \text{and} \quad \frac{\partial^2 \mathbf{x}}{\partial p^2} = \ddot{\mathbf{x}} = k\mathbf{N}.$$

Now, from (4.13) we have

$$\begin{aligned}\frac{d\nu}{dp} &= \det\left(\frac{\partial \mathbf{x}}{\partial p}, \frac{\partial^2 \mathbf{x}}{\partial p^2}\right)^{1/3} \\ &= \det(\mathbf{T}, k\mathbf{N})^{1/3} \\ &= k^{1/3} \det(\mathbf{T}, \mathbf{N})^{1/3} \\ &= k^{1/3}\end{aligned}$$

(since $\mathbf{T}$ and $\mathbf{N}$ are orthonormal vectors). Now we are ready to write the affine normal in terms of Euclidean quantities: From the chain rule

$$\begin{aligned}\mathbf{N_a} = \frac{\partial^2 \mathbf{x}}{\partial \nu^2} &= \frac{\partial^2 \mathbf{x}}{\partial p^2}\left(\frac{dp}{d\nu}\right)^2 + \frac{\partial \mathbf{x}}{\partial p}\frac{d^2 p}{d\nu^2} \\ &= k\mathbf{N}\left(\frac{1}{k}\right)^{2/3} + \frac{dp}{d\nu}\frac{\partial}{\partial p}(k^{-1/3})\mathbf{T} \\ &= k^{1/3}\mathbf{N} - \frac{\partial k}{\partial p}\frac{1}{3k^{5/3}}\mathbf{T}.\end{aligned}$$

Defining $k_p := \partial k/\partial p$ we can write the affine curve evolution as

$$\frac{\partial \mathbf{x}}{\partial t} = k^{1/3}\mathbf{N} - \frac{k_p}{3k^{5/3}}\mathbf{T}.$$

From (4.10) we can see that only the component of $\partial \mathbf{x}/\partial t$ in the normal direction, $\mathbf{N}$, contributes to shrinking the curve. The component of $\partial \mathbf{x}/\partial t$ in the tangential direction $\mathbf{T}$ gives a rotation of the curve and thus only affects the parametrization of the family of curves. Because of this the affine curve shortening flow is geometrically equivalent to

$$\frac{\partial \mathbf{x}}{\partial t}(p,t) = k^{1/3}(p,t)\mathbf{N}(p,t).$$

Therefore, geometrically, the only difference between Euclidean and Affine curve shortening is $k\mathbf{N}$ versus $k^{1/3}\mathbf{N}$. However the affine curve shortening flow has a component of $\partial \mathbf{x}/\partial t$ which is parallel to the curve and which induces a rotation. In terms of shortening

the perimeter of a curve, this rotation is an unwanted motion, and therefore the affine curve shortening flow is not as "efficient" at shortening the perimeter as the Euclidean curve shortening flow.

4.3 Polygon shortening

With the beautiful results of Euclidean and affine curve shortening in mind, we now turn our attention to multi-agent systems. We can consider a group of n agents lying in the plane to be the vertices of an n-sided polygon. By creating a polygon shortening scheme analogous to that of curve shortening, the vertices, and thus the agent's positions, will converge to a point. In addition, the shape of the polygon as it shrinks to a point will have properties which are analogous to the curve shortening theory. In this section we will formally define a polygon and introduce two polygon shortening schemes.

4.3.1 n-gons

We begin by formally defining a polygon and a non-self-intersecting polygon in $\mathbb{R}^2$ (or equivalently $\mathbb{C}$), which we will refer to as an n-gon and a simple n-gon respectively [11].

Definition 4.5. An *n-gon* (n-sided polygon) is a (possibly intersecting) circuit of n line segments $z_1z_2, z_2z_3, \ldots, z_nz_1$, joining consecutive pairs of n distinct points $z_1, z_2, \ldots, z_n$. The segments are called *sides* and the points are called *vertices*.

Definition 4.6. A *simple n-gon* is a non-self-intersecting n-gon.

We denote the counterclockwise *internal angle* between consecutive sides z_iz_{i+1} and $z_{i-1}z_i$ of an n-gon as β_i, where $i = 1, \ldots, n$ modulo n. For a simple n-gon these angles satisfy

$$\sum_{i=1}^{n} \beta_i = (n-2)\pi.$$

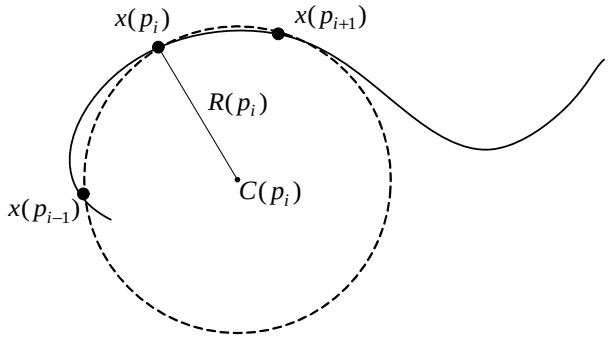

Figure 4.4: The circumcenter for three points on the curve $\mathbf{x}(p)$.

Definition 4.7. An n-gon is *convex* if it is simple and its internal angles satisfy

$$0 < \beta_i \leq \pi, \quad \forall i = 1, \ldots, n.$$

Definition 4.8. An n-gon is *strictly convex* if it is simple and its internal angles satisfy

$$0 < \beta_i < \pi, \quad \forall i = 1, \ldots, n.$$

4.3.2 Shortening by Menger-Melnikov curvature

To introduce the polygon shortening scheme studied in [4, 22], consider the case where we know only discrete points $\mathbf{x}(p_i)$, $i = 1, \ldots, n$, along a smooth curve $\mathbf{x}(p)$. By connecting these points we create an n-gon. As $n \to \infty$ the n-gon becomes the smooth curve $\mathbf{x}(p)$. The idea is to create a polygon shortening scheme such that as $n \to \infty$, and the polygon tends to a smooth curve, the scheme becomes Euclidean curve shortening.

There exists a unique circle (the *circumcircle*) which passes through any three non-collinear points, $\mathbf{x}(p_{i-1})$, $\mathbf{x}(p_i)$, $\mathbf{x}(p_{i+1})$, where $p_{i-1} < p_i < p_{i+1}$, on the curve $\mathbf{x}(p)$. We will denote the radius of the circle $R(p_i)$, and the center of this circle, which is called the *circumcenter*, $C(p_i)$, as shown in Figure 4.4. The quantity $1/R(p_i)$ is called the Menger-Melnikov curvature and has the property that

$$\lim_{p_{i-1}, p_{i+1} \to p_i} \frac{1}{R(p_i)} = |k(p_i)|.$$

In addition, as the points $\mathbf{x}(p_{i-1})$ and $\mathbf{x}(p_{i+1})$ approach $\mathbf{x}(p_i)$, the quantity $(C(p_i) - \mathbf{x}(p_i))/R(p_i)$ approaches $\mathbf{N}(p_i)$ if $k(p_i) > 0$ and $-\mathbf{N}(p_i)$ if $k(p_i) < 0$. Therefore, multiplying this quantity by the Menger-Melnikov curvature we have

$$\lim_{p_{i-1},p_{i+1}\to p_i} \frac{C(p_i) - \mathbf{x}(p_i)}{R(p_i)^2} = k(p_i)\mathbf{N}(p_i).$$

Hence, a discrete analogue to Euclidean curve shortening can be created using this method.

Consider the situation in which we have n agents, $z_1, \dots z_n$, lying in the complex plane, which form an n-gon. For any three consecutive vertices z_{i-1}, z_i, z_{i+1} define the function

$$c_i := c(z_{i-1}, z_i, z_{i+1}) = \left(\frac{z_{i-1} - z_i}{\overline{z_{i-1} - z_i}} - \frac{z_{i+1} - z_i}{\overline{z_{i+1} - z_i}} \right) \frac{1}{z_{i-1} - z_{i+1}},$$

where $\overline{z_{i-1} - z_i}$ denotes the complex conjugate. In [22] it is shown that $|c_i|$ is the Menger-Melnikov curvature of the three vertices, z_{i-1}, z_i, z_{i+1}, and the circumcenter of the three vertices is given by $z_i + c_i/|c_i|^2$. Therefore, the normal vector for z_i is approximated by $c_i/|c_i|$. Hence, the Menger-Melnikov flow described above can be written as

$$\dot{z}_i = c(z_{i-1}, z_i, z_{i+1}). \tag{4.16}$$

The polygon evolution given by (4.16) is studied in [4, 22]. However, due to the complexity of the system the results are quite limited. In fact, in [4] the author's point out the difficulty in obtaining analytical results for this scheme. It has been shown that a simple n-gon collapses to a point in finite time, and for $n = 4$ most quadrilaterals tend to regular polygons as they shrink to a point. However when n is small, the scheme in (4.16) may yield a very poor approximation of the normal vector. This is depicted in Figure 4.5. In fact, for a convex n-gon, there may be a $\dot{z}_i$ which does not point into the interior of the n-gon. Finally, as the polygon collapses, the velocity of the vertices becomes infinitely large, which is not ideal for a multi-agent (vehicle) system. Because of these points we propose a simple linear scheme for polygon shortening.

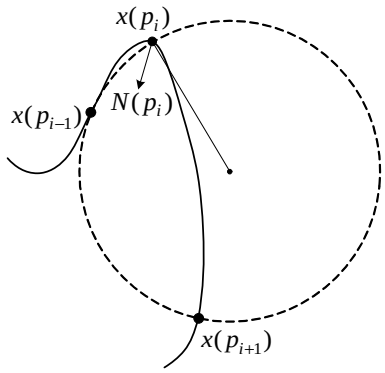

Figure 4.5: The normal vector, and the Menger-Melnikov approximation, when the number of points n is small. The approximation to $\mathbf{N}(p_i)$ is very rough.

4.3.3 Linear scheme

The linear polygon shortening scheme that we propose can be described as follows. A group of n agents, modeled as point masses are numbered from 1 to n. The position of each agent can be described in the complex plane by the point $z_i = x_i + jy_i$, $i = 1, \ldots, n$. These agents make up the vertices of an n-gon. The strategy is for agent i to chase the centroid of agents $i-1$ and $i+1$. The i^{th} agent's velocity points in the direction of the centroid of its neighbors and the magnitude of the velocity is equal to the distance from agent i to the centroid. This is described in (4.2) as

$$\dot{z}_i = \frac{1}{2}(z_{i+1} - z_i) + \frac{1}{2}(z_{i-1} - z_i),$$

where all indices are evaluated modulo n. This system can be written in the form $\dot{z} = Az$ where the matrix A is given by

$$A = \operatorname{circ}\left(-1, \frac{1}{2}, 0, \ldots, 0, \frac{1}{2}\right).$$

The matrix A can be written in terms of the polynomial

$$q_A(s) = \frac{1}{2}s^{n-1} + \frac{1}{2}s - 1,$$

and the matrix $P = \text{circ}(0, 1, 0, \ldots, 0)$, as $A = q_A(P)$. By the Spectral Mapping Theorem we obtain

$$\text{eigs}(A) = \{q_A(1), q_A(\omega), q_A(\omega^2), \ldots, q_A(\omega^{n-1})\},$$

where $\omega = \mathrm{e}^{2\pi j/n}$. Therefore, denoting $\lambda_i := q_A(\omega^{i-1})$, we have $\text{eigs}(A) = \{\lambda_i : i = 1, \ldots, n\}$. Evaluating λ_i we get

$$\begin{aligned}\lambda_i &= \frac{1}{2}\mathrm{e}^{2\pi j(n-1)(i-1)/n} + \frac{1}{2}\mathrm{e}^{2\pi j(i-1)/n} - 1 \\ &= \cos(2\pi(i-1)/n) - 1,\end{aligned}$$

where $i = 1, \ldots, n$. Hence, the eigenvalues of A are real, with one eigenvalue at zero, and all others lie on the negative real line. The zero eigenvalue dictates that the agents converge to their stationary centroid rather than to the origin. The rightmost nonzero eigenvalue of A gives the rate of convergence of the agents to their centroid [47]. This eigenvalue, which we will denote as γ, is given by $i = 2$ (or equivalently $i = n$), and is

$$\gamma := \lambda_2 = \cos(2\pi/n) - 1. \tag{4.17}$$

The following theorem describes the geometrical shape of the points $z_i(t)$ as they converge to their centroid. This theorem is proved for discrete time in [4]. The following result, which was inspired by [4], was proved by Laura Krick. Joshua Marshall [30] proved this result for a general circulant pursuit matrix.

Theorem 4.9. *Consider n points, $z_1(t), \ldots, z_n(t)$ evolving according to (4.2). As $t \to \infty$ these points converge to an ellipse. That is, $z_1(t), \ldots, z_n(t)$ collapse to an elliptical point.*

Proof. The matrix A can be diagonalized by the matrix

$$F = \frac{1}{\sqrt{n}}[f_1, \ldots, f_n],$$

where

$$f_i = \left[\omega^0, \omega^{(i-1)}, \omega^{2(i-1)}, \ldots, \omega^{(n-1)(i-1)}\right]^T, \tag{4.18}$$

and $\omega = \mathrm{e}^{2\pi j/n}$. We have $A = F\Lambda F^*$ where Λ is a diagonal matrix consisting of the eigenvalues of A. Because of this, we can write

$$z(t) = F\mathrm{e}^{\Lambda t}F^* z(0).$$

This can equivalently be written as the modal decomposition

$$\begin{aligned} z(t) &= \frac{1}{n}\sum_{i=1}^{n} \mathrm{e}^{\lambda_i t} f_i f_i^* z(0) \\ &= \frac{1}{n}\mathrm{e}^{0t}\begin{bmatrix} 1 \\ \vdots \\ 1 \end{bmatrix}\begin{bmatrix} 1 & \cdots & 1 \end{bmatrix} z(0) + \frac{1}{n}\sum_{i=2}^{n} \mathrm{e}^{\lambda_i t} f_i f_i^* z(0) \\ z(t) &= \tilde{z}\mathbf{1} + \frac{1}{n}\sum_{i=2}^{n} \mathrm{e}^{\lambda_i t} f_i f_i^* z(0), \end{aligned}$$

where

$$\tilde{z} := \frac{1}{n}\sum_{i=1}^{n} z_i(0)$$

is the agents' centroid, and $\mathbf{1}$ is the $n \times 1$ vector of 1's. As $t \to \infty$ the terms in the summation tend to zero and thus the agent's converge to their centroid. The rate of convergence is dictated by γ in (4.17). Since γ is the rightmost nonzero eigenvalue, the modes corresponding to all the other eigenvalues will die away more quickly. Therefore, by subtracting off the vector of centroids, and dividing by γ we can scale the system by the slowest eigenvalues and thus study the shape as $t \to \infty$. Define

$$w(t) := \frac{1}{\mathrm{e}^{j\gamma}}(z(t) - \tilde{z}\mathbf{1}) = \frac{1}{n\mathrm{e}^{j\gamma}}\sum_{i=2}^{\infty} \mathrm{e}^{\lambda_i t} f_i f_i^* z(0).$$

Taking the limit of $w(t)$ as $t \to \infty$ we obtain

$$\lim_{t\to\infty} w(t) =: w^\infty = \frac{1}{n}(f_2 f_2^* + f_n f_n^*)z(0).$$

The vector w^∞ gives the final shape of the points. Defining the complex numbers, which are independent of i,

$$a\mathrm{e}^{j\alpha} := \frac{1}{n} f_2^* z(0) \quad \text{and} \quad b\mathrm{e}^{j\beta} := \frac{1}{n} f_n^* z(0),$$

we can write w^∞ as

$$w^\infty = f_2 a e^{j\alpha} + f_n b e^{j\beta}.$$

Using the definition of f_2 and f_n from (4.18) we can write the components of w^∞ as

$$\begin{aligned} w_i^\infty &= a e^{j\alpha} e^{2\pi j(i-1)/n} + b e^{j\beta} e^{2\pi j(i-1)(n-1)/n}, \\ &= a e^{j\alpha} e^{2\pi j(i-1)/n} + b e^{j\beta} e^{-2\pi j(i-1)/n}. \end{aligned}$$

Letting $\theta_i = 2\pi(i-1)/n$, we can write this as

$$w^\infty = a e^{j\alpha} e^{j\theta_i} + b e^{j\beta} e^{-j\theta_i}.$$

Finally, defining

$$\psi = \frac{\alpha+\beta}{2} \quad \text{and} \quad \bar{\psi} = \frac{\alpha-\beta}{2},$$

we have $\alpha = \psi + \bar{\psi}$ and $\beta = \psi - \bar{\psi}$ and thus

$$\begin{aligned} w_i^\infty &= a e^{j\psi} e^{j\bar{\psi}} e^{j\theta_i} + b e^{j\psi} e^{j\bar{\psi}} e^{-j\theta_i} \\ &= e^{j\psi}(a e^{j(\bar{\psi}+\theta_i)} b e^{-j(\bar{\psi}+\theta_i)}) \\ &= e^{j\psi}\left((a+b)\cos(\bar{\psi}+\theta_i) + j(a-b)\sin(\bar{\psi}+\theta_i)\right). \end{aligned} \tag{4.19}$$

Since the variables $a, b, \psi, \bar{\psi}$ depend only on the initial condition $z(0)$, (4.19) describes an ellipse which is parametrized by $\theta_i \in [0, 2\pi]$. The quantity $e^{j\psi}$ gives the rotation of the semimajor axis of the ellipse relative to the positive real axis, and $\bar{\psi}$ defines the starting point $\theta_1 = 0$ of the ellipse relative to the semimajor axis. □

4.4 Star formations

In this section we will show that a group of agents, arranged in a star formation about their centroid (see Figure 4.7), remain in a star formation for all time. We require some preliminary tools which are introduced in the following lemmas. In what follows, $\bar{z}$ denotes the complex conjugate of the complex number z.

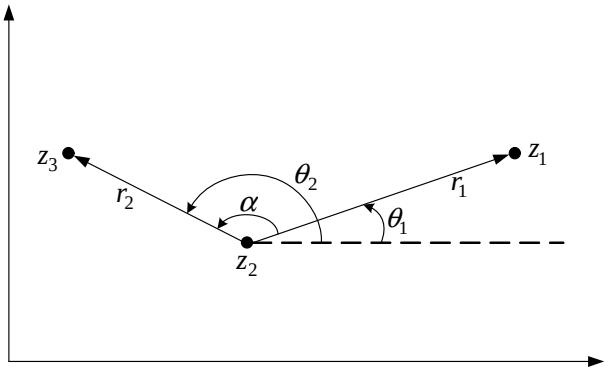

Figure 4.6: The setup for the definition of the function F.

Lemma 4.10 (Lin et al. [25])**.** *Let z_1, z_2, and z_3 be three points in the complex plane, as shown in Figure 4.6. Let $r_1 := |z_1 - z_2|$, $r_2 := |z_3 - z_2|$ and*

$$F = \Im\{\overline{(z_1 - z_2)}(z_3 - z_2)\}.$$

Then

(i) $0 < \alpha < \pi$, $r_1 > 0$, and $r_2 > 0$ if and only if $F > 0$.

(ii) $\pi < \alpha < 2\pi$, $r_1 > 0$, and $r_2 > 0$ if and only if $F < 0$.

(iii) the points are collinear if and only if $F = 0$.

Proof. Introduce the polar form

$$z_1 - z_2 = r_1 \mathrm{e}^{j\theta_1}, \quad z_3 - z_2 = r_2 \mathrm{e}^{j\theta_2}$$

where θ_1, θ_2 are the angles of the line segments in the global coordinate system. Then

$$F = \Im\{\overline{(z_1 - z_2)}(z_3 - z_2)\} = \Im\{r_1 \mathrm{e}^{-j\theta_1} r_2 \mathrm{e}^{j\theta_2}\} = r_1 r_2 \sin(\alpha).$$

Thus, $0 < \alpha < \pi$, $r_1 > 0$, and $r_2 > 0$ iff $F > 0$; and $\pi < \alpha < 2\pi$, $r_1 > 0$, and $r_2 > 0$ iff $F < 0$. Also, the points are collinear iff $F = 0$. □

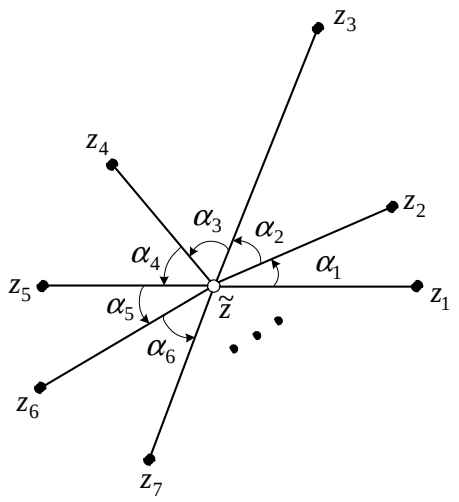

Figure 4.7: A counterclockwise star formation.

Now consider our system of n agents, whose positions, not all collinear, are denoted by $z_1, \ldots, z_n$. Let $\tilde{z}$ be the centroid and r_i be the distance from the centroid to z_i. Let α_i denote the counterclockwise angle from $\tilde{z}z_i$ to $\tilde{z}z_{i+1}$ for $i = 1, \ldots, n-1$, and α_n denote the counterclockwise angle from $\tilde{z}z_n$ to $\tilde{z}z_1$.

Definition 4.11 (Lin et al. [25])**.** The n points are said to be arranged in a counterclockwise star formation if $r_i > 0$ and $\alpha_i > 0$, for all $i = 1, \ldots, n$, and $\sum_{i=1}^{n} \alpha_i = 2\pi$. They are said to be arranged in a clockwise star formation if $r_i > 0$ and $\alpha_i < 0$, for all $i = 1, \ldots, n$, and $\sum_{i=1}^{n} \alpha_i = -2\pi$.

This formation is shown in Figure 4.7. In what follows we will only consider counterclockwise star formations, since the treatment for clockwise star formations is analogous. Also, the case where $n = 2$ is trivial, so it is omitted.

Lemma 4.12 (Lin et al. [25])**.** *Suppose that n distinct points, $z_1, \ldots, z_n$, with $n > 2$ are in a counterclockwise star formation. Then $\alpha_i < \pi$, $\forall i$.*

Proof. Suppose by way of contradiction and by renumbering the points, if necessary, that $\alpha_1 \geq \pi$. Fix a coordinate system centered at $\tilde{z}$ with the positive real axis given by the

ray from $\tilde{z}$ passing through z_1. Then we have $\Im\{z_1\} = 0$, $\Im\{z_2\} \leq 0$ and $\Im\{z_k\} < 0$, for $k = 3, \ldots, n$. Therefore, $\Im\{\tilde{z}\} = \sum_{i=1}^{n} \Im\{z_i\} < 0$, a contradiction. □

Lemma 4.13 (Lin et al. [25])**.** *If n points, $z_1, \ldots, z_n$, which are evolving according to* (4.2)*, are collinear at some time t_1, then they are collinear for all $t < t_1$ and $t > t_1$.*

Proof. Suppose n points are all collinear at $t = t_1$. Reorient the coordinate system such that all points lie on the real axis, $\mathbb{R}$. Since

$$\dot{z}_i = \frac{1}{2}(z_{i+1} + z_{i-1}) - z_i,$$

and $z_i \in \mathbb{R}$, $\forall i$, it follows that $\dot{z}_i \in \mathbb{R}$, $\forall i$. This means that $\mathbb{R}^n$ is an invariant subspace of $\mathbb{C}^n$ under the dynamics (4.2). Hence, $z_i(t) \in \mathbb{R}$ for all time, implying the points are collinear for all time. □

We will now use these tools to prove the main theorem of this section.

Theorem 4.14. *Suppose that n distinct points, with $n > 2$, are initially arranged in a counterclockwise star formation. If these points evolve according to* (4.2) *they will remain in a counterclockwise star formation for all time.*

Proof. We begin by considering the function

$$\begin{aligned} F_i(t) &= \Im\{\overline{(z_i(t) - \tilde{z}(t))}(z_{i+1}(t) - \tilde{z}(t))\} \\ &= r_i r_{i+1} \sin(\alpha_i). \end{aligned}$$

By the definition of a counterclockwise star formation we have $r_i(0) > 0$, and $0 < \alpha_i(0) < \pi$, $\forall i$. Hence by Lemma 4.10, $F_i(0) > 0$, $\forall i$. We want to show that $F_i(t) > 0$, $\forall t$, which by Lemma 4.10 shows that the vertices are in a counterclockwise star formation for all time.

Suppose by way of contradiction that t_1 is the first time that an F_i becomes zero. We can select $i = m$ such that $F_m(t_1) = 0$ and $F_{m+1}(t_1) > 0$, for if all the F_i's are zero at t_1,

then the points are collinear, which by Lemma 4.13 is a contradiction. Hence, we have

$$\begin{aligned} F_i(t) > 0 \quad \forall\, t \in [0, t_1), \quad i = 1, \ldots, n, \\ F_m(t_1) = 0, \\ F_{m+1}(t_1) > 0. \end{aligned}$$

Taking the derivative of F_m along the trajectories of the system $\dot{z} = Az$, and noting that $\dot{\tilde{z}} = 0$, we have

$$\dot{F}_m = \Im\{\overline{\dot{z}_m}(z_{m+1} - \tilde{z}) + \overline{(z_m - \tilde{z})}\dot{z}_{m+1}\}.$$

Substituting in the expressions for $\dot{z}_m$ and $\dot{z}_{m+1}$ we get

$$\begin{aligned} \dot{F}_m = \frac{1}{2}\Im\Big\{&\overline{(z_{m+1} - z_m)}(z_{m+1} - \tilde{z}) + \overline{(z_{m-1} - z_m)}(z_{m+1} - \tilde{z}) \\ &+ \overline{(z_m - \tilde{z})}(z_{m+2} - z_{m+1}) + \overline{(z_m - \tilde{z})}(z_m - z_{m+1})\Big\} \end{aligned}$$

Adding and subtracting $\tilde{z}$ from each of the 4 terms and simplifying we obtain

$$\dot{F}_m = -2F_m + G_m, \tag{4.20}$$

where

$$G_m = \frac{1}{2}\Im\{\overline{(z_{m-1} - \tilde{z})}(z_{m+1} - \tilde{z}) + \overline{(z_m - \tilde{z})}(z_{m+2} - \tilde{z})\}. \tag{4.21}$$

We can equivalently write G_m as

$$G_m = \frac{1}{2}\left(r_{m-1}r_{m+1}\sin(\alpha_{m-1} + \alpha_m) + r_m r_{m+2}\sin(\alpha_m + \alpha_{m+1})\right).$$

Now, if $F_m(t_1) = 0$, by Lemma 4.10, one of the four following conditions must be satisfied.

(i) $\alpha_m(t_1) = \pi$ and $r_m(t_1), r_{m+1}(t_1) > 0$.

(ii) $\alpha_m(t_1) = 0$ and $r_m(t_1), r_{m+1}(t_1) > 0$.

(iii) $r_m(t_1) = 0$.

(iv) $r_{m+1}(t_1) = 0$.

Condition (iv), in which $r_{m+1}(t_1) = 0$, cannot be satisfied since $F_{m+1}(t_1) > 0$. Condition (i) cannot be satisfied since $\alpha_i(t_1) \geq 0$, $\forall i$, and so all the points lie on, or to one side of, the line formed by z_{m+1} and z_m, a contradiction by either Lemma 4.12 or 4.13. Assume that condition (ii) is satisfied. Then $\alpha_m(t_1) = 0$, and from (4.21) we obtain

$$\begin{aligned} G_m(t_1) &= \frac{1}{2}\left(r_{m-1}r_{m+1}\sin(\alpha_{m-1}) + r_m r_{m+2}\sin(\alpha_{m+1})\right) \\ &= \frac{1}{2}\left(\frac{r_{m+1}}{r_m}F_{m-1}(t_1) + \frac{r_m}{r_{m+1}}F_{m+1}(t_1)\right). \end{aligned}$$

Since $r_m(t_1), r_{m+1}(t_1) > 0$, $F_{m+1}(t_1) > 0$, and $F_{m-1}(t_1) \geq 0$, it follows that $G_m(t_1) > 0$. By continuity of G_m there exists $0 \leq t_0 < t_1$ such that

$$G_m(t) > 0 \quad \forall\, t \in [t_0, t_1].$$

Also, by assumption, $F_m(t) > 0$ for $t \in [0, t_1)$. Therefore

$$\dot{F}_m(t) = -2F_m + G_m > -2F_m, \quad t \in [t_0, t_1).$$

Integrating this we obtain

$$F_m(t) > \mathrm{e}^{-2(t-t_0)}F_m(t_0), \quad t \in [t_0, t_1).$$

By continuity of F_m,

$$F_m(t_1) \geq \mathrm{e}^{-2(t_1-t_0)}F_m(t_0) > 0,$$

which is a contradiction.

Finally, suppose condition (iii) is satisfied and $r_m(t_1) = 0$. This condition implies that $z_m(t_1)$ is positioned at the centroid, $\tilde{z}$. Assume without loss of generality that $\tilde{z} = 0$. Notice that if $z_i(t_1) = 0$, the angle $\theta_i(t_1)$ is not defined. We will now establish the fact that if $z_i(t_1) = 0$ and $\dot{z}_i(t_1) \neq 0$, then $\lim_{t \uparrow t_1} \theta_i(t)$ is well defined. The expansion for z_i about t_1 is defined as

$$z_i(t_1) - z_i(t_1 - h) = h\dot{z}_i(t_1) - \mathcal{O}(h),$$

where $\mathcal{O}(h)/h \to 0$ as $h \to 0$. If $z_i(t_1) = 0$ then

$$z_i(t_1 - h) = -h\dot{z}_i(t_1) + \mathcal{O}(h).$$

Hence, $\lim_{h\to 0} z_i(t_1 - h)/h = -\dot{z}_i(t_1)$. Therefore the limiting motion of $z_i(t)$ as $t \uparrow t_1$ is along the ray defined by $-\dot{z}_i(t_1)$. Because of this, $\lim_{t\uparrow t_1} \theta_i(t)$ is well defined and is given by the angle of this ray, as shown in Figure 4.8. Therefore we can define

$$\theta_i(t_1) := \begin{cases} \theta_i(t_1) & \text{if} \quad r_i(t_1) > 0, \\ \arctan\left(\dfrac{\Im\{-\dot{z}_i(t_1)\}}{\Re\{-\dot{z}_i(t_1)\}}\right) & \text{if} \quad r_i(t_1) = 0. \end{cases} \tag{4.22}$$

With this definition we can talk about $\theta_i(t_1)$, and $\alpha_i(t_1)$, when $r_i(t_1) = 0$.

Suppose that by a rotation of the coordinate system, if necessary, that

$$\frac{z_{m+1}(t_1) + z_{m-1}(t_1)}{2} = -r, \quad \text{where} \quad r > 0. \tag{4.23}$$

This is possible since if $r = 0$ then $z_{m-1}(t_1), z_m(t_1), z_{m+1}(t_1)$ all lie on a line through the centroid, and all other points must lie either on or to one side of this line, implying that 0 is not the centroid, or all the points are collinear, both contradictions. Since $z_m(t_1) = 0$, we have $\dot{z}_m(t_1) = -r$, as shown in Figure 4.9. If $n = 3$ then $z_m(t_1) = 0$ and the centroid of $z_{m+1}(t_1)$ and $z_{m-1}(t_1)$ is at $-r$, implying that 0 is not the centroid of the three points, a contradiction. Therefore we need only consider $n > 3$. Since $\dot{z}_m(t_1) = -r$, from (4.22) we obtain

$$\theta_m(t_1) = 0. \tag{4.24}$$

To obtain a contradiction for $n > 3$ we will show that (4.23) and (4.24) cannot both be satisfied. To do this we will consider the two cases, $r_{m-1}(t_1) = 0$ and $r_{m-1}(t_1) > 0$. Since the points are in a star formation until t_1, we know that $\forall i$, $\alpha_i(t) \in (0, \pi)$ for $t \in [0, t_1)$. Hence, if $\theta_i(t_1)$ and $\theta_{i+1}(t_1)$ are defined via (4.22), then by continuity $\alpha_i(t_1) \in [0, \pi]$.

If $r_{m-1}(t_1) = 0$ then from (4.23) we have $z_{m+1}(t_1) = -2r$. Therefore $\theta_{m+1}(t_1) = \pi$ and from (4.24), $\theta_m(t_1) = 0$. However this implies that all other $\theta_i(t_1)$'s which are defined

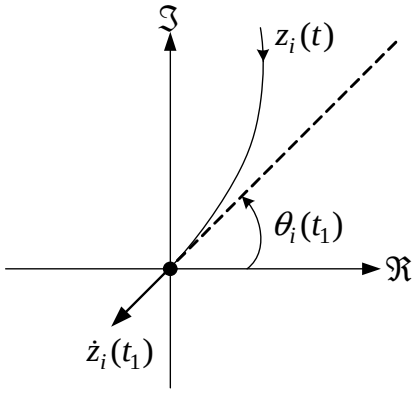

Figure 4.8: The limiting $\theta_i(t)$ as $t \uparrow t_1$ when $z_i(t_1) = 0$.

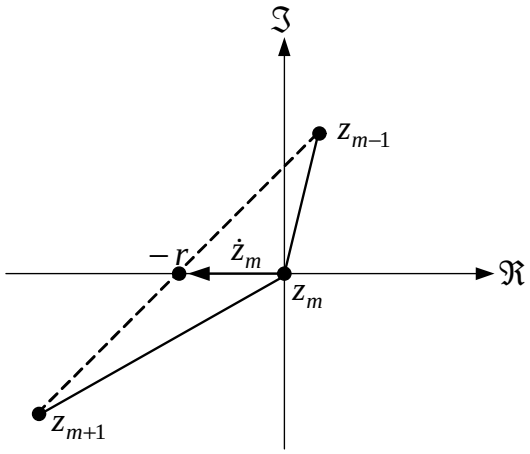

Figure 4.9: The position of the points z_{m-1}, z_m, and z_{m+1} at $t = t_1$.

must lie in $[-\pi, 0]$. Hence $\Im\{z_i(t_1)\} \leq 0 \ \forall i$, which implies that all points are collinear, or that 0 is not the centroid, both contradictions.

If $r_{m-1}(t_1) > 0$ then from (4.24), and since $\alpha_m(t_1), \alpha_{m-1}(t_1) \in [0, \pi]$, we have that $\theta_{m+1}(t_1) \in [0, \pi]$ and $\theta_{m-1}(t_1) \in [-\pi, 0]$. This means that $\Im\{z_{m+1}(t_1)\} \geq 0$ and $\Im\{z_{m-1}(t_1)\} \leq 0$. Because of this, as can be verified in Figure 4.10, for (4.23) to be satisfied either $z_{m-1}(t_1)$ and $z_{m+1}(t_1)$ are both real, in which case $\theta_{m+1}(t_1) - \theta_{m-1}(t_1) = \pi$, or they are not real and $\theta_{m+1}(t_1) - \theta_{m-1}(t_1) > \pi$. But this implies that all points lie on, or to one side of the line formed by $z_{m-1}(t_1)$ (or equivalently, the line formed by $z_{m+1}(t_1)$). Thus all points are collinear, or 0 is not the centroid, both contradictions.

□

Figure 4.11 shows the evolution of a polygon which is in a star formation about its centroid. Notice that the polygon remains in a star formation, becomes convex, and collapses to a point.

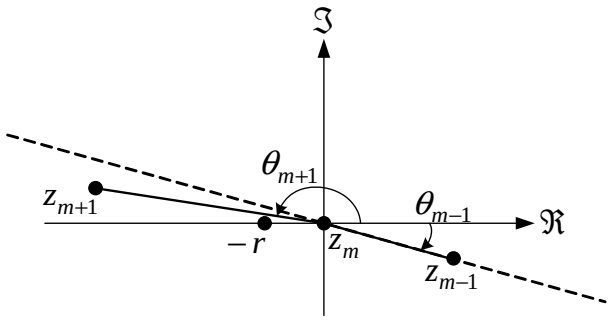

Figure 4.10: The required geometry such that $\theta_{m-1}(t_1) \in [-\pi, 0]$, $\theta_{m+1}(t_1) \in [0, \pi]$, and $z_{m+1}(t_1) + z_{m-1}(t_1) = -2r$. All points lie either on or to one side of the dotted line.

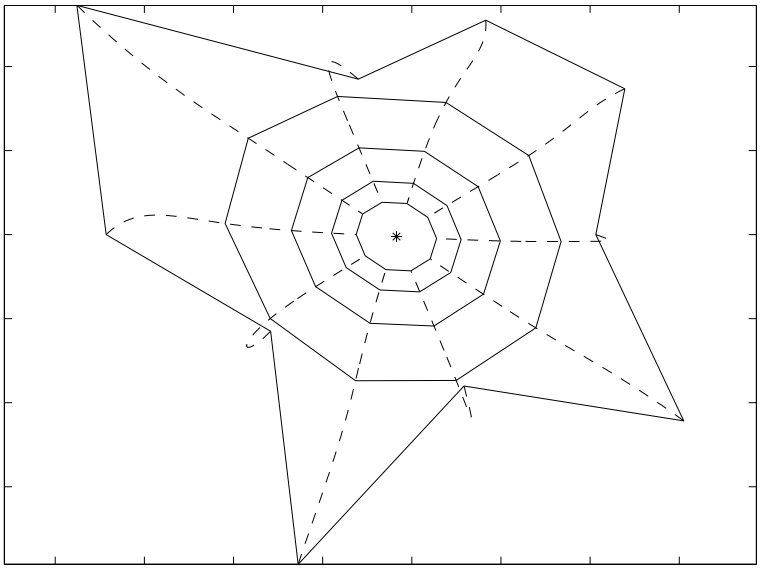

Figure 4.11: The evolution of a polygon whose vertices are in a star formation about their centroid $*$. The solid lines show the trajectories of each vertex.

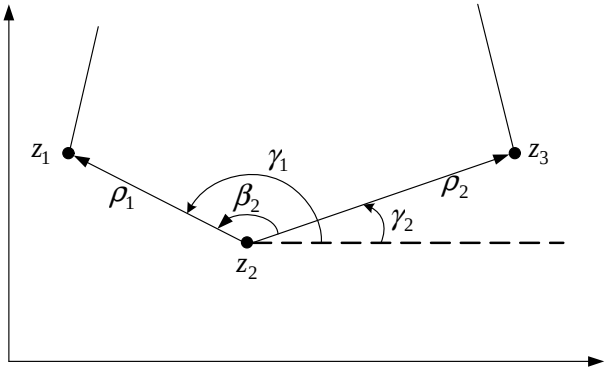

Figure 4.12: The setup for the definition of the function H.

4.5 Convex stays convex

In this section we will show that as a convex n-gon evolves according to (4.2), it remains convex. To do this we require a function similar to that in Lemma 4.10, but which measures the counterclockwise internal angle between two sides of a n-gon.

Lemma 4.15. *Consider a simple n-gon lying in the complex plane, whose vertices z_i are numbered counterclockwise around the n-gon. Let z_1, z_2, and z_3 be three vertices of the n-gon as shown in Figure 4.12. Let β_2 denote the counterclockwise angle from the side z_2z_3 to the side z_1z_2, and define $\rho_1 = |z_1 - z_2|$, $\rho_2 = |z_3 - z_2|$ and*

$$H = \Im\{(z_1 - z_2)\overline{(z_3 - z_2)}\}.$$

Then

(i) $0 < \beta_2 < \pi$, $\rho_1 > 0$, *and* $\rho_2 > 0$ *if and only if* $H > 0$.

(ii) $\pi < \beta_2 < 2\pi$, $\rho_1 > 0$, *and* $\rho_2 > 0$ *if and only if* $H < 0$.

(iii) the points are collinear if and only if $H = 0$.

Proof. We introduce the polar form:

$$z_1 - z_2 = \rho_1 e^{j\gamma_1}, \quad z_3 - z_2 = \rho_2 e^{j\gamma_2},$$

where γ_1, γ_2 are the angles shown in Figure 4.12. Then

$$H = \Im\{(z_1 - z_2)\overline{(z_3 - z_2)}\} = \Im\{\rho_1 e^{j\gamma_1}\rho_2 e^{-j\gamma_2}\} = \rho_1\rho_2 \sin(\beta_2)$$

Thus, $0 < \beta_2 < \pi$, $\rho_1 > 0$, and $\rho_2 > 0$ iff $H > 0$; and $\pi < \beta_2 < 2\pi$, $\rho_1 > 0$, and $\rho_2 > 0$ iff $H < 0$. Also, the points are collinear iff $H = 0$. □

Lemma 4.16. *If an n-gon is convex, with its vertices z_i, $i = 1, \ldots, n$, numbered counterclockwise around the n-gon, then these vertices are in a counterclockwise star formation about their centroid.*

Proof. Denote the centroid of the n vertices as $\tilde{z}$. The centroid must lie in the interior of the n-gon for if it lies on the boundary or in the exterior, we could draw a separating line through the centroid for which all vertices lie either on the line or to one side of it, a contradiction by Lemma 4.12 or 4.13. Since the centroid is in the interior, and the polygon is convex, we must have that $\sum_{i=1}^{n} \alpha_i = 2\pi$.

Since the n-gon is convex, we can draw a line from the centroid, $\tilde{z}$, to any vertex without exiting the interior of the n-gon. Consider an arbitrary vertex, z_m. Fix a coordinate system centered at $\tilde{z}$ with the positive real axis given by the ray from $\tilde{z}$ passing through z_m. The internal angle from the side $z_m z_{m+1}$ to the side $z_{m-1}z_m$ is $\beta_m \in (0, \pi]$. The real axis divides β_m into two angles, $\zeta_1, \zeta_2 > 0$ where $\zeta_1 + \zeta_2 = \beta_m$ as shown in Figure 4.13. The angle ζ_1 is the counterclockwise angle between the real axis and the side $z_{m-1}z_m$, and ζ_2 is the counterclockwise angle between $z_m z_{m+1}$ and the real axis. But since $\zeta_1, \zeta_2 \in (0, \pi)$, we have that $\Im\{z_{m-1}\} < 0$, $\Im\{z_m\} = 0$, and $\Im\{z_{m+1}\} > 0$. Hence, $\alpha_{m-1} > 0$, and $\alpha_m > 0$. Since this can be performed for each vertex, we have that $\alpha_i > 0$, $\forall i$ and thus the n-gon is in a counterclockwise star formation. □

With the use of these two lemmas, and the main result from Section 4.4, we will now prove the main result of this section.

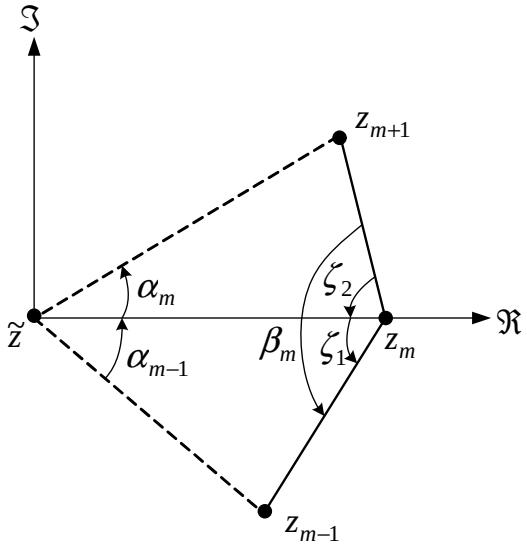

Figure 4.13: A convex n-gon whose vertices are therefore in a star formation about their centroid $\tilde{z}$.

Theorem 4.17. *Consider a strictly convex n-gon at time $t = 0$ whose vertices z_i, $i = 1, \ldots, n$, are numbered counterclockwise around the n-gon. If these vertices evolve according to* (4.2) *the n-gon will remain strictly convex for all time.*

Proof. We begin by considering the function

$$\begin{aligned} H_i(t) &= \Im\{(z_{i-1}(t) - z_i(t))\overline{(z_{i+1}(t) - z_i(t))}\}. \\ &= \rho_{i-1}\rho_i \sin(\beta_i) \end{aligned}$$

By the definition of a strictly convex n-gon we have that $\rho_i(0) > 0$, and $0 < \beta_i(0) < \pi$, $\forall i$. Hence by Lemma 4.15, $H_i(0) > 0$, $\forall i$. We want to show that $H_i(t) > 0$ for all t, which by Lemma 4.15 shows that the n-gon remains strictly convex for all time.

Suppose by way of contradiction that t_1 is the first time that an H_i becomes zero. We can select $i = m$ such that $H_m(t_1) = 0$ and $H_{m+1}(t_1) > 0$, for if all the H_i's are zero at t_1, then the points are collinear, which by Lemma 4.13 is a contradiction since the

points started in a convex n-gon formation. Hence, we have

$$\begin{aligned} H_i(t) > 0 \quad \forall\, t \in [0, t_1), \quad i = 1, \ldots, n, \\ H_m(t_1) = 0, \\ H_{m+1}(t_1) > 0. \end{aligned}$$

Taking the derivative of H_m along the trajectories of (4.2), we have

$$\dot{H}_m = \Im\{(\dot{z}_{m-1} - \dot{z}_m)\overline{(z_{m+1} - z_m)} + (z_{m-1} - z_m)\overline{(\dot{z}_{m+1} - \dot{z}_m)}\}.$$

Substituting in (4.2) for $\dot{z}_{m-1}, \dot{z}_m, \dot{z}_{m+1}$, we have

$$\begin{aligned} \dot{H}_m = \frac{1}{2}\Im\Big\{&(z_m - z_{m-1})\overline{(z_{m+1} - z_m)} + (z_{m-2} - z_{m-1})\overline{(z_{m+1} - z_m)} \\ &- (z_{m+1} - z_m)\overline{(z_{m+1} - z_m)} - (z_{m-1} - z_m)\overline{(z_{m+1} - z_m)} + (z_{m-1} - z_m)\overline{(z_{m+2} - z_{m+1})} \\ &+ (z_{m-1} - z_m)\overline{(z_m - z_{m+1})} - (z_{m-1} - z_m)\overline{(z_{m+1} - z_m)} - (z_{m-1} - z_m)\overline{(z_{m-1} - z_m)}\Big\}. \end{aligned}$$

The imaginary part of the 1^{st}, 4^{th}, 6^{th}, and 7^{th} terms are each equal to $-H_m$. The 3^{rd} and 8^{th} terms are equal to $-\rho_{m+1}^2$ and $-\rho_{m-1}^2$ respectively, which have zero imaginary part. Therefore we have

$$\dot{H}_m = -2H_m + G_m, \tag{4.25}$$

where

$$G_m = \frac{1}{2}\Im\{(z_{m-2} - z_{m-1})\overline{(z_{m+1} - z_m)} + (z_{m-1} - z_m)\overline{(z_{m+2} - z_{m+1})}\} \tag{4.26}$$

Now, if $H_m(t_1) = 0$, by Lemma 4.15, one of the following four conditions must be satisfied.

(i) $\beta_m(t_1) = \pi$ and $\rho_{m-1}(t_1), \rho_m(t_1) > 0$.

(ii) $\beta_m(t_1) = 0$ and $\rho_{m-1}(t_1), \rho_m(t_1) > 0$.

(iii) $\rho_m(t_1) = 0$.

(iv) $\rho_{m-1}(t_1) = 0$.

Condition (iii), in which $\rho_m(t_1) = 0$, cannot be satisfied since $H_{m+1}(t_1) > 0$. Also, since the n-gon is initially convex, by Lemma 4.16 it is in a counterclockwise star formation. By Theorem 4.14 the vertices remain in a star formation for all time and thus remain distinct. Therefore, condition (iv) in which $\rho_{m-1}(t_1) = 0$, cannot be satisfied.

Assume condition (i) is satisfied. Then $\beta_m(t_1) = \pi$, $\rho_{m-1}(t_1), \rho_m(t_1) > 0$ and $H_m(t_1) = 0$, $H_{m+1}(t_1) > 0$. Since $\beta_m(t_1) = \pi$, we have that

$$\frac{z_{m+1}(t_1) - z_m(t_1)}{\rho_m} = -\frac{z_{m-1}(t_1) - z_m(t_1)}{\rho_{m-1}}.$$

Combining this with the expression for G_m we have

$$\begin{aligned} G_m(t_1) &= \frac{1}{2}\Im\{-\frac{\rho_m}{\rho_{m-1}}(z_{m-2} - z_{m-1})\overline{(z_{m-1} - z_m)} - \frac{\rho_{m-1}}{\rho_m}(z_{m+1} - z_m)\overline{(z_{m+2} - z_{m+1})}\} \\ &= \frac{1}{2}\left(\frac{\rho_m}{\rho_{m-1}}H_{m-1}(t_1) + \frac{\rho_{m-1}}{\rho_m}H_{m+1}(t_1)\right). \end{aligned} \tag{4.27}$$

Since $\rho_{m-1}(t_1), \rho_m(t_1) > 0$, $H_{m+1}(t_1) > 0$, and $H_{m-1}(t_1) \geq 0$, it follows that $G_m(t_1) > 0$. By continuity of G_m there exists $0 \leq t_0 < t_1$ such that $G_m(t) > 0 \ \forall t \in [t_0, t_1]$. Also, by assumption, $H_m(t) > 0$ for $t \in [0, t_1)$. Therefore

$$\dot{H}_m(t) = -2H_m + G_m > -2H_m, \quad t \in [t_0, t_1).$$

Integrating this and using the continuity of H_m, we obtain

$$H_m(t_1) \geq \mathrm{e}^{-2(t_1 - t_0)}H_m(t_0) > 0,$$

which is a contradiction.

Finally, assume condition (ii) is satisfied. Then $\beta_m(t_1) = 0$ and $\rho_{m-1}, \rho_m > 0$. The angle β_m is the interior angle between the edges $z_{m-1}z_m$ and $z_m z_{m+1}$. For all $t \in [0, t_1)$, we have $\beta_i(t) \in (0, \pi)$ and $\rho_i(t) > 0$ for all i. Moving z_m to the origin, we can define the (positive) cone created by the edges of the n-gon $z_{m-1}z_m$ and $z_m z_{m+1}$, as

$$\mathrm{cone}\{z_{m-1}z_m, z_m z_{m+1}\} := \{a(z_{m-1} - z_m) + b(z_{m+1} - z_m) | a, b \geq 0\}.$$

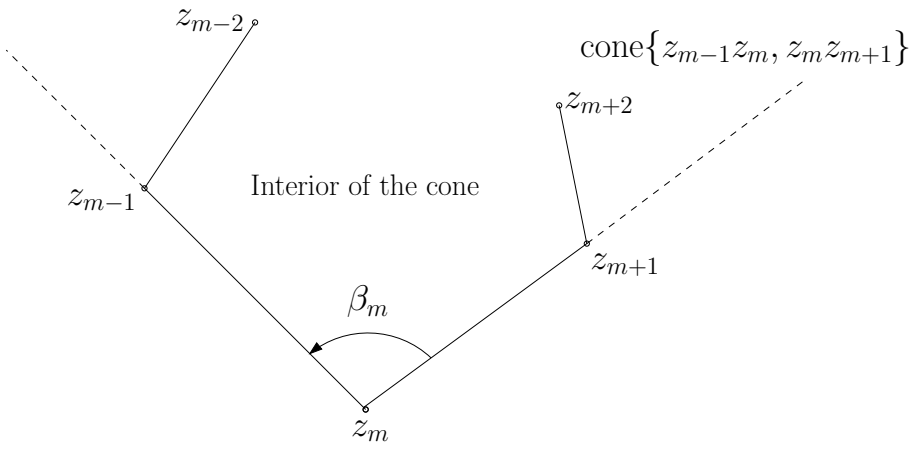

Figure 4.14: The convex n-gon lying within the boundaries of the shaded cone.

The $n-3$ vertices which are not involved in creating the cone must lie in the interior of this cone for all $t \in [0, t_1)$. This is shown in Figure 4.14. By continuity of the z_i's, at time t_1 the vertices must lie either in the interior or on the boundary of this cone. But we have $\beta_m(t_1) = 0$, implying that $z_{m-1}z_m$ and z_mz_{m+1} are collinear and the cone is a line. Hence all the vertices are collinear, a contradiction by Lemma 4.13. □

Corollary 4.18. *Consider an n-gon which is convex at $t = 0$. If the vertices evolve according to* (4.2)*, then for any $t > 0$, the n-gon will be strictly convex.*

Proof. Consider a vertex m for which $\beta_m(0) = \pi$, and thus $H_m(0) = 0$. We can choose this vertex such that $H_{m+1}(0) > 0$ since if $H_i(0) = 0$, $\forall i$, then the n-gon is not initially convex. From the proof of Theorem 4.17 we have

$$\dot{H}_m(t) = -2H_m(t) + G_m(t).$$

But $H_m(0) = 0$ and we have shown in (4.27) that $G_m(0) > 0$. Therefore, $\dot{H}_m(0) > 0$. By continuity of $\dot{H}_m$ there exists a $t_0 > 0$ such that $\dot{H}_m(t) > 0$ for $t \in [0, t_0]$. Thus, $H_m(t) > 0$, for all $t \in (0, t_0]$ and by Theorem 4.17, $H_m(t) > 0$ for all $t > t_0$. □

Figure 4.15 shows the evolution of a convex n-gon. Notice that the polygon remains convex and collapses to a point.

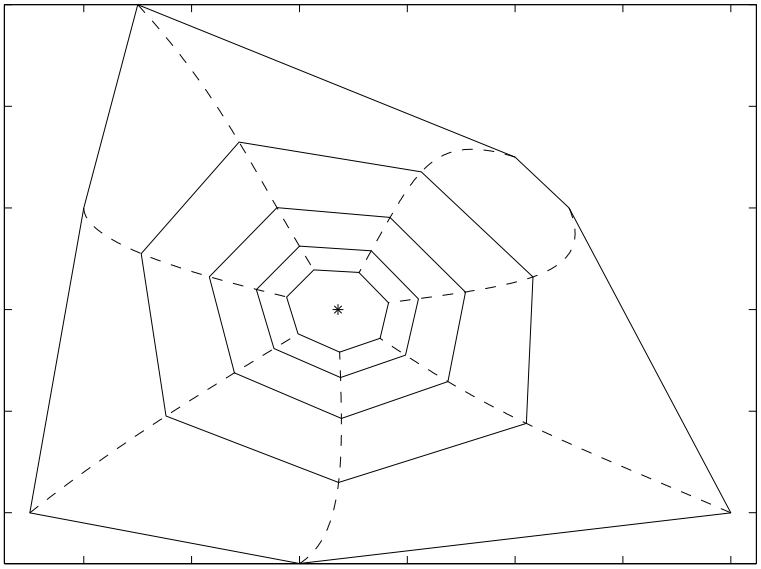

Figure 4.15: The evolution of a convex n-gon. The solid lines show the trajectories of each vertex.

4.6 Optimal control law for perimeter shortening

Given a polygon with vertices $z_1, \ldots, z_n$ and sides $z_1z_2, \ldots, z_nz_1$ we can write the perimeter of the polygon as

$$P(t) = \sum_{i=1}^{n} |z_{i+1} - z_i|. \tag{4.28}$$

We would like to compute an expression for $\dot{P}(t)$ analogous to that in Section 4.2.3. In order to take the time derivative of $P(t)$ consider taking the derivative of $|z_{i+1} - z_i|^2 = \langle z_{i+1} - z_i, z_{i+1} - z_i \rangle$ (for $u, v \in \mathbb{C}^n, \langle u, v \rangle = u^*v$, where * denotes complex conjugate transpose). This yields

$$\begin{aligned} \frac{d}{dt}|z_{i+1} - z_i|^2 &= \frac{d}{dt}\langle z_{i+1} - z_i, z_{i+1} - z_i \rangle \\ &= 2\Re\left\{\langle z_{i+1} - z_i, \dot{z}_{i+1} - \dot{z}_i \rangle\right\}. \end{aligned}$$

But also,

$$\frac{d}{dt}|z_{i+1} - z_i|^2 = 2|z_{i+1} - z_i|\frac{d}{dt}|z_{i+1} - z_i|.$$

Letting $\dot{z}_i = u_i$ for $i = 1, \ldots, n$ and rearranging we have

$$\frac{d}{dt}|z_{i+1} - z_i| = \Re\left\{\left\langle \frac{z_{i+1} - z_i}{|z_{i+1} - z_i|}, u_{i+1} - u_i \right\rangle\right\}.$$

Therefore

$$\begin{aligned}\dot{P}(t) &= \sum_{i=1}^{n} \Re\left\{\left\langle \frac{z_{i+1} - z_i}{|z_{i+1} - z_i|}, u_{i+1} - u_i \right\rangle\right\} \\ &= \sum_{i=1}^{n} \Re\left\{\left\langle \frac{z_{i+1} - z_i}{|z_{i+1} - z_i|}, u_{i+1} \right\rangle - \left\langle \frac{z_{i+1} - z_i}{|z_{i+1} - z_i|}, u_i \right\rangle\right\}.\end{aligned}$$

Since all indices are evaluated modulo n this can be rewritten as

$$\begin{aligned}\dot{P}(t) &= \sum_{i=1}^{n} \Re\left\{\left\langle \frac{z_i - z_{i-1}}{|z_i - z_{i-1}|}, u_i \right\rangle - \left\langle \frac{z_{i+1} - z_i}{|z_{i+1} - z_i|}, u_i \right\rangle\right\} \\ &= -\sum_{i=1}^{n} \Re\left\{\left\langle \frac{z_{i-1} - z_i}{|z_{i-1} - z_i|} + \frac{z_{i+1} - z_i}{|z_{i+1} - z_i|}, u_i \right\rangle\right\}. \qquad (4.29)\end{aligned}$$

To maximize the rate of decrease of $P(t)$ the two vectors in the inner product must point in the same direction. This implies that u_i should point in the direction of

$$\frac{z_{i-1} - z_i}{|z_{i-1} - z_i|} + \frac{z_{i+1} - z_i}{|z_{i+1} - z_i|}.$$

That is, u_i should point in the direction which bisects the internal angle β_i of the polygon. In general, neither the linear scheme (4.2) nor the shortening by Menger-Melnikov curvature points in this direction. However, this direction does not ensure that the polygon becomes circular (or elliptical); in simulation, adjacent vertices may capture each other and the polygon may collapse to a line. An example is shown in Figure 4.16.

Using (4.29) and the linear scheme (4.2) we can determine $\dot{P}(t)$. For $\dot{P}(t)$ to be defined we require that adjacent vertices be distinct. This is ensured, for example, if the vertices start in a star formation about their centroid.

Theorem 4.19. *Consider an n-gon whose distinct vertices evolve according to* (4.2)*. If adjacent vertices remain distinct, the perimeter $P(t)$ of the n-gon (defined in* (4.28)*) monotonically decreases to zero.*

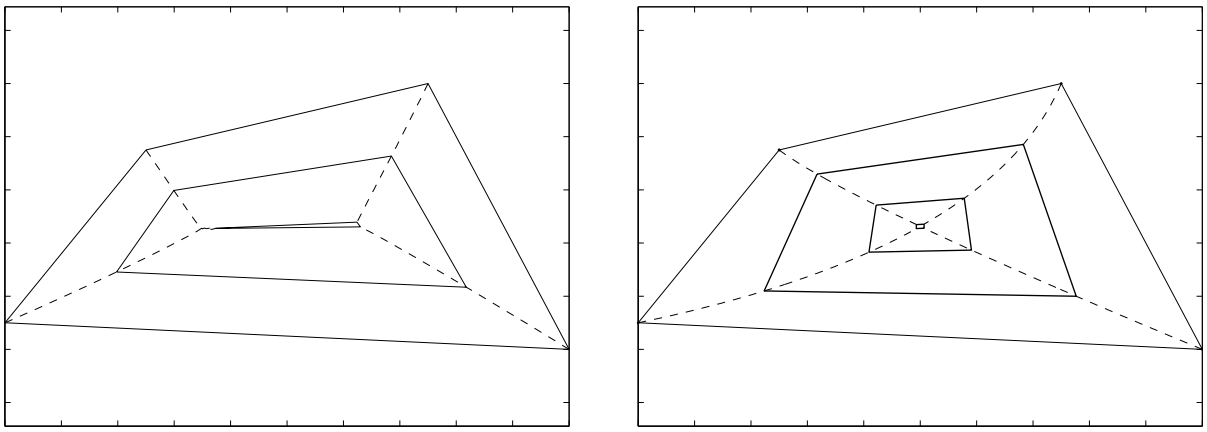

(a) A polygon evolving in the optimal direction. Notice that the polygon collapses to a line.

(b) The same initial polygon evolving according to the linear curve shortening scheme.

Figure 4.16: Evolving in the optimal direction.

Proof. Substituting (4.2) into (4.29) we have

$$\dot{P}(t) = -\frac{1}{2}\sum_{i=1}^{n} \Re\left\{\left\langle \frac{z_{i-1}-z_i}{|z_{i-1}-z_i|} + \frac{z_{i+1}-z_i}{|z_{i+1}-z_i|}, (z_{i+1}-z_i)+(z_{i-1}-z_i)\right\rangle\right\}.$$

Expanding this expression we obtain

$$\dot{P}(t) = \frac{1}{2}\sum_{i=1}^{n} \Re\left\{-|z_i-z_{i-1}| - |z_{i+1}-z_i| + \left\langle \frac{z_i-z_{i-1}}{|z_i-z_{i-1}|}, z_{i+1}-z_i\right\rangle + \left\langle \frac{z_{i+1}-z_i}{|z_{i+1}-z_i|}, z_i-z_{i-1}\right\rangle\right\}.$$

Each term in this summation has the form $\Re\{-|u|-|v|+\langle u/|u|, v\rangle + \langle v/|v|, u\rangle\}$. From the Cauchy-Schwarz inequality we have $\Re\{\langle u/|u|, v\rangle\} \leq |v|$, $\Re\{\langle v/|v|, u\rangle\} \leq |u|$, and thus $\Re\{-|u|-|v|+\langle u/|u|, v\rangle + \langle v/|v|, u\rangle\} \leq 0$. Therefore, $\dot{P}(t) \leq 0$. Equality is achieved if and only if $u/|u| = v/|v|$ for each term in the summation; that is, if and only if

$$\frac{z_i - z_{i-1}}{|z_i - z_{i-1}|} = \frac{z_{i+1}-z_i}{|z_{i+1}-z_i|}, \quad \forall i. \tag{4.30}$$

However, assume by way of contradiction that (4.30) is satisfied. Rotate the coordinate system such that z_1 and z_2 lie on the real axis and $z_2 - z_1 > 0$. Setting $i = 2$ in (4.30) we have $z_3 - z_2 > 0$, setting $i = 3$ we have $z_4 - z_3 > 0$, and so on. Hence $z_{i+1} - z_i > 0$,

$\forall i = 1, \ldots, n-1$, which implies that $z_n > z_1$. But setting $i = n$ in (4.30) we have $z_1 - z_n > 0$, a contradiction. Therefore (4.30) cannot be satisfied, $\dot{P}(t) < 0$, and since the vertices converge to their stationary centroid, $P(t)$ monotonically decreases to zero. □

4.7 Limitations of the linear scheme

There are two ways in which the linear scheme does not mimic Euclidean curve shortening. First of all, if an embedded curve is evolved via Euclidean curve shortening, its area is monotonically decreasing. However, for the linear scheme, in general, the area of a simple polygon is not monotonically decreasing. This is shown in Figure 4.17.

Remark 4.20. If a convex polygon evolves according to (4.2), its area is monotonically decreasing. To see this, consider a convex polygon at time $t = 0$ with vertices z_i, $i = 1, \ldots, n$, evolving according to (4.2). For each i, $\dot{z}_i(0)$ is either zero, or points into the interior of the polygon, with $\dot{z}_i(0) \neq 0$ for some i. Therefore, the area is initially decreasing. By Corollary 4.18 the polygon is strictly convex for all $t > 0$, and thus $\dot{z}_i(t)$ points into the interior of the polygon for all i and for all $t > 0$. Therefore, the area decreases for all time. ◀

Second, if an embedded curve evolves according to the Euclidean curve shortening flow, it remains embedded. In contrast, a simple polygon can become self-intersection under the linear scheme, as is shown in Figure 4.18. However, this is to be expected since the vertices in Figure 4.18(a) are not equally spaced around the polygon. The regions of the polygon with smaller spacing between adjacent vertices will move more slowly than the regions where the spacing is large. This is why, in Figure 4.18(b), the outer edge of the boomerang has intersected the inner edge.

These two limitations show that in some respects, the linear scheme does not mimic the curve shortening flows. However, as shown throughout this chapter, their are many striking similarities between these two schemes. For a simple linear scheme, (4.2) does a

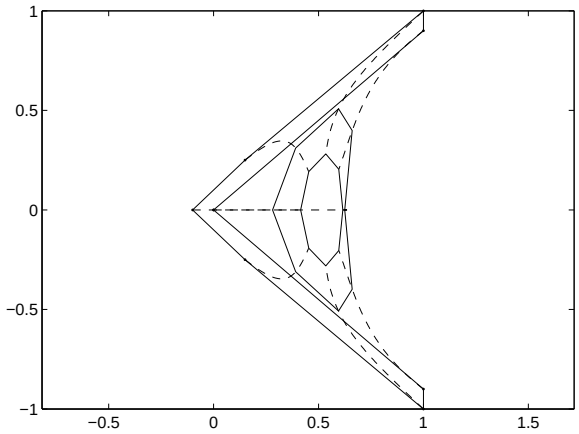

(a) The evolution of a simple polygon. The dashed lines show the trajectories of the vertices.

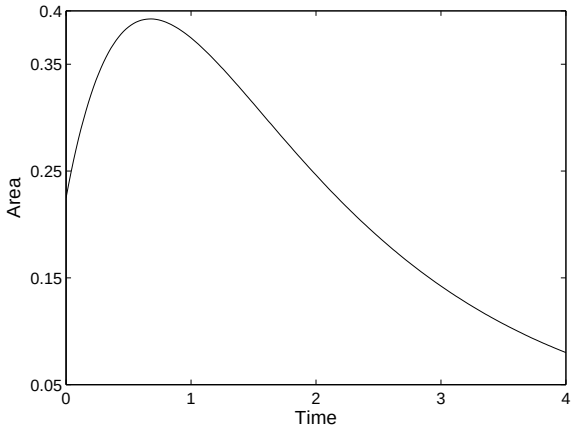

(b) A plot of the area as a function of time. Notice that the area is initially increasing.

Figure 4.17: An embedded polygon for which the area initially increases.

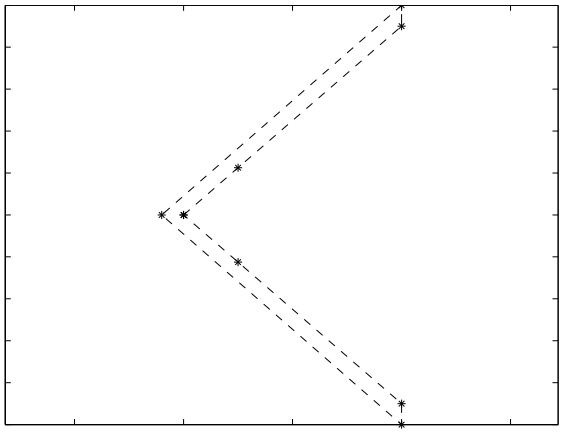

(a) A simple polygon. The vertices are marked by $*$'s.

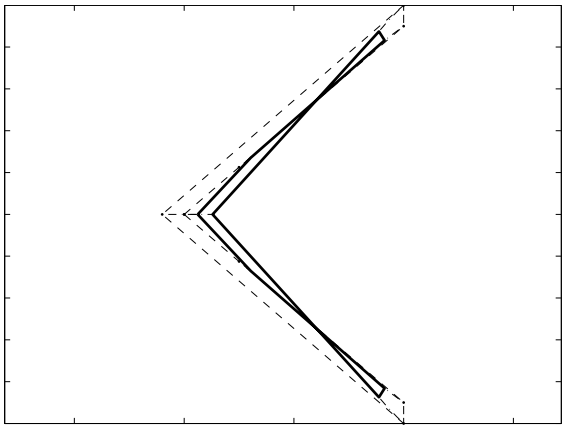

(b) The initial polygon evolves to the self-intersecting polygon shown by the thick solid line.

Figure 4.18: A simple polygon becomes self-intersecting.

remarkable job of mimicking the behavior of the curve shortening flows.

4.8 Summary

Motivated by the rendezvous problem in multi-agent systems we reviewed the theory of curve shortening. We proposed a simple linear scheme for polygon shortening and showed that it exhibits several properties similar to the curve shortening theory.

Chapter 5

Stabilizing to an equilateral polygon

In this chapter, the problem of stabilizing a group of agents to a stationary formation is analyzed. A local control scheme is proposed to stabilize the agents to the vertices of an equilateral polygon (a polygon for which every side has equal length). The centroid of the agents is stationary during the evolution. For three agents a full stability analysis is performed: If three agents start distinct and non-collinear, they converge to the vertices of a stationary equilateral triangle, while maintaining a stationary centroid.

5.1 Introduction

There has been a considerable amount of work on formation stabilization in the multi-agent systems literature. The two main types of formation stabilization that are studied are stabilization to a moving formation, and stabilization to a stationary formation. Much of the work was been on stabilizing a group of agents (most commonly unicycles) to a moving formation. For example, Justh and Krishnaprasad [23] develop a control law to stabilize two unicycles moving at constant speed to a common heading. In [41] by Paley et al., the same problem is approached by using potential functions to maintain spacing between unicycles. Marshall et al. [31] create a control strategy based on cyclic pursuit in which the unicycles can converge to a circle formation. In formation the unicycles are

moving around the circle, equally spaced. In [51, 52] by Tanner et al., moving formations are studied in the context of flocking. The agents are modeled as double integrators (i.e., the control input is the acceleration) and the stability of a flocking control law is studied for both fixed and dynamic communication topologies.

In the area of stabilization to a stationary formation there are some interesting results. Sugihara and Suzuki [48] propose a heuristic distributed algorithm to stabilize a group of agents (modeled as point masses) to stationary positions, equally spaced around a circle. Each agent adjusts its position based on the position of the nearest agent and the farthest agent. Through simulation, it is shown that the agents form a rough approximation of a circle. The formation stabilization problem has also been studied using graph theory, as in, for example, [38, 39]. In this work a formation is viewed as a rigid graph, where the links on the graph represent the distance constraints between agents. Problems such as determining the best way to split a large rigid formation into smaller rigid formations are studied in this framework.

An interesting scheme for formation stabilization of point masses is given by Lin et al. [25]. This scheme requires that each agent be equipped with a compass, so that they share a common direction. If the agents have this property then a local control strategy can be designed to stabilize to any stationary formation. This scheme will be described in detail in the next section. In [26] this idea is extended to unicycles.

In this chapter we look at the problem of stabilizing a group of agents to a stationary formation. As in the previous chapters, we model the agents as point masses, and we uniquely identify each of the n agents with a number between 1 and n. The position of the i^{th} agent is given by the vector $z_i = (x_i, y_i)$ in $\mathbb{R}^2$. The input to each agent is a velocity vector u_i:

$$\dot{z}_i = u_i.$$

The agents' positions can also be represented as points in the complex plane $z_i = x_i + jy_i$, $i = 1, \ldots, n$. The agents are not equipped with a compass, and thus they do not share a

common heading (i.e., the agents are disoriented). The fact that the agents are disoriented makes formation stabilization significantly more complicated then when the agents are oriented. The problem we address is to find a local control strategy such that for each i, agent i is stabilized to a distance $b > 0$ from agents $i + 1$ and $i - 1$.

The organization of this chapter is as follows. In Section 5.2 we explore the strategy in [25] in more detail and discuss the limitation of working in the complex plane. In Section 5.3 we introduce the control strategy, which is based on the linear polygon shortening scheme of Chapter 4, and analyze the system for n agents. Finally, in Section 5.4 we study the special case of three agents and show that they stabilize to an equilateral triangle.

5.2 Background

We will briefly explore the scheme for formation stabilization in [25]. We will also briefly talk about the limitations of representing the positions of the agents as points in the complex plane.

5.2.1 Formation stabilization with a compass

Consider the strategy, as introduced in Chapter 2, where each agent pursues a displacement of the next

$$\dot{z}_i = (z_{i+1} + d_i) - z_i, \quad i = 1, ..., n,$$

where the index i is evaluated modulo n and $\sum_{i=1}^{n} d_i = 0$. In vector form, this can be written as $\dot{z} = A_1 z + d$, where $A_1 = \mathrm{circ}(-1, 1, 0, \ldots, 0)$. A result from [25] is that the centroid of $z_1(t), \ldots, z_n(t)$ is stationary, and there exists a unique vector h orthogonal to $\ker A_1$ such that $A_1 h + d = 0$. Every $z_i(t)$ converges to the stationary centroid displaced by h_i.

By appropriate choice of d, a group of agents can be stabilized to a formation about their centroid. For example, let

$$d_i = \mathrm{e}^{2\pi ij/n}.$$

Notice that $\sum_{i=1}^{n} d_i = 0$ and therefore the centroid of the n points is stationary. In equilibrium $z_{i+1} - z_i = \mathrm{e}^{2\pi ij/n}$. Therefore, this stabilizes a group of agents to the vertices of a regular polygon centered at the centroid. However, notice that in order to implement this scheme, each agent must be able to calculate the vector $\mathrm{e}^{2\pi ij/n}$. This vector resides in the global coordinate system, which in this case is a global complex plane. Therefore, in order to implement this scheme, each agent must agree on a real and imaginary axis. Hence, each agent must be equipped with a compass. In this chapter, the agents are not equipped with compasses. This makes the problem considerably more difficult.

5.2.2 Limitations of the complex plane representation

Throughout this thesis we have been dealing with problems consisting of n agents lying in the plane. To simplify the analysis it is often convenient to represent the agents' positions as points in the complex plane. However, there are limitations to working in the complex plane, most if which occur when differentiating. As an example let $v = (v_x, v_y)$ be a vector in $\mathbb{R}^2$. Consider the function $f : \mathbb{R}^2 \to \mathbb{R}^2$, defined as $f(v) = (v_x, -v_y)$. This function is continuous and $\partial f/\partial v$ is a real matrix. However, if we introduce the notation $z = v_x + jv_y$, we can write $f : \mathbb{C} \to \mathbb{C}$, as $f(z) = \bar{z}$, where $\bar{z}$ is the complex conjugate of z. However $f(z)$ is not holomorphic and thus is not differentiable at any point in $\mathbb{C}$. Therefore, in this case the complex representation of f cannot be used when differentiating with respect to v.

5.3 Adapting linear polygon shortening

Consider a group of n agents, numbered from $1, \ldots, n$, lying in the plane. The i^{th} agents' position is given by (x_i, y_i), which we can represent in the complex plane as $z_i = x_i + jy_i$. We can view the group of agents as the vertices of an n-gon by joining consecutive pairs of points $z_1, z_2, \ldots, z_n$ to create the sides $z_1z_2, z_2z_3, \ldots, z_nz_1$. In this section we will introduce a control scheme for stabilizing the agents to an equilateral n-gon and study the stability of its equilibria.

5.3.1 The z dynamics

In order to stabilize a group of agents to an equilateral polygon, consider the following control strategy:

$$\dot{z}_i = u_i = \frac{1}{2}(z_{i+1} - z_i)\left(1 - \frac{b^2}{|z_{i+1} - z_i|^2}\right) + \frac{1}{2}(z_{i-1} - z_i)\left(1 - \frac{b^2}{|z_{i-1} - z_i|^2}\right), \quad i = 1, \ldots, n, \tag{5.1}$$

where b is a positive constant. In this expression all indices are evaluated modulo n (i.e., $n+1 = 1$ and $0 = n$). To better understand the motivation behind this scheme, consider the first term on the right-hand side of (5.1). If $|z_{i+1} - z_i| > b$ then $1 - b^2/|z_{i+1} - z_i|^2 > 0$ and thus the agent moves towards z_{i+1}. Similarly, if $|z_{i+1} - z_i| < b$ then $1 - b^2/|z_{i+1} - z_i|^2 < 0$ and the agent moves away from z_{i+1}. Therefore, the effect of this term is to stabilize z_i to a distance b from z_{i+1}. We add the second term to the right hand-side of (5.1) (which stabilizes z_i to a distance b from z_{i-1}) so that the centroid will remain stationary throughout the evolution.

Notice that if $b = 0$ we simply have the linear polygon shortening scheme of Chapter 4. Also notice that the system is undefined if $|z_{i+1} - z_i| = 0$ for some i. Letting $z \in \mathbb{C}^n$ denote the $n \times 1$ vector of positions, $(z_1, \ldots, z_n)$, the system (5.1) is defined on the set

$$\mathcal{T} := \{z \in \mathbb{C}^n : |z_{i+1} - z_i| > 0, \ \forall i\}.$$

The system (5.1) has been chosen to stabilize to the configuration $|z_{i+1} - z_i| = b$, $\forall i$. However, it is difficult to study the stability of this formation in the z dynamics, since z_{i+1} and z_i could be going off to infinity together, and yet $|z_{i+1} - z_i|$ could be converging to b. Because of this, we introduce the notation $e_i = z_{i+1} - z_i$ and study the stability of the e dynamics with respect to the equilibrium $|e_i| = b$, $\forall i$. From this analysis we will be able to infer the stability of the z dynamics.

5.3.2 The e dynamics

We introduce the notation

$$e_i = z_{i+1} - z_i.$$

Notice that by the definition of e_i,

$$\sum_{i=1}^{n} e_i = 0. \tag{5.2}$$

Let $e \in \mathbb{C}^n$ denote the $n \times 1$ vector $(e_1, \ldots, e_n)$. Then, by introducing the permutation matrix $P = \text{circ}(0, 1, 0, \ldots, 0)$, and the matrix $A_1 := P - I = \text{circ}(-1, 1, 0, \ldots, 0)$, we have

$$e = A_1 z.$$

We can rewrite (5.1) in terms of e as

$$u_i = \frac{1}{2} e_i \left(1 - \frac{b^2}{|e_i|^2}\right) - \frac{1}{2} e_{i-1} \left(1 - \frac{b^2}{|e_{i-1}|^2}\right), \quad i = 1, \ldots, n. \tag{5.3}$$

We can also write the dynamics $\dot{e}_i = \dot{z}_{i+1} - \dot{z}_i$ as

$$\dot{e}_i = \frac{1}{2} e_{i+1} \left(1 - \frac{b^2}{|e_{i+1}|^2}\right) - e_i \left(1 - \frac{b^2}{|e_i|^2}\right) + \frac{1}{2} e_{i-1} \left(1 - \frac{b^2}{|e_{i-1}|^2}\right), \quad i = 1, \ldots, n. \tag{5.4}$$

Notice that both (5.3) and (5.4) have a singularity if $e_i = 0$ for some i, and thus (5.3) and (5.4) are defined on the set

$$\mathcal{S} := \{e \in \mathbb{C}^n : |e_i| > 0, \ \forall i\}.$$

The topology of $\mathcal{S}$ is inherited from the topology of $\mathbb{R}^{2n}$. The system (5.4) on the set $\mathcal{S}$ can be viewed as a completely separate system from (5.1). If we impose condition (5.2) on the e_i's and hence relate the system to (5.1), then (5.4) evolves on the set $\mathcal{S}_0 \subset \mathcal{S}$:

$$\mathcal{S}_0 := \{e \in \mathbb{C}^n : |e_i| > 0,\ \forall i,\ \sum_{i=1}^{n} e_i = 0\}.$$

Note that with the relation $e = A_1 z$, $e \in \mathcal{S}_0$ if and only if $z \in \mathcal{T}$.

We can rewrite the equations (5.1) and (5.4) in vector form as follows. First, we introduce the function $\phi : \mathbb{C} \setminus \{0\} \to \mathbb{C}$

$$\phi(s) = \frac{1}{2} s \left(1 - \frac{b^2}{|s|^2}\right). \tag{5.5}$$

Using this function we can write (5.3) as

$$u_i = \phi(e_i) - \phi(e_{i-1}). \tag{5.6}$$

We can extend this function up to vectors by defining $\Phi : \mathcal{S} \to \mathbb{C}^n$ as

$$\Phi(e) = (\phi(e_1), \ldots, \phi(e_n)).$$

Noting that

$$-{A_1}^T = \operatorname{circ}(1, 0, \ldots, 0, -1) = \begin{bmatrix} 1 & 0 & \cdots & 0 & -1 \\ -1 & 1 & \cdots & 0 & 0 \\ \vdots & \vdots & \vdots & \vdots & \vdots \\ 0 & 0 & \cdots & -1 & 1 \end{bmatrix},$$

we can write (5.1) as

$$\dot{z} = -{A_1}^T \Phi(A_1 z) = -{A_1}^T \Phi(e). \tag{5.7}$$

Finally, writing (5.4) as

$$\dot{e}_i = \phi(e_{i+1}) - 2\phi(e_i) + \phi(e_{i-1}),$$

and using the fact that

$$-A_1 {A_1}^T = \operatorname{circ}(-2, 1, 0, \ldots, 0, 1),$$

we can write the e dynamics as

$$\dot{e} = -A_1 {A_1}^T \Phi(e). \tag{5.8}$$

Remark 5.1. In the development of (5.8) we have taken e_i as a point in the complex plane. However, we can equivalently let e_i be a vector in $\mathbb{R}^2$, and thus $e \in \mathbb{R}^{2n}$. The set $\mathcal{S}$ can be written as $\mathcal{S} = \{e \in \mathbb{R}^{2n} : \|e_i\| > 0,\ \forall i\}$. The function $\phi : \mathbb{R}^2 \setminus \{0\} \to \mathbb{R}^2$ is then defined as

$$\phi(e_i) = e_i \left(1 - \frac{b^2}{\|e_i\|^2}\right),$$

and $\Phi : \mathcal{S} \to \mathbb{R}^{2n}$ is defined as before. Finally, (5.8) becomes

$$\dot{e} = -\left(A_1 {A_1}^T \otimes I_2\right) \Phi(e),$$

where $\otimes$ is the Kronecker product and I_2 is the 2×2 identity matrix. ◀

This chapter will proceed in the following manner. We will study the stability of the system (5.8) on the set $\mathcal{S}$. From this study we will be able to determine the stability of the system (5.8) on $\mathcal{S}_0$. This is performed through an application of LaSalle's Theorem. In Lemmas 5.2 to 5.9 we will establish the results required to apply LaSalle's Theorem, and in Theorem 5.11 we state the main result for the system (5.8). From this result we will be able to infer the stability of system (5.1) on the set $\mathcal{T}$. This takes place in Theorem 5.13.

In order to perform a stability analysis of the system (5.8) on the set $\mathcal{S}$, we need to establish that $\mathcal{S}$ is open and connected. We say that an open and connected set is a *domain* [24].

Lemma 5.2. *The set $\mathcal{S}$ is a domain.*

Proof. It is clear that the set $\mathcal{S}$ is open. We will show that $\mathcal{S}$ is path-connected, which implies that $\mathcal{S}$ is connected. Consider a point $e \in \mathcal{S}$. This point consists of n complex numbers $e_1, \ldots e_n$, which satisfy $e_i \neq 0$, $\forall i$. That is, no component e_i of $e \in \mathcal{S}$, can lie

at the origin of the complex plane. Consider two arbitrary points $p, p' \in \mathcal{S}$. The set $\mathcal{S}$ is path-connected if there exists a function $\sigma(t) : [0,\ 1] \mapsto \mathcal{S}$, such that $\sigma(0) = p$ and $\sigma(1) = p'$. Consider the i^{th} component of p and p':

$$p_i := |p_i|\mathrm{e}^{j\theta_i} \quad \text{and} \quad p_i' := |p_i'|\mathrm{e}^{j\theta_i'}.$$

We would like to find a function $\sigma_i(t) : [0,1] \mapsto \mathbb{C}/\{0\}$, such that $\sigma_i(0) = p_i$ and $\sigma_i(1) = p_i'$. We can simply let $\sigma_i(t)$ be any smooth function that satisfies the boundary conditions, and does not pass through the origin. For example, $\sigma_i(t)$ could be a function which rotates and scales p_i to p_i'. Hence, letting $\sigma_i(t)$ be any such function, and defining $\sigma(t) = [\sigma_1(t), \ldots, \sigma_n(t)]$, we obtain the result that $\mathcal{S}$ is path-connected. This implies that $\mathcal{S}$ is connected. A set which is open and connected is a domain. □

In order to talk about a solution of the system (5.8), we must ensure local existence and uniqueness of solutions. A sufficient condition for this is that the right-hand side (RHS) of (5.8) is locally Lipschitz on $\mathcal{S}$. To show this we must compute the Jacobian of the RHS. This is an instance where the complex representation has its limitations. We will therefore show this using $e \in \mathbb{R}^{2n}$ as developed in Remark 5.1.

Lemma 5.3. *The right hand side of* (5.8) *is locally Lipschitz on* $\mathcal{S}$.

Proof. From Remark 5.1, we can let $e \in \mathbb{R}^{2n}$ and write (5.8) as $\dot{e} = -\left(A_1 {A_1}^T \otimes I_2\right)\Phi(e) =: f(e)$. From Lemma 3.2 of Khalil [24], f is locally Lipschitz on $\mathcal{S}$ if $f(e)$ and $\partial f/\partial e$ are continuous on $\mathcal{S}$. Letting $e_i = (e_{ix}, e_{iy})$, we can see that the function

$$\phi(e_i) = e_i\left(1 - \frac{b^2}{\|e_i\|^2}\right) = \begin{bmatrix} e_{ix} \\ e_{iy} \end{bmatrix}\left(1 - \frac{b^2}{e_{ix}^2 + e_{iy}^2}\right)$$

is continuous for all $\|e_i\| > 0$ (i.e., on the set $\mathbb{R}^2 \setminus \{0\}$), and thus $f(e)$ is continuous on $\mathcal{S}$. Therefore, it remains to be shown that $\partial f/\partial e$ is continuous on $\mathcal{S}$. We have

$$\frac{\partial f}{\partial e} = -\left(A_1 {A_1}^T \otimes I_2\right)\frac{\partial \Phi}{\partial e}.$$

The matrix $\partial\Phi/\partial e$ is a block diagonal matrix with the 2×2 blocks $\partial\phi(e_i)/\partial e_i$ along the diagonal. By computing the Jacobian $\partial\phi(e_i)/\partial e_i$, it can easily be verified that each block is continuous on $\mathbb{R}^2 \setminus \{0\}$. Therefore, $\partial\Phi/\partial e$ is continuous on $\mathcal{S}$ which implies that $\partial f/\partial e$ is continuous on $\mathcal{S}$. □

Note that at this point in the development we are not saying that $\mathcal{S}$ is positively invariant with respect to the dynamics (5.8). Later this will be shown to be true. In the following three lemmas we will establish some properties of the systems (5.1) and (5.8).

Lemma 5.4. *Under the dynamics* (5.8)*, if the trajectory* $e(t)$ *lies entirely in* $\mathcal{S}$*, the centroid of* $e_1, \ldots, e_n$ *is stationary. In particular, if a trajectory contained in* $\mathcal{S}$ *starts in* $\mathcal{S}_0$*, it remains in* $\mathcal{S}_0$ *for all time.*

Proof. Defining the $n \times 1$ vector of 1's as $\mathbf{1}$, the centroid of $e_1, \ldots, e_n$ is given by

$$\tilde{e} := \frac{1}{n}\mathbf{1}^T e.$$

From (5.8) we have

$$\dot{e} = -A_1 {A_1}^T \Phi(e).$$

Pre-multiplying this by $\mathbf{1}^T$ we have

$$n\dot{\tilde{e}} = -\mathbf{1}^T A_1 {A_1}^T \Phi(e) = -\mathbf{1}^T (P - I) {A_1}^T \Phi(e) = -(\mathbf{1}^T P - \mathbf{1}^T) {A_1}^T \Phi(e).$$

But, $\mathbf{1}$ is an eigenvector of P^T with eigenvalue 1, so $P^T\mathbf{1} = \mathbf{1}$ and thus $\mathbf{1}^T P - \mathbf{1}^T = 0$. Therefore $\dot{\tilde{e}} = 0$, and the centroid of the e_i's is stationary.

Consider a trajectory $e(t) \in \mathcal{S}$, $\forall t \geq 0$. If $e(0) \in \mathcal{S}_0$ then by the definition of $\mathcal{S}_0$, $\mathbf{1}^T e(0) = 0$. Since the centroid is stationary, $\mathbf{1}^T e(t) = 0$ and thus $e(t) \in \mathcal{S}_0$, $\forall t$. □

Similarly, the centroid of the z dynamics is stationary.

Lemma 5.5. *Under the dynamics* (5.1)*, if the trajectory* $z(t)$ *lies entirely in* $\mathcal{T}$*, the centroid of* $z_1, \ldots, z_n$ *is stationary.*

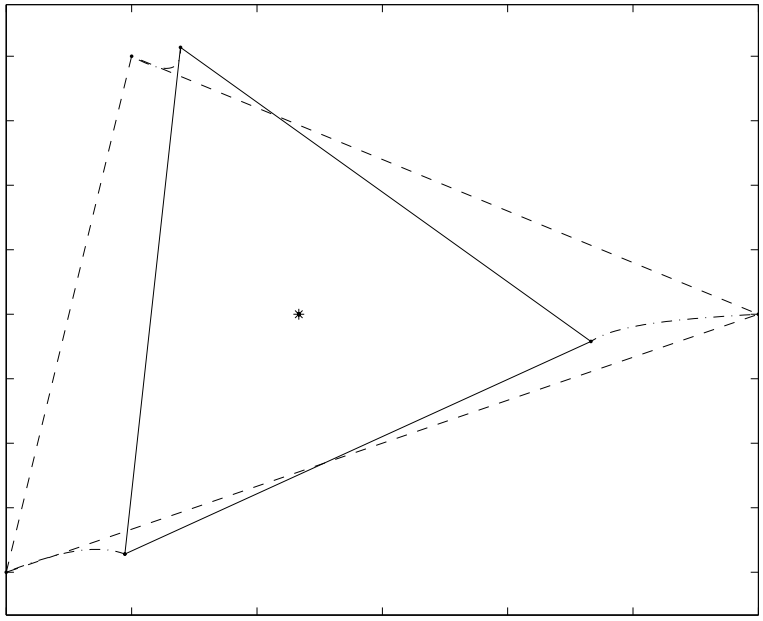

Figure 5.1: The evolution of a triangle. The initial triangle is given by the dashed line and the final triangle by the solid line. The stationary centroid is denoted by the $*$.

Proof. The centroid of the n points is given by $\tilde{z} := \frac{1}{n}\mathbf{1}^T z$. From (5.7) we have $\dot{z} = -{A_1}^T\Phi(e)$. Pre-multiplying this by $\mathbf{1}^T$ we have

$$n\dot{\tilde{z}} = -\mathbf{1}^T{A_1}^T\Phi(e) = -\mathbf{1}^T(P-I)^T\Phi(e) = -(\mathbf{1}^TP^T - \mathbf{1}^T)\Phi(e) = 0,$$

since $\mathbf{1}^TP^T = \mathbf{1}^T$. Therefore $\dot{\tilde{z}} = 0$, and the centroid of the n points is stationary. □

In Figure 5.1 the evolution of a triangle is shown. Notice that the centroid is stationary and the triangle evolves to an equilateral triangle.

Lemma 5.6. *Consider a trajectory $e(t)$ of (5.8) which lies entirely in $\mathcal{S}$. If the components $e_1, \ldots, e_n$ are collinear at some time t_1, then they are collinear for all $t < t_1$ and $t > t_1$.*

Proof. Let $x := \Re\{e\} \in \mathbb{R}^n$. If the points $e_1, \ldots, e_n$ are all collinear at t_1, then we can rotate the coordinate system such that they all lie on the imaginary axis. Then $x(t_1) = 0$.

Therefore, defining the function $\psi(x) = x$, and the set

$$\mathcal{L} := \{x \in \mathbb{R}^n : \psi(x) = 0\},$$

we have $x(t_1) \in \mathcal{L}$. Notice that $\partial\psi/\partial x = I_n$, where I_n is the $n \times n$ identity matrix. Therefore, if $L_{\dot{x}}\psi(x(t_1)) = 0$ for all $x(t_1) \in \mathcal{L}$, then $\mathcal{L}$ is an invariant set. We have

$$L_{\dot{x}}\psi(x) = \frac{\partial\psi}{\partial x}\dot{x} = \dot{x}.$$

From (5.8) we have $\dot{x} = -A_1 {A_1}^T \Re\{\Phi(e)\}$. However, notice that from (5.5) we can write $\phi(e_i) = e_i k(e_i)$ where

$$k(e_i) := \frac{1}{2}\left(1 - \frac{b^2}{|e_i|^2}\right) \in \mathbb{R}.$$

Therefore, defining $K(e) = \text{diag}(k(e_1), \ldots, k(e_n))$ we have $\Phi(e) = K(e)e$ and thus $\Re\{\Phi(e)\} = K(e)x$. Hence

$$L_{\dot{x}}\psi(x(t_1)) = -A_1 {A_1}^T K(e)x(t_1) = 0,$$

since $x(t_1) = 0$. This implies that $\mathcal{L}$ is an invariant set and if the points are collinear at some time t_1, they are collinear for all time. □

Note that this implies that the same collinearity property holds for the z dynamics. In the following lemma we prove two properties of ϕ which will be useful for the upcoming analysis.

Lemma 5.7. *The function* $\phi : \mathbb{C} \setminus \{0\} \to \mathbb{C}$

$$\phi(s) = \frac{1}{2}s\left(1 - \frac{b^2}{|s|^2}\right),$$

has the following properties:

(i) $\phi(s) = 0$ *if and only if* $|s| = b$, *and*

(ii) the restriction of ϕ *to* $\mathbb{R}^+$ *is one-to-one.*

Proof. To show (i), set $\phi(s) = 0$. Then clearly $|\phi(s)| = 0$. Hence

$$|\phi(s)| = \frac{1}{2}\left|s\left(1 - \frac{b^2}{|s|^2}\right)\right| = \frac{1}{2}|s|\left|1 - \frac{b^2}{|s|^2}\right| = 0.$$

Since $|s| > 0$ we must have that

$$1 - \frac{b^2}{|s|^2} = 0 \quad \Rightarrow \quad |s| = b.$$

For (ii), let q be a positive real number. Then

$$\phi(q) = \frac{1}{2}\left(q - \frac{b^2}{q}\right).$$

Taking the derivative of $\phi(q)$ with respect to q we obtain

$$\frac{d\phi}{dq} = \frac{1}{2} + \frac{b^2}{2q^2} > 0, \quad \forall q \in \mathbb{R}^+.$$

Therefore ϕ is monotonically increasing on $\mathbb{R}^+$ which implies that the restriction of ϕ to $\mathbb{R}^+$ is one-to-one. □

In general, the function ϕ is not one-to-one. For example, let $s_1 = b/\sqrt{2}$ and $s_2 = -b\sqrt{2}$. Then $\phi(s_1) = \phi(s_2) = -b/\sqrt{2}$.

We will now characterize the equilibria of the system (5.8) on the set $\mathcal{S}$. To keep the notation compact we introduce the set

$$\mathcal{I} := \{1, 2, \ldots, n\}.$$

We also introduce the unit vector notation

$$\hat{e}_i := \frac{e_i}{|e_i|}. \tag{5.9}$$

Lemma 5.8. *The equilibria of the system* (5.8) *on the set* $\mathcal{S}$ *are given by*

$$E := \{e \in \mathcal{S} : \Phi(e) \in \ker {A_1}^T\} = \{e \in \mathcal{S} : \phi(e_i) = \phi(e_j),\ \forall i, j \in \mathcal{I}\}.$$

Proof. From (5.8), at equilibrium we have

$$A_1 {A_1}^T \Phi(e) = 0.$$

Pre-multiplying both sides by $\Phi(e)^T$ we have that

$$\Phi(e)^T A_1 A_1^T \Phi(e) = 0 \quad \Rightarrow \quad \|A_1^T \Phi(e)\|^2 = 0.$$

Therefore, in equilibrium, $\Phi(e) \in \ker {A_1}^T$. Since ${A_1}^T = \text{circ}(-1, 0, \ldots, 0, 1)$, this implies that all components of $\Phi(e)$ are equal. □

Now we will characterize the equilibria of (5.8) on the set $\mathcal{S}_0 \subset \mathcal{S}$.

Lemma 5.9. *Let $e \in \mathcal{S}_0$ be an equilibrium of (5.8). If the components $e_1, \ldots, e_n$ are not all collinear, then e lies in the set*

$$E_1 := \{e \in \mathcal{S}_0 : |e_i| = b, \ \forall i\}.$$

If the components are collinear, then e lies in

$$E_2 := \left\{ e \in \mathcal{S}_0 : e_i = e_j \ \text{ or } \ e_i = -e_j \frac{b^2}{|e_j|^2}, \ \forall i, j \in \mathcal{I} \right\}.$$

Proof. From Lemma 5.8, at equilibrium all components of $\Phi(e)$ are equal. If $\Phi(e) = 0$, then $\phi(e_i) = 0$, $\forall i$, which from Lemma 5.7 implies that $|e_i| = b$, $\forall i$.

If $\Phi(e) \neq 0$, then $\phi(e_i)$ must take the same nonzero value in the complex plane for every i. That is,

$$\phi(e_i) = \phi(e_j) \quad \forall i, j \in \mathcal{I}. \tag{5.10}$$

From (5.9), we can write this as

$$\hat{e}_i \phi(|e_i|) = \hat{e}_j \phi(|e_j|), \quad \forall i, j \in \mathcal{I}, \tag{5.11}$$

and so e_i and e_j must be collinear, for all $i, j \in \mathcal{I}$. For simplicity, rotate the coordinate system so that e_i points along the positive real axis. Then we have $\hat{e}_i = 1$ and $\hat{e}_j = \pm 1$,

where the sign depends on e_j's orientation relative to e_i. Therefore, from (5.11) we have $\phi(|e_i|) = \pm\phi(|e_j|)$.

If $\hat{e}_j = 1$ then $\phi(|e_i|) = \phi(|e_j|)$. From Lemma 5.7, this is satisfied only if $|e_i| = |e_j|$. Combining this with the fact that $\hat{e}_i = \hat{e}_j$ we obtain that (5.10) is satisfied if $e_i = e_j$.

The other option is that $\hat{e}_j = -1$, in which case $\phi(|e_i|) = -\phi(|e_j|)$, and thus

$$|e_i| - \frac{b^2}{|e_i|} = -\left(|e_j| - \frac{b^2}{|e_j|}\right).$$

Solving this we obtain $|e_i||e_j| = b^2$. Combining this with the fact that $\hat{e}_i = -\hat{e}_j$ we obtain $e_i = -e_j b^2/|e_j|^2$.

So the equilibria fall into two categories. If the points are not all collinear then they lie in the set

$$E_1 := \{e \in \mathcal{S}_0 : |e_i| = b,\ \forall i\}.$$

If they are collinear, they lie in the set

$$E_2 := \left\{e \in \mathcal{S}_0 : e_i = e_j \ \text{ or } \ e_i = -e_j \frac{b^2}{|e_j|^2},\ \forall i, j \in \mathcal{I}\right\}.$$

□

Notice that if $e \in \mathcal{S}_0$, $e_i = e_j$ cannot be satisfied for all $i, j \in \mathcal{I}$, for if it were then $e_1 = e_2 = \cdots = e_n$, and $\sum_{i=1}^{n} e_i = ne_1 \neq 0$, which implies that $e \notin \mathcal{S}_0$. Also, the sets E_1 and E_2 are not disjoint if n is even. If an even number of points are in equilibrium and are non-collinear, they must lie in E_1. However, if they are collinear, they can lie in both E_1 and E_2. An example is shown in Figure 5.2. Figure 5.3 shows three possible equilibrium formations for $n = 5$ agents on the set $\mathcal{S}_0$. In Figures 5.3(a) and 5.3(b), $e \in E_2$, and in Figure (5.3(c)) we have $e \in E_1$.

With these preliminary results in place, we will now introduce two functions which will be used in the application of LaSalle's Theorem. First we introduce the function $g : \mathbb{R}^+ \to \mathbb{R}$:

$$g(q) = \frac{q^2}{2} - b^2 \ln(q) - C, \tag{5.12}$$

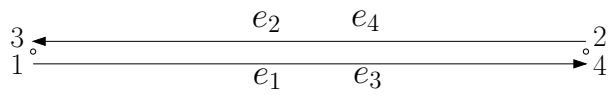

Figure 5.2: An equilibrium for $n = 4$ which is in both E_1 and E_2. Here the points are collinear and $|e_i| = b$, $\forall i$.

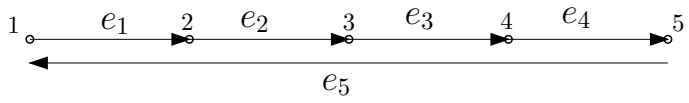

(a) collinear: $|e_1|, |e_2|, |e_3|, |e_4| = b/\sqrt{6}$, $|e_5| = 5|e_1|$.

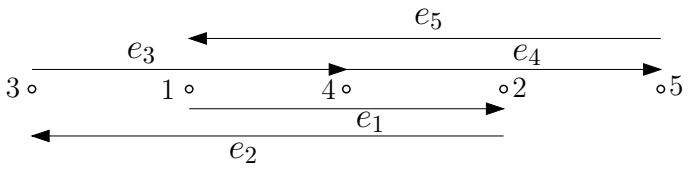

(b) collinear: $|e_1|, |e_3|, |e_4| = b\sqrt{2/3}$, $|e_2|, |e_5| = b\sqrt{3/2}$

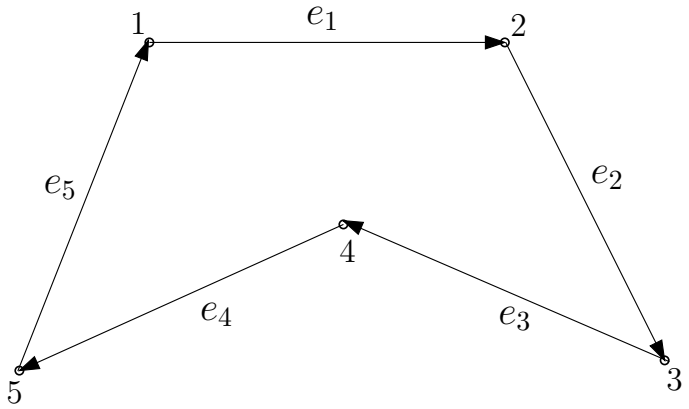

(c) non-collinear: $|e_i| = b$, $\forall i$.

Figure 5.3: Example equilibrium formations for $n = 5$ agents.

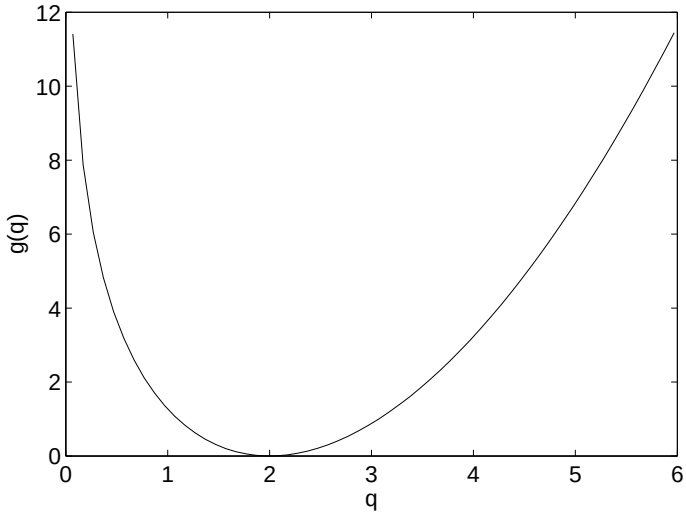

Figure 5.4: The function $g(q)$ with $b = 2$. Notice that $g(b) = 0$ is the minimum of the function.

where $C = b^2/2 - b^2 \ln(b)$. Using this function we define the continuously differentiable function $V : \mathcal{S} \to \mathbb{R}$:

$$V(e) := \sum_{i=1}^{n} g(|e_i|). \tag{5.13}$$

Taking the derivative of $g(q)$ with respect to q we obtain:

$$\frac{dg}{dq} = q - \frac{b^2}{q} = 2\phi(q). \tag{5.14}$$

From Lemma 5.7 we have that $\phi(q)$ is monotonically increasing and $\phi(q) = 0$ if and only if $q = b$. Therefore $g(q)$ takes its minimum at $g(b) = 0$, as shown in Figure 5.4. This implies that $V(e) \geq 0$ with $V(e) = 0$ if and only if $|e_i| = b$, $\forall i$. A plot of the level sets of V for $n = 2$ is shown in the $|e_1|, |e_2|$ space in Figure 5.5.

Lemma 5.10. *If the derivative of $V(e)$ is taken with respect to the dynamics* (5.8)*, then $\dot{V} \leq 0$ on $\mathcal{S}$, with $\dot{V} = 0$ if and only if $e \in E$ (where E is defined in Lemma 5.8).*

Proof. Taking the Lie derivative of V in (5.13) we have

$$\dot{V} = \sum_{i=1}^{n} \frac{dg}{de_i}\frac{de_i}{dt} = \sum_{i=1}^{n} \frac{dg}{d|e_i|}\frac{d|e_i|}{de_i}\frac{de_i}{dt} = \sum_{i=1}^{n} \frac{dg(|e_i|)}{d|e_i|}\frac{d|e_i|}{dt}.$$

Recall from Section 4.6 in Chapter 4 that

$$\frac{d}{dt}|e_i| = \frac{d}{dt}\langle e_i, e_i\rangle^{1/2} = \frac{1}{|e_i|}\Re\{\langle e_i, \dot{e}_i\rangle\} = \Re\{\langle \hat{e}_i, \dot{e}_i\rangle\}.$$

From (5.14) we also have that

$$\frac{dg(|e_i|)}{d|e_i|} = 2\phi(|e_i|).$$

Therefore, we can write $\dot{V}$ as

$$\dot{V} = 2\sum_{i=1}^{n} \phi(|e_i|)\Re\{\langle \hat{e}_i, \dot{e}_i\rangle\} = 2\sum_{i=1}^{n} \Re\{\langle \phi(|e_i|)\hat{e}_i, \dot{e}_i\rangle\}.$$

However, using the fact that $\phi(|e_i|)\hat{e}_i = \phi(e_i)$, we can write this as

$$\dot{V} = 2\sum_{i=1}^{n} \Re\{\langle \phi(e_i), \dot{e}_i\rangle\} = 2\Re\{\langle \Phi(e), \dot{e}\rangle\}.$$

From (5.8) this becomes

$$\dot{V} = -2\Re\{\langle \Phi(e), A_1 A_1{}^T \Phi(e)\rangle\} = -2\Re\{\Phi(e)^T A_1 A_1{}^T \Phi(e)\} = -2\|A_1{}^T \Phi(e)\|^2 \leq 0.$$

Therefore, $\dot{V} \leq 0$ on $\mathcal{S}$, with equality if and only if $\Phi(e) \in \ker A_1{}^T$. That is, $\dot{V} = 0$ if and only if $e \in E$ (where E is defined in Lemma 5.8). □

We say that a trajectory $e(t)$ approaches a set M as $t \to \infty$ if

$$\lim_{t\to\infty} \operatorname{dist}(e(t), M) = 0,$$

where

$$\operatorname{dist}(e(t), M) = \inf_{v\in M} \|e(t) - v\|.$$

Theorem 5.11. *Consider the system* (5.8). *For any initial condition* $e(0) \in \mathcal{S}$, *the solution* $e(t)$ *approaches* E *(defined in Lemma 5.8) as* $t \to \infty$. *Moreover, for any initial condition* $e(0) \in \mathcal{S}_0$, $e(t) \to E_1 \cup E_2$ *(defined in Lemma 5.9) as* $t \to \infty$.

Proof. From (5.12) we have

$$g(|e_i|) = |e_i|^2/2 - b^2 \ln(|e_i|) - C,$$

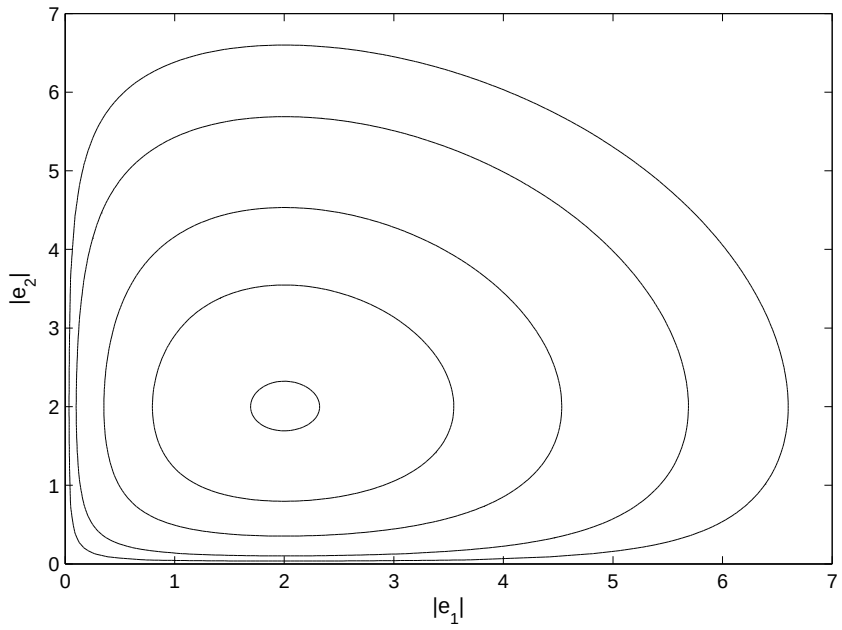

Figure 5.5: A few level sets of the function V. In this plot $b = 2$ and so as V decreases, the level sets approach $|e_1| = |e_2| = b$.

and thus

$$\lim_{|e_i|\to\infty} g(|e_i|) = \infty, \quad \text{and} \quad \lim_{|e_i|\to 0} g(|e_i|) = \infty.$$

Therefore, from the definition of V in (5.13),

$$\lim_{\|e\|\to\infty} V(e) = \infty,$$

implying that $V(e)$ is radially unbounded, and

$$\lim_{e\to\mathbb{C}^n\setminus\mathcal{S}} V(e) = \infty,$$

implying that $V(e)$ is proper. We define the set

$$\Omega_c = \{e \in \mathbb{C}^n : V(e) \leq c\}, \quad c > 0.$$

Since $V(e)$ is radially unbounded, Ω_c is compact, for all $c > 0$. Also, since $V(e)$ is proper, no level set of $V(e)$ contains a point in $\mathbb{C}^n \setminus \mathcal{S}$ (i.e., no level set of $V(e)$ contains

a singularity). Hence, $\Omega_c \subset \mathcal{S}$, for all c. Finally, since $\dot{V} \leq 0$ on $\mathcal{S}$, we have that Ω_c is positively invariant with respect to the dynamics (5.8).

Therefore, we have a dynamical system (5.8) which is locally Lipschitz (Lemma 5.3) on the domain $\mathcal{S}$ (Lemma 5.2). We have a set $\Omega_c \subset \mathcal{S}$ which is compact and positively invariant with respect to (5.8). Finally, we have a continuously differentiable function $V : \mathcal{S} \to \mathbb{R}$ such that $\dot{V} \leq 0$ on Ω_c. The set of all points in $\mathcal{S}$ where $\dot{V} = 0$ is given by

$$E = \{e \in \mathcal{S} : \Phi(e) \in \ker {A_1}^T\}.$$

From Lemma 5.8, E is an invariant set under (5.8). Therefore, By LaSalle's Theorem (see Theorem 4.4 of [24]), for every initial condition $e(0) \in \Omega_c$, the solution $e(t)$ of (5.8) approaches $E \cap \Omega_c$ as $t \to \infty$. In addition, for any initial condition $e(0) \in \mathcal{S}$, we can choose c such that $e(0) \in \Omega_c$. Therefore, for every $e(0) \in \mathcal{S}$, $e(t) \to E$ as $t \to \infty$.

If $e(0) \in \mathcal{S}_0$ then by Lemma 5.4, $e(t) \in \mathcal{S}_0$, $\forall t > 0$. Therefore, $e(t)$ must converge to a point in the set $\mathcal{S}_0 \cap E$ as $t \to \infty$. From Lemma 5.9, $\mathcal{S}_0 \cap E = E_1 \cup E_2$. Therefore, for every $e(0) \in \mathcal{S}_0$, $e(t) \to E_1 \cup E_2$ as $t \to \infty$. □

From this theorem the we have determined that the sets $\mathcal{S}$ and $\mathcal{S}_0$ are positively invariant under the dynamics (5.8). Therefore, a trajectory which starts in one of these sets is contained in that set for all time.

Corollary 5.12. *Let $e(t)$ be a trajectory of (5.8). If $e(0)$ is in $\mathcal{S}_0$, and its components $e_1(0), \ldots, e_n(0)$ are collinear, then $e(t) \to E_2$ as $t \to \infty$.*

Proof. From Theorem 5.11 we have that if $e(0) \in \mathcal{S}_0$, $e(t) \to E_1 \cup E_2$ as $t \to \infty$. From Lemma 5.9 the collinear equilibria on the set $\mathcal{S}_0$ are given by E_2. Also, from Lemma 5.6, if $e_1, \ldots, e_n$ are collinear at some time, they are collinear for all time. Therefore, if $e(0) \in \mathcal{S}_0$ and $e_1(0), \ldots, e_n(0)$ are collinear, then $e(t) \to E_2$ as $t \to \infty$. □

In the previous corollary we have shown that if the e_i's start collinear, then $e(t)$ converges to a collinear equilibrium. Unfortunately, if the points start non-collinear, we have not determined whether they will converge to a collinear or non-collinear equilibrium.

Theorem 5.13. *Let $z(t)$ be a trajectory of (5.7). If $z(0)$ is in $\mathcal{T}$, then:*

(i) $z(t)$ converges to a stationary equilibrium,

(ii) if the components of $z(0)$ are non-collinear, then in the limit as $t \to \infty$, $|z_{i+1} - z_i| = b$, $\forall i$, or the components are collinear,

(iii) if the components of $z(0)$ are collinear, they remain collinear.

Proof. If $z(0) \in \mathcal{T}$, then $e(0) = A_1 z(0) \in \mathcal{S}_0$. From Theorem 5.11 we have that $e(t) \to E_1 \cup E_2$ as $t \to \infty$. On the set $E_1 \cup E_2$, $\Phi(e) \in \ker {A_1}^T$. From (5.7) we have that $\dot{z} = -{A_1}^T \Phi(e)$, and so on $E_1 \cup E_2$, $\dot{z} = 0$. Therefore, $z(t)$ converges to a stationary equilibrium.

Since $e(t) \to E_1 \cup E_2$ as $t \to \infty$, either $|e_i| \to b$, $\forall i$, which implies $|z_{i+1} - z_i| \to b$, $\forall i$, or $e(t) \to E_2$ which implies that $z(t)$ converges to a collinear equilibrium.

Finally, if $z_1, \ldots, z_n$ are collinear, then $e_1, \ldots, e_n$ are collinear. By Corollary 5.12, $e(t)$ converges to a collinear equilibrium point, which implies that $z(t)$ converges to a collinear equilibrium. □

In Figure 5.6 the evolution of a ten sided polygon is shown. The length of each side of the polygon converges to the value b.

5.4 Special case of a triangle

In simulation it appears that if the points start non-collinear, they converge to a non-collinear equilibrium. However, through the prior analysis we have not been able to show this for n agents. In this section we will prove it for three agents. To do this we will begin by determining the equilibria of the e dynamics on the set $\mathcal{S}_0$ for three agents.

Lemma 5.14. *For $n = 3$, the collinear equilibria of (5.8) on the set $\mathcal{S}_0$ are given by*

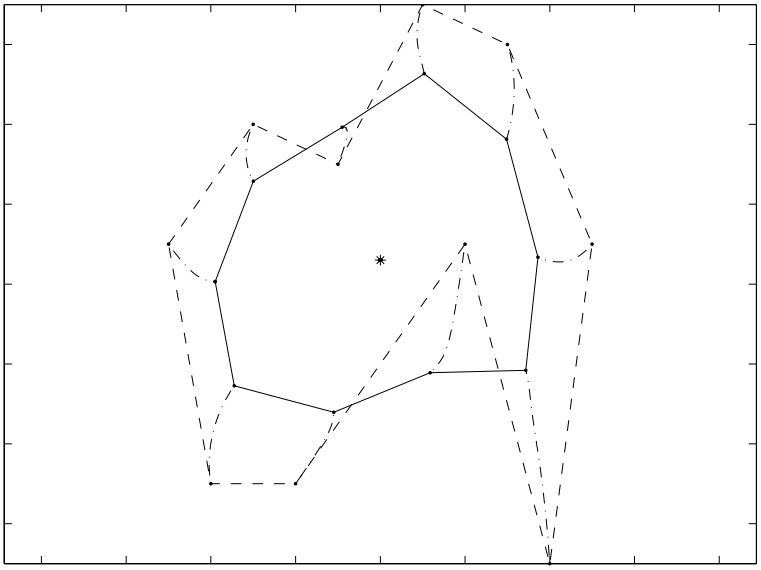

Figure 5.6: The evolution of a ten-sided polygon. The initial polygon is given by the dashed line, and the final polygon by the solid line. The length of each side converges to the value b.

$C_1 \cup C_2 \cup C_3$, *where*

$$C_k := \left\{ e \in \mathbb{C}^3 : |e_k| = \frac{b}{\sqrt{2}}, \quad e_k = e_{k-1}, \quad e_{k+1} = -2e_k \right\}, \quad k = 1, 2, 3.$$

Proof. From Lemma 5.6, the collinear equilibria on the set $\mathcal{S}_0$ are given by

$$E_2 := \left\{ e \in \mathcal{S}_0 : e_i = e_j \text{ or } e_i = -e_j \frac{b^2}{|e_j|^2}, \ \forall i, j \in \mathcal{I} \right\}$$

With $n = 3$, we have that $e \in E_2$ if $\sum_{i=1}^{3} e_i = 0$, and for each i,

(i) $e_i = e_{i-1}$, or

(ii) $e_i = -e_{i-1} \frac{b^2}{|e_{i-1}|^2}$.

To determine the equilibria we introduce the index $k \in \{1, 2, 3\}$. Notice that (i) cannot be satisfied for both $i = k$ and $i = k + 1$ for if it were, then $e_{k-1} = e_k = e_{k+1}$ and so either $\sum_{i=1}^{3} e_i \neq 0$, or $e_i = 0 \ \forall i$, both of which imply that $e \notin \mathcal{S}_0$. Therefore, we have three possible equilibria cases:

Case 1: (i) is satisfied for $i = k$, (ii) is satisfied for $i = k + 1$.

Case 2: (i) is satisfied for $i = k + 1$, (ii) is satisfied for $i = k$.

Case 3: (ii) is satisfied for $i = k$ and $i = k + 1$.

First consider Case 1. From (i) we have $e_k = e_{k-1}$. Substituting this into (5.2) we have $e_{k+1} = -2e_k$. From (ii) we have

$$e_{k+1} = -e_k \frac{b^2}{|e_k|^2},$$

which, when combined with $e_{k+1} = -2e_k$, gives $|e_k| = b/\sqrt{2}$. Therefore, from Case 1 we obtain

$$|e_k| = \frac{b}{\sqrt{2}}, \quad e_k = e_{k-1}, \quad e_{k+1} = -2e_k.$$

Case 2 is similar. From (i) we have $e_{k+1} = e_k$ and thus from (5.2), $e_{k-1} = -2e_k$. Setting $i = k$ in (ii) and combining that with $e_{k-1} = -2e_k$ we obtain $|e_k| = b/\sqrt{2}$. Therefore, from Case 2 we obtain

$$|e_k| = \frac{b}{\sqrt{2}}, \quad e_{k+1} = e_k, \quad e_{k-1} = -2e_k.$$

Finally, from Case 3 we have

$$e_k = -e_{k-1} \frac{b^2}{|e_{k-1}|^2} \quad \text{and} \quad e_{k+1} = -e_k \frac{b^2}{|e_k|^2}. \tag{5.15}$$

From this we have $\hat{e}_k = -\hat{e}_{k-1}$ and $\hat{e}_{k+1} = -\hat{e}_k$ which implies that $\hat{e}_{k-1} = \hat{e}_{k+1}$. Taking the magnitude of the expressions in (5.15) we obtain $|e_k||e_{k-1}| = b^2 = |e_{k+1}||e_k|$, and thus $|e_{k-1}| = |e_{k+1}|$. Therefore, $e_{k-1} = e_{k+1}$. From (5.2), we obtain $e_k = -2e_{k-1}$. Combining this with (5.15) we have $|e_{k-1}| = b/\sqrt{2}$. Therefore, from Case 3 we obtain

$$|e_{k-1}| = \frac{b}{\sqrt{2}}, \quad e_{k+1} = e_{k-1}, \quad e_k = -2e_{k-1}.$$

Notice that the equilibria obtained from the three cases are simply cyclic index shifts of each other. Therefore, the collinear equilibria of the system for $n = 3$ are given by

$$C_k := \left\{ e \in \mathbb{C}^3 : |e_k| = \frac{b}{\sqrt{2}}, \quad e_k = e_{k-1}, \quad e_{k+1} = -2e_k \right\}, \quad k = 1, 2, 3.$$

□

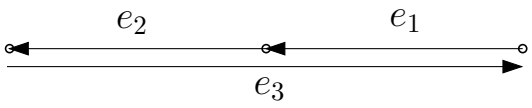

Figure 5.7: Three agents in collinear equilibrium with $|e_1| = |e_2| = b/\sqrt{2}$, $|e_3| = 2|e_1|$.

In Figure 5.7 an equilibrium for $n = 3$ agents is shown. It is interesting to note that $C_k \cap C_{k+1} = \emptyset$, $\forall k$. This can be seen by noting that in equilibrium the magnitudes of the e_i's satisfy

$$|e_{k-1}| = |e_k| = \frac{b}{\sqrt{2}}, \quad |e_{k+1}| = \sqrt{2}b.$$

For $C_k \cap C_{k+1}$ to be nonempty, we require that $b/\sqrt{2} = \sqrt{2}b$, which is satisfied only if $b = 0$.

We would like to show that if the points start non-collinear, the converge to a non-collinear equilibrium point. To do this we require a known result in planar geometry. For completeness, we will prove it here.

Lemma 5.15. *Consider a simple n-sided polygon lying in the complex plane whose vertices, $z_1, \ldots, z_n$, are numbered counterclockwise around the polygon. The area inclosed by the polygon is given by*

$$A = \frac{1}{2} \sum_{i=1}^{n} \Im\{\langle z_i, z_{i+1} \rangle\}.$$

Proof. Consider a simple closed curve in $\mathbb{R}^2$, $\mathbf{x}(p) = (x_1(p), x_2(p))$. Here $p \in [0, 1]$ parameterizes the points on the curve in the counterclockwise direction (i.e, as p increases, $\mathbf{x}(p)$ runs counterclockwise around the curve). Green's Theorem states that the area enclosed by the simple curve is

$$A = \frac{1}{2} \int (x_1 \dot{x}_2 - x_2 \dot{x}_1) dp,$$

where $\dot{x}_i = dx_i/dp$. We can write this as

$$\begin{aligned} A &= \frac{1}{2}\int \left(x_1 \frac{dx_2}{dp} - x_2 \frac{dx_1}{dp} \right) dp \\ &= \frac{1}{2}\int (x_1 dx_2 - x_2 dx_1) \\ &= \frac{1}{2}\int (x_1(x_2 + dx_2) - x_2(x_1 + dx_1)) \,. \end{aligned}$$

This can be written as the infinite summation

$$A = \frac{1}{2}\sum_{i=1}^{\infty}(x_1(p_i)x_2(p_{i+1}) - x_2(p_i)x_1(p_{i+1})),$$

where $p_{i+1} > p_i$ and thus $(x_1(p_{i+1}), x_2(p_{i+1}))$ is an infinitesimal distance counterclockwise around the curve from $(x_1(p_i), x_2(p_i))$. Therefore, the area of a simple n-sided polygon can be written as the finite summation

$$A = \frac{1}{2}\sum_{i=1}^{n}(x_1(p_i)x_2(p_{i+1}) - x_2(p_i)x_1(p_{i+1})),$$

where $(x_1(p_i), x_2(p_i))$ denotes the position of the i^{th} vertex of the polygon. Letting $z_i = x_1(p_i) + jx_2(p_i)$ we have

$$\langle z_i, z_{i+1} \rangle = \{x_1(p_i)x_1(p_{i+1}) + x_2(p_i)x_2(p_{i+1})\} + j\{x_1(p_i)x_2(p_{i+1}) - x_2(p_i)x_1(p_{i+1})\}$$

and thus

$$A = \frac{1}{2}\sum_{i=1}^{n} \Im\{\langle z_i, z_{i+1} \rangle\}.$$

□

Because of system (5.8)'s nonlinear circulant structure, the dynamics of the system are invariant under an index shift. To see this consider the shift $\check{e} := Pe$ where P is the permutation matrix. From (5.8), we have $\dot{e} = -A_1 {A_1}^T \Phi(e)$. Hence

$$\dot{\check{e}} = P\dot{e} = -PA_1 {A_1}^T \Phi(P^{-1}\check{e}).$$

But $\Phi(P^{-1}\check{e}) = (\phi(\check{e}_n), \phi(\check{e}_1), \ldots, \phi(\check{e}_{n-1})) = P^{-1}\Phi(\check{e}) = P^T\Phi(\check{e})$, where the last step comes from the fact that $P^{-1} = P^T$. Therefore,

$$\dot{\check{e}} = -PA_1 {A_1}^T P^T \Phi(\check{e}) = -(A_1^T P^T P A_1)^T \Phi(\check{e}) = -(A_1^T A_1)^T \Phi(\check{e}) = -A_1 {A_1}^T \Phi(\check{e}).$$

Therefore, if $e(t)$ evolves according to (5.8) then $\check{e}(t)$ also evolves according to (5.8). Also, notice that if $e \in C_1$ then $\check{e} = Pe \in C_2$ and $P^2\check{e} \in C_3$. Hence, by studying the stability of, say C_2, we are studying the stability of all three collinear equilibrium sets. By exploiting this fact, and using the two previous lemmas, we are now able to prove the main result of this section.

Theorem 5.16. *Let $e(t)$ be a trajectory of (5.8) starting in $\mathcal{S}_0$ (and thus always lying in $\mathcal{S}_0$). If the components e_1, e_2, e_3 of e start non-collinear, then the components of $\lim_{t\to\infty} e(t)$ are not collinear.*

Proof. Since $e(0) \in \mathcal{S}_0$, from Theorem 5.11, $e(t) \to E_1 \cup E_2$ as $t \to \infty$. For $n = 3$, the collinear equilibria are given by $E_2 := C_1 \cup C_2 \cup C_3$. Since $e_1(0), e_2(0), e_3(0)$ are non-collinear, by Lemma 5.6, they are non-collinear for all time. Assume by way of contradiction that $e(t) \to C_1 \cup C_2 \cup C_3$ as $t \to \infty$. Because of the circulant structure of (5.8), this is equivalent to assuming that $e(t) \to C_2$ as $t \to \infty$, where

$$C_2 = \left\{ e \in \mathbb{C}^3 : |e_1| = \frac{b}{\sqrt{2}}, \quad e_2 = e_1, \quad e_3 = -2e_2 \right\}.$$

We can write $e(t) = A_1 z(t)$, where $z(t) \in \mathcal{T}$. Since the e_i's are non-collinear, the z_i's are also non-collinear. Therefore, the z_i's define the vertices of a triangle as shown in Figure 5.8. We assume without loss of generality that the vertices are initially numbered counterclockwise around the triangle. This implies that that they are numbered counterclockwise for all time; otherwise the vertices would become collinear at some finite time, a contradiction by Lemma 5.6. From Lemma 5.15, we can write the area of the triangle as a function of time as

$$A(t) = \frac{1}{2} \sum_{i=1}^{3} \Im\{\langle z_i(t), z_{i+1}(t) \rangle\}.$$

Since we have assumed that $e(t) \to C_2$ as $t \to \infty$, it must also be that $A(t) \to 0$ as $t \to \infty$. Also, since the points are non-collinear for all time, $A(t) > 0$, $\forall t$.

Evaluating the time derivative of A, and using the fact that for $u, v \in \mathbb{C}^n$, $\Im\{\langle u, v \rangle\} =$

$-\Im\{\langle v, u\rangle\}$, we obtain

$$\dot{A} = \frac{1}{2}\sum_{i=1}^{3} \Im\{\langle u_i, z_{i+1}\rangle + \langle z_i, u_{i+1}\rangle\} = -\frac{1}{2}\sum_{i=1}^{3} \Im\{\langle z_{i+1}, u_i\rangle - \langle z_{i-1}, u_i\rangle\}$$
$$= -\frac{1}{2}\sum_{i=1}^{3} \Im\{\langle z_{i+1} - z_{i-1}, u_i\rangle\}.$$

However, notice that for $n = 3$, $z_{i+1} - z_{i-1} = -e_{i+1}$. Therefore, we have

$$\dot{A} = \frac{1}{2}\sum_{i=1}^{3} \Im\{\langle e_{i+1}, u_i\rangle\}.$$

From (5.6) we have $u_i = \phi(e_i) - \phi(e_{i-1}) = \phi(|e_i|)\hat{e}_i - \phi(|e_{i-1}|)\hat{e}_{i-1}$. Substituting this in we obtain

$$\dot{A} = \frac{1}{2}\sum_{i=1}^{3} \Im\left\{\phi(|e_i|)\langle e_{i+1}, \hat{e}_i\rangle - \phi(|e_{i-1}|)\langle e_{i+1}, \hat{e}_{i-1}\rangle\right\}.$$

In order to simplify the presentation we let $\phi_i := \phi(|e_i|)$. Introducing this notation we can write $\dot{A}$ as

$$\dot{A} = \frac{1}{2}\sum_{i=1}^{3} \Im\left\{\phi_i|e_{i+1}|\langle \hat{e}_{i+1}, \hat{e}_i\rangle - \phi_{i-1}|e_{i+1}|\langle \hat{e}_{i+1}, \hat{e}_{i-1}\rangle\right\}.$$

Expanding this expression we get

$$\dot{A} = \frac{1}{2}\Im\{\phi_1|e_2|\langle \hat{e}_2, \hat{e}_1\rangle - \phi_3|e_2|\langle \hat{e}_2, \hat{e}_3\rangle + \phi_2|e_3|\langle \hat{e}_3, \hat{e}_2\rangle - \phi_1|e_3|\langle \hat{e}_3, \hat{e}_1\rangle$$
$$+ \phi_3|e_1|\langle \hat{e}_1, \hat{e}_3\rangle - \phi_2|e_1|\langle \hat{e}_1, \hat{e}_2\rangle\}.$$

Collecting inner products we obtain

$$\dot{A} = -\frac{1}{2}\Im\{(\phi_1|e_2| + \phi_2|e_1|)\langle \hat{e}_1, \hat{e}_2\rangle + (\phi_3|e_2| + \phi_2|e_3|)\langle \hat{e}_2, \hat{e}_3\rangle + (\phi_1|e_3| + \phi_3|e_1|)\langle \hat{e}_3, \hat{e}_1\rangle\}.$$

Recall from Lemma 4.15 in Chapter 4 that we defined the function:

$$H_i := \Im\{(z_{i-1} - z_i)\overline{(z_{i+1} - z_i)}\} = \rho_{i-1}\rho_i \sin(\beta_i),$$

where β_i is the counterclockwise internal angle from the side $z_i z_{i+1}$ to the side $z_{i-1}z_i$ of a polygon. We can write $\Im\{\langle \hat{e}_{i-1}, \hat{e}_i\rangle\}$ in terms of this function as:

$$\Im\{\langle \hat{e}_{i-1}, \hat{e}_i\rangle\} = \frac{1}{|e_{i-1}||e_i|}\Im\{\overline{(z_i - z_{i-1})}(z_{i+1} - z_i)\} = -\frac{1}{\rho_{i-1}\rho_i}\Im\{(z_i - z_{i-1})\overline{(z_{i+1} - z_i)}\}$$
$$= \frac{1}{\rho_{i-1}\rho_i}\Im\{(z_{i-1} - z_i)\overline{(z_{i+1} - z_i)}\} = \frac{1}{\rho_{i-1}\rho_i}H_i = \sin(\beta_i).$$

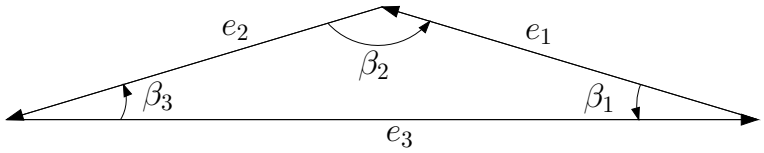

Figure 5.8: The triangle for sufficiently large t, showing the three internal angles.

The angles are shown in Figure 5.8. Using this, and the fact that $\sin(\beta_2) = \sin(\pi - \beta_1 - \beta_3) = \sin(\beta_1 + \beta_3)$ we obtain:

$$\dot{A} = -\frac{1}{2}\left((\phi_1|e_2| + \phi_2|e_1|)\sin(\beta_1+\beta_3) + (\phi_3|e_2| + \phi_2|e_3|)\sin(\beta_3) + (\phi_1|e_3| + \phi_3|e_1|)\sin(\beta_1)\right).$$

To simplify the following presentation we introduce $\mu := b/\sqrt{2}$. Multiplying $\dot{A}$ by 2, and dividing by $\mu\beta_3 > 0$ we obtain

$$\frac{2}{\mu\beta_3}\dot{A} = -\frac{1}{\mu}\left((\phi_1|e_2| + \phi_2|e_1|)\frac{\sin(\beta_1+\beta_3)}{\beta_3} + (\phi_3|e_2| + \phi_2|e_3|)\frac{\sin(\beta_3)}{\beta_3} + (\phi_1|e_3| + \phi_3|e_1|)\frac{\sin(\beta_1)}{\beta_3}\right) \quad (5.16)$$

As $t \to \infty$, $e(t) \to C_2$. From the definition of C_2 we have that,

$$\lim_{t\to\infty}|e_1| = \mu, \quad \lim_{t\to\infty}|e_2| = \mu, \quad \lim_{t\to\infty}|e_3| = 2\mu. \quad (5.17)$$

This implies that

$$\lim_{t\to\infty}\phi_1 = \phi(\mu) = -\mu, \quad \lim_{t\to\infty}\phi_2 = \phi(\mu) = -\mu, \quad \lim_{t\to\infty}\phi_3 = \phi(2\mu) = \mu. \quad (5.18)$$

Also from C_2, as $t \to \infty$, $\hat{e}_1(t) \to \hat{e}_2(t) \to -\hat{e}_3(t)$, which implies that $\beta_1(t), \beta_3(t) \to 0$. Finally, since $|e_1(t)| \to |e_2(t)|$ as $t \to \infty$, it follows that the triangle is becoming an isosceles triangle and thus $\beta_1(t) \to \beta_3(t) \to 0$ (that is, β_1 and β_3 approach each other as they approach zero). Therefore, we also have the limits

$$\lim_{t\to\infty}\frac{\sin(\beta_3)}{\beta_3} = 1, \quad \lim_{t\to\infty}\frac{\sin(\beta_1)}{\beta_3} = 1, \quad \lim_{t\to\infty}\frac{\sin(\beta_1+\beta_3)}{\beta_3} = 2. \quad (5.19)$$

Taking the limit of (5.16) as $t \to \infty$, and using the expressions in (5.17), (5.18), and (5.19) we obtain

$$\begin{aligned}\lim_{t\to\infty} \frac{2}{\mu\beta_3}\dot{A} &= -\frac{1}{\mu}\{(-\mu\mu - \mu\mu)(2) + (\mu\mu - \mu(2\mu))(1) + (-\mu(2\mu) + \mu\mu)(1)\} \\ &= 6\mu > 0.\end{aligned}$$

This implies that as $t \to \infty$, $\dot{A}(t) \downarrow 0$. Therefore, there exists a time t_1 such that, $\dot{A}(t) > 0$, $\forall t \geq t_1$. But, $A(t_1) > 0$, and thus

$$A(t) = \int_{t_1}^{t} \dot{A}(s)ds + A(t_1) > A(t_1), \quad \forall t > t_1,$$

a contradiction with our assumption that $e(t) \to C_2$ as $t \to \infty$ (and thus $A(t) \to 0$). Therefore, $e(t)$ does not converge to C_2. This implies that $Pe(t)$ does not converge to C_3 and $P^2e(t)$ does not converge to C_1. Thus, $e(t)$ does not converge to a collinear equilibrium point. □

Corollary 5.17. *Let $e(t)$ be a trajectory of (5.8) starting in $\mathcal{S}_0$. If the components, e_1, e_2, e_3, of e start non-collinear, then $e(t) \to E_1$ as $t \to \infty$.*

Proof. From Theorem 5.11 we know that for every $e(0) \in \mathcal{S}_0$, $e(t)$ converges to the equilibrium set $E_1 \cup E_2$. In Theorem 5.16 we have shown that $e(t)$ does not converge to the set of collinear equilibria $E_2 = C_1 \cup C_2 \cup C_3$. Therefore $e(t) \to E_1$ as $t \to \infty$. □

Theorem 5.18. *Let $z_1(0), z_2(0), z_3(0)$ be distinct, non-collinear points. Under the dynamics of (5.1), $z_1(t), z_2(t), z_3(t)$ converge to a stationary equilateral triangle with side length equal to b. In addition, their centroid is stationary throughout the evolution.*

Proof. Since the points are initially distinct, from Theorem 5.13, they converge to a stationary equilibrium. Also, since $z \in \mathcal{T}$, this implies that $e = A_1 z \in \mathcal{S}_0$. Since z_1, z_2, z_3 start non-collinear, e_1, e_2, e_3 are also initially non-collinear. Therefore, from Corollary 5.17, $|e_i| \to b$, $\forall i$ as $t \to \infty$. This implies that $|z_{i+1} - z_i| \to b$, $\forall i$ as $t \to \infty$. Therefore, z_1, z_2, z_3 converge to the vertices of an equilateral triangle, with side length b. From Lemma 5.4 the centroid of the three points is stationary. □

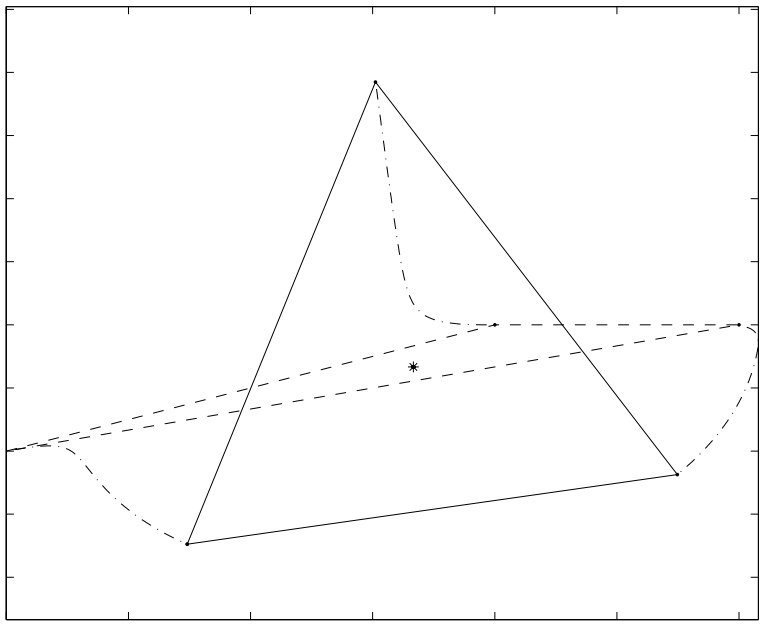

Figure 5.9: The evolution of a triangle. The initial triangle is given by the dashed line and the final triangle by the solid line. The stationary centroid is denoted by the $*$.

The evolution of a triangle is shown in Figure 5.9. Even when the vertices start close to being collinear, they converge to an equilateral triangle.

5.5 Summary

In this chapter a local control scheme was proposed to stabilize the agents to the vertices of an equilateral polygon. The centroid of the agents is stationary during the evolution. For n agents, we have shown that the agents converge either to the desired formation, or to a collinear equilibrium. In simulation, if the points start non-collinear, they converge to a non-collinear equilibrium. However, this could not be determined from our analysis. For three agents, a full stability analysis was performed. If three agents start distinct and non-collinear, they converge to the vertices of a stationary equilateral triangle, while maintaining a stationary centroid.

Chapter 6

Conclusions

Several interesting problems in multi-agent systems have been addressed in this thesis. In Chapter 2 the idea of creating a hierarchy within the sensing structure of a multi-agent system is introduced. A hierarchical cyclic pursuit scheme is created which yields a very significant increase in the rate of convergence of a group of vehicles to a common point. It is shown that this hierarchical structure can be applied to any linear circulant pursuit scheme. In Chapter 3 the stability analysis of a beetle and a unicycle in cyclic pursuit is completed. The stability analysis is global, and considers all possible values for the controller gains on the linear velocity of the beetle and the linear and angular velocities of the unicycle. Depending on these gains, the agents can either spiral in to a point, converge to concentric circles, or diverge. In Chapter 4, curve shortening theory is adapted to the multi-agent setting. A simple linear scheme is developed for polygon shortening and it is shown to yield some interesting parallels to curve shortening. The polygon shrinks to an elliptical point; convex polygons remain convex; and, the perimeter of the polygon monotonically decreases to zero. Finally, in Chapter 5 a control strategy is introduced to stabilize a group of agents to the vertices of an equilateral polygon. For the case of three agents, the analysis shows that the agents will converge to a stationary equilateral triangle while keeping their centroid stationary.

6.1 Summary of contributions

Chapter 2 introduced the novel concept of hierarchy within the sensing structure of a multi-agent system. The local strategy developed is the first hierarchical local control strategy in the multi-agent systems literature.

Chapter 3 is the first analytical study of a local control strategy for a heterogeneous multi-agent system. A complete global stability analysis is performed for a two agent heterogeneous system.

Chapter 4 is the first research to directly relate the curve shortening theory to multi-agent systems. The theory is used to design a simple local control strategy and reveal some of its interesting properties.

Chapter 5 introduced a novel local control strategy for stabilizing a multi-agent system to a vertices of a stationary equilateral polygon. The control strategy does not require that the agents have a common orientation (i.e., they are not equipped with compasses).

6.2 Future research

The work in this thesis has created several areas for future research. A few of these areas will be briefly described here.

6.2.1 Heterogeneous cyclic pursuit

There are two areas for future work on the subject of cyclic pursuit for heterogeneous groups of agents. The first is to perform a stability analysis for a constant speed beetle and unicycle. In this case we have

$$u_{\|} = -1 \quad \text{and} \quad v = 1.$$

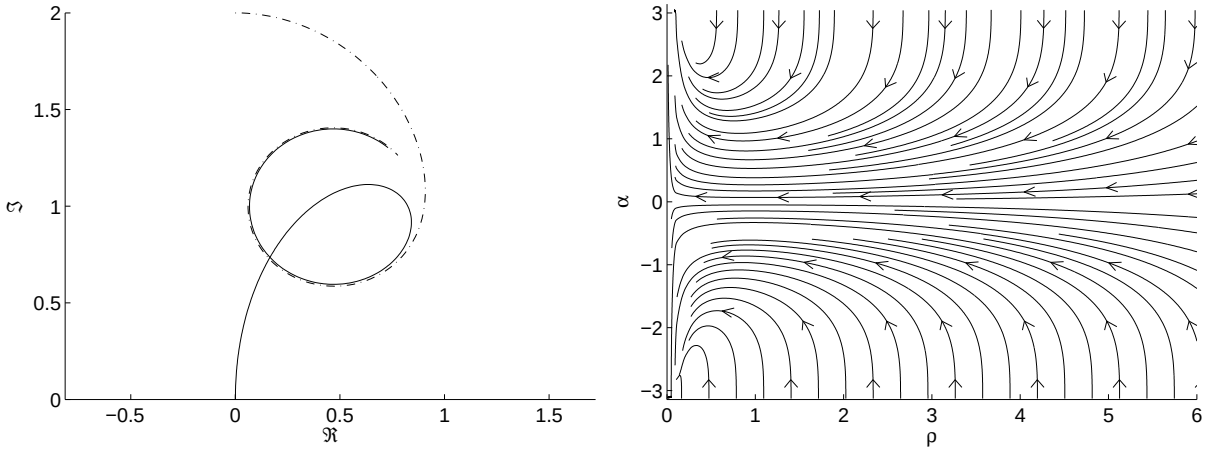

(a) A unicycle (dashed line) and a beetle (solid line) approach $(\rho, \alpha) = (0, \pi)$.

(b) The corresponding phase portrait.

Figure 6.1: A unicycle and a beetle in cyclic pursuit at constant speed. Here $k_\alpha = 1$.

The dynamics of the system becomes

$$\dot{\rho} = -1 - \cos\alpha$$
$$\dot{\alpha} = \frac{1}{\rho}\sin\alpha - k_\alpha \alpha.$$

Notice that the α dynamics is undefined if $\rho = 0$. Through simulation it appears that the system converges to the point $(\rho, \alpha) = (0, \pm\pi)$. This is shown in Figure 6.1. In this figure, the agents are moving around a circle defined by the maximum turning rate of the unicycle, with the beetle positioned an infinitesimal distance behind the unicycle.

Another area of future work would be to extend the heterogeneous analysis to a group of $n > 2$ agents. A good starting point would be to analyze a system of alternating beetles and unicycles. That is, given an even number of agents which we call n, agents $1, 3, 5, \ldots, n-1$ are beetles and $2, 4, 6, \ldots, n$ are unicycles.

6.2.2 Polygon shortening

In Chapter 4 we developed a linear polygon shortening scheme which "mimics" some of the important properties of curve shortening. There are a few limitations to this scheme.

We have shown that a polygon collapses to an elliptical point rather than a circular point. In addition, for a simple polygon, the area enclosed may initially increase, and the polygon may become self-intersecting.

Another approach to this problem would be to design a controller u_i for each agent (vertex) based on the isoperimetric inequality

$$\frac{L(t)^2}{A(t)} \geq 4\pi.$$

That is, we would like to find a controller such that

$$\lim_{t\to\infty} \frac{P(t)^2}{A(t)} = 4\pi, \tag{6.1}$$

where $P(t)$ is the perimeter of the polygon. Differentiating the left hand-side of this inequality we have

$$\frac{d}{dt}\left(\frac{P(t)^2}{A(t)}\right) = \frac{P}{A}\left(2\dot{P} - \frac{P}{A}\dot{A}\right).$$

But in Chapter 4 we derived that

$$\dot{P}(t) = -\sum_{i=1}^{n} \Re\left\{\left\langle \frac{z_{i-1}-z_i}{|z_{i-1}-z_i|} + \frac{z_{i+1}-z_i}{|z_{i+1}-z_i|}, u_i \right\rangle\right\}.$$

Also, from Chapter 5 we can write

$$\dot{A} = -\frac{1}{2}\sum_{i=1}^{n} \Im\{\langle z_{i+1}-z_{i-1}, u_i\rangle\}.$$

Therefore, the problem becomes finding the control input u_i such that the right hand side of

$$\frac{d}{dt}\left(\frac{P^2}{A}\right) = -\frac{P}{A}\left(2\sum_{i=1}^{n} \Re\left\{\left\langle \frac{z_{i-1}-z_i}{|z_{i-1}-z_i|} + \frac{z_{i+1}-z_i}{|z_{i+1}-z_i|}, u_i \right\rangle\right\} - \frac{P}{2A}\sum_{i=1}^{n} \Im\{\langle z_{i+1}-z_{i-1}, u_i\rangle\}\right),$$

is negative and (6.1) is satisfied. This analysis would ideally follow along the lines of [13] and [14].

6.2.3 Stabilizing to an equilateral polygon

For $n > 3$ agents, the analysis in Chapter 5 simply shows that the agents converge to an equilibrium point. This point could be a collinear equilibrium. However, in simulation, the agents do not converge to a collinear equilibrium point if they start non-collinear. A proof is needed to show that for general n, the collinear equilibria are unstable. This could be done by extending the result for $n = 3$ or by using a different technique.

6.2.4 Primary assumptions

Throughout this thesis we have used the assumption that the agents are not anonymous; they are each given a unique number between 1 and n. However, the agents do not know a common direction (they are disoriented), and they base their movements on a small number of other agents. In some research, the agents are anonymous (they do not have a unique number) but they are oriented (they have a compass). In other research the agents are anonymous and disoriented, but each agents' motion is based on the positions of every agent that it can sense. In the latter case, each agent must have sufficient computational power onboard to be able to compute a real-time heading based on the positions of, possibly, five or ten other agents. An interesting question is, how does one determine the "cost" of each of these assumptions.

It would be beneficial for the entire field of research in multi-agent systems to have an unbiased way of comparing these different schemes. This comparison would ideally be performed in terms of a cost function. The cost function would depend in some way on three criteria:

(i) How much information is required to initialize the system for a task,

(ii) How complex is the system (i.e., how complex is the hardware installed on each agent), and

(iii) How efficient is the system at completing the task.

The ideal system minimizes (i) and (ii) and maximizes (iii).

6.3 Concluding remarks

Throughout this thesis we have approached the control of multi-agent systems from a completely analytic point of view. We have devised local control strategies and attempted to prove their global outcomes. After seeing the difficulty and complexity of this approach, one might wonder why we didn't consider heuristic, or behavior-based techniques. After all, humans are constantly performing distributed and coordinated tasks: They flock on the sidewalks, avoid collisions on the roads, and line-up at the cash register. By definition, the strategies they employ are behavior-based. But there is a lack of precision in these behaviors: People bump into each other on the sidewalk; there are car crashes on the roads; and the line at the cash register can become a complete mess. What is so powerful about a multi-agent system based purely on analytic strategies (strategies with provable outcomes) is that the agents never "mess up." Their flocking is flawless, the collisions on the road just don't happen, and their line is perfectly straight every time. The power of a multi-agent system is not in emulating the behavior of humans, it is in doing things that humans cannot. It is in providing a degree of reliability and precision that is not possible through human behaviors. And it is my belief that the only way to achieve this is through the analytic approach of designing local strategies which result in provable global outcomes.

Bibliography

[1] S. Angenent, G. Sapiro, and A. Tannenbaum. On the affine heat equation for nonconvex curves. *J. of the American Math. Soc.*, 11:601–634, 1998.

[2] Birkhoff. Dynamical systems with two degress of freedom. *Trans. American Mathematical Society*, 18:199–300, 1917.

[3] D. A. Brannan, M. F. Esplen, and J. J. Gray. *Geometry.* Cambridge University Press, 1999.

[4] A. M. Bruckstein, N. Cohen, and A. Efrat. Ants, crickets and frogs in cyclic pursuit. *CIS Report No. 9105, Technion, IIT, Haifa, Israel*, July 1991.

[5] S. Buchin. *Affine Differential Geometry.* Gordon and Breach, Science Publishers, Inc., New York, 1983.

[6] E. Calabi, P. Olver, and A. Tannenbaum. Affine geometry, curve flows, and invariant numerical approximations. *Advances in Mathematics*, 124:154–196, 1996.

[7] F. Cao. *Geometric Curve Evolution and Image Processing.* Springer, 2003.

[8] Y. U. Cao, A. S. Fukunaga, and A. B. Kahng. Cooperative mobile robotics: Antecedents and directions. *Autonomous Robots*, 4(1):1–23, 1997.

[9] K-S. Chou and X-P. Zhu. *The Curve Shortening Problem.* Chapman and Hall, 2001.

[10] J. Cortes, S. Martinez, and F. Bullo. Spatially-distributed coverage optimization and control with limited-range interactions. *ESAIM. Control, Optimization and Calculus of Variations. To Appear.*

[11] H. S. M. Coxeter. *Regular Polytopes.* Dover Publications, Inc., New York, third edition, 1973.

[12] P. J. Davis. *Circulant Matrices.* Chelsea Publishing, New York, 2nd edition, 1979.

[13] M. E. Gage. An isoperimetric inequality with applications to curve shortening. *Duke Mathematical Journal*, 50(3):1225–1229, 1983.

[14] M. E. Gage. Curve shortening makes convex curves circular. *Inventiones mathematicae*, 76:357–364, 1984.

[15] M. E. Gage and R. S. Hamilton. The heat equation shrinking convex plane curves. *J. Differential Geometry*, 23:69–96, 1986.

[16] V. Gazi and K.M. Passino. Stability analysis of swarms. *IEEE Trans. Automatic Control*, 8(4):692–697, April 2003.

[17] R. Grabowski, L. E. Navarro-Serment, C. J.J. Paredis, and P. K. Khosla. Heterogeneous teams of modular robots for mapping and exploration. *Autonomous Robots*, 8(3):293–308, 2000.

[18] M. A. Grayson. The heat equation shrinks embedded plane curves to round points. *J. Differential Geometry*, 26:285–314, 1987.

[19] M. A. Grayson. Shortening embedded curves. *Annals of Mathematics*, 129:71–111, 1989.

[20] H. W. Guggenheimer. *Differential Geometry.* Dover Publications, Inc., New York, 1977.

[21] J. K. Hedrick, R. Sengupta, and T. Zohdi. Center for collaborative control of unmanned vehicles. *http://www.calccit.org/c3uv/*.

[22] T. Jecko and J-C. Leger. Polygon shortening makes (most) quadrilaterals circular. *Bull. Korean Math. Society*, 39(1):97–111, 2002.

[23] E. W. Justh and P. S. Krishnaprasad. Equilibria and steering laws for planar formations. *Systems and Control Letters*, 52(1):25–38, 2004.

[24] H. K. Khalil. *Nonlinear Systems*. Prentice Hall, 3rd edition, 2002.

[25] Z. Lin, M. Broucke, and B. Francis. Local control strategies for groups of mobile autonomous agents. *IEEE Trans. on Automatic Control*, 49(4):622–629, 2004.

[26] Z. Lin, B. Francis, and M. Maggiore. Necessary and sufficient conditions for formation control of unicycles. *IEEE Trans. on Automatic Control*, 50(1):121–127, 2005.

[27] Y. Liu and K. M. Passino. Stable social foraging swarms in a noisy environment. *IEEE Trans. on Automatic Control*, 49(1):30–44, 2004.

[28] J. Lui and J. Wu. *Multi-agent Robotic Systems*. CRC Press International Series on Computational Intelligence, 2001.

[29] R. Madhavan, K. Fregene, and L.E. Parker. Distributed cooperative outdoor multirobot localization and mapping. *Autonomous Robots*, 17(1):23–39, 2004.

[30] J. A. Marshall. *Coordinated Autonomy: Pursuit Formations of Multivehicle Systems*. PhD thesis, University of Toronto, 2005.

[31] J. A. Marshall, M. E. Broucke, and B. A. Francis. A pursuit strategy for wheeled-vehicle formations. In *Proc. of the 42nd IEEE Conference on Decision and Control*, volume 3, pages 2555–2560, December 2003.

[32] M. S. Mel'nikov. Analytic capacity: discrete approach and curvature of measure. *Sbornik: Math.*, 186(6):827–846, 1995.

[33] L. Moreau. Leaderless coordination via bidirectional and unidirectional time-dependent communication. In *Proc. of the 42nd IEEE Conference on Decision and Control*, pages 3070–3075, December 2003.

[34] K. Nakayama, H. Segur, and M Wadati. A discrete curve-shortening equation. *Methods and Applications of Analysis*, 4(2):162–172, 1997.

[35] K. Nomizu and T. Sasaki. *Affine Differential Geometry: Geometry of Affine Immersions*. Cambridge University Press, 1994.

[36] R. Olfati-Saber and R. Murray. Agreement problems in networks with directed graphs and switching topology. In *Proc. of the 42nd IEEE Conference on Decision and Control*, pages 4126–4132, December 2003.

[37] R. Olfati-Saber and R. Murray. Consensus protocols for networks of dynamic agents. In *Proc. of the American Control Conference*, pages 951–956, July 2003.

[38] R. Olfati-Saber and R. M. Murray. Distributed structural stabilization and tracking for formations of dynamic multi-agents. In *Proc. of the 41st IEEE Conference on Decision and Control*, volume 1, pages 209–215, 2002.

[39] R. Olfati-Saber and R. M. Murray. Graph rigidity and distributed formation stabilization of multi-vehicle systems. In *Proc. of the 41st IEEE Conference on Decision and Control*, volume 3, pages 2965–2971, 2002.

[40] R. Osserman. Bonnesen-style isoperimetric inequalities. *Amer. Math. Monthly*, 86:1–29, 1979.

[41] D. Paley, N. E. Leonard, and R. Sepulchre. Collective motion: bistability and trajectory tracking. In *Proc. of the 43rd IEEE Conference on Decision and Control*, volume 2, pages 1932–1937, 2004.

[42] L.E. Parker, B. Kannan, and M. Bailey. Tightly-coupled navigation assistance in heterogeneous multi-robot teams. In *Proc. of IEEE International Conference on Intelligent Robots and Systems*, volume 1, pages 1016 – 1022, 2004.

[43] W. Ren and R. Beard. Consensus of information under dynamically changing interaction topologies. In *Proc. of the American Control Conference*, pages 4939–4944, July 2004.

[44] H. G. Rotstein, S. Brandon, and A. Novick-Cohen. Hyperbolic flow by mean curvature. *Journal of Crystal Growth*, 198/199:1256–1261, 1999.

[45] G. Sapiro and A. Tannenbaum. On affine plane curve evolution. *Journal of Functional Analysis*, 119:79–120, 1994.

[46] S. L. Smith, M. E. Broucke, and B. A. Francis. Curve shortening and its application to multi-agent systems. *Submitted to the 44th IEEE Conference on Decision and Control*, 2005.

[47] S. L. Smith, M. E. Broucke, and B. A. Francis. A hierarchical cyclic pursuit scheme for vehicle networks. *Automatica*, 41(6):1045–1053, 2005.

[48] K. Sugihara and I. Suzuki. Distributed motion coordination of multiple robots. In *Proc. of the 5th IEEE International Symposium on Intelligent Control*, pages 138–143, 1990.

[49] I. Suzuki and M. Yamashita. Distributed anonymous mobile robots: Formation of geometric patterns. *SIAM J. Comput.*, 28(4):1347–1363, 1999.

[50] P. Tabuada, G.J. Pappas, and P. Lima. Feasible formations of multi-agent systems. In *Proceedings of the American Control Conference*, June 2001.

[51] H. Tanner, A. Jadbabaie, and G. Pappas. Stable flocking of mobile agents, part i: Fixed topology. In *Proc. of the 42nd IEEE Conference on Decision and Control*, pages 2010–2015, December 2003.

[52] H. Tanner, A. Jadbabaie, and G. Pappas. Stable flocking of mobile agents, part ii: Dynamic topology. In *Proc. of the 42nd IEEE Conference on Decision and Control*, pages 2016–2021, December 2003.

[53] I. A. Wagner and A. M. Bruckstein. From ants to a(ge)nts: A special issue on ant-robotics. *Annals of Mathematics and Artificial Intelligence*, 31(1):1–5, 2001.

[54] A. Williams, S. Glavaski, and Tariq Samad. Formations of formations: Hierarchy and stability. In *Proc. of the American Control Conference*, pages 2992–2997, July 2004.